INSTABILITY IN ACTION POTENTIAL MORPHOLOGY UNDERLIES PHASE 2 REENTRY INITIATION

by Anat Maoz

INSTABILITY IN ACTION POTENTIAL MORPHOLOGY UNDERLIES PHASE 2 REENTRY INITIATION

A Dissertation

Presented to the Faculty of the Graduate School

of Cornell University

In Partial Fulfillment of the Requirements for the Degree of

Doctor of Philosophy

by

Anat Maoz

August 2010

INSTABILITY IN ACTION POTENTIAL MORPHOLOGY UNDERLIES PHASE 2 REENTRY INITIATION

Anat Maoz, Ph. D.

Cornell University 2010

Phase-2 reentry (P2R) occurs when electrotonic current propagates from sites of normal notch-and-dome action potentials (AP) to loss-of-dome abbreviated AP sites, causing abnormal reexcitation. If sufficiently large and ill-timed, the secondary activation associated with P2R may initiate ventricular fibrillation and cause sudden cardiac death. AP heterogeneity consisting of the two AP morphologies, the notch-and-dome and the loss-of-dome, in adjacent regions is required for P2R development. Although P2R is well defined, the mechanisms underlying its initiation and the factors determining its development are still unknown. In this computational modeling study, a number of aspects of P2R initiation were explored. In the first part of this study, P2R development within the right ventricle epicardium was investigated using a systematic approach exploring homogeneous and heterogeneous one-dimensional cables. As expected, notch-and-dome morphologies were produced when the inward current overwhelmed the outward current while loss-of-dome morphologies were produced when the opposite occurred. However, when this fine balance was in an intermediate range, cells switched intermittently between a prolonged notch-and-dome morphology and the loss-of-dome morphology during constant pacing. P2R occurred in homogeneous and heterogeneous cable simulations, but only when a significant percentage of cells manifested this unstable “switching” behavior. In the second

part of this study, P2R initiation was studied in the transmural direction. The ventricular wall is thought to be comprised of three distinct layers: the epicardium, the midmyocardium, and the endocardium. Myocytes from each layer exhibit different action potential morphologies. We found that P2R occurred in one-dimensional transmural cables where the epicardial end manifested the unstable AP switching behavior. The last part of the study combined the first two parts; i.e., the initiation and development of P2R in two-dimensional transmural tissue was investigated. It was found that P2R could develop in two-dimensional tissues, expanding and creating macroscopic reentry. A notable increase in P2R incidence in two-dimensional transmural simulations compared to one-dimensional epicardial and transmural simulations was demonstrated as well. Hence, we conclude that an important factor facilitating P2R is not the presence of two different morphologies in adjacent regions but rather a switching AP behavior in which cells switch intermittently between the two morphologies.

BIOGRAPHICAL SKETCH

Anat Maoz was awarded a bachelor's of science in Computer Science, Statistics and Operations Research from Tel Aviv University in 1998. She graduated *Magna cum Laude* with a dean award for outstanding academic achievements. After working in the software industry, she enrolled in the Cornell/Rockefeller/Sloan-Kettering Tri-Institutional Ph.D. Program in Computational Biology and Medicine in July 2003.

To my children, husband and parents

ACKNOWLEDGEMENTS

First, I would like to thank my advisor, Dr. David Christini, for all his support throughout the years of my PhD. David's professionalism, help, ideas and most importantly his undeterred optimism were all crucial in achieving the goals of my research.

A special thanks goes to Dr. Trine Krogh-Madsen for her help and involvement in this project. Trine's eye for details always provided exciting directions to explore. Her advice and constant feedback were instrumental in the completion of this thesis.

I would also like to thank my committee members: Dr. Colleen Clancy, Dr. Larry Palmer and Dr. Jonathan Victor for their valuable feedback, comments, ideas and assistance.

I would like to extend my gratitude to my lab members: Becca Ahrens-Nicklas, Jonathan Bettencourt, Steve Gaeta, Uche Kanu, Jonathan Moreno, Francis Ortega and Byron Roberts.

I would like to thank my family and friends both in New York and Israel. Especially, I would like to thank my parents for their everlasting support. They were always close even if geographically far. Thank you.

I would like to thank my husband, Lior, who stole my heart long ago. Without him, all this would not have been possible. Thank you for supporting me

from the very beginning of the whole process, for always putting my work first, and more than all, for your never-ending love.

I would like to thank my two little children, Shira and Yahel. When you get older you will understand what it meant that mommy worked on her *“doctoran”*. You were to me a fountain of love. Your amazing development, your happiness, tricks and dances were the best I could have ever asked for.

TABLE OF CONTENTS

LIST OF FIGURES

LIST OF ABBREVIATIONS

4-AP	**4-aminopyridine**
AP	**action potential**
APD	**action potential duration**
AV	**atrial-ventricular**
BCL	**basic cycle length**
CV	**conduction velocity**
dmLSB	**dimethyl lithospermate B**
EAD	**early after depolarization**
ECG	**electrocardiogram**
$G_{Ca,L}$	**macroscopic conductance of the L-type calcium current**
G_{Na}	**macroscopic conductance of the sodium current**
G_{to}	**macroscopic conductance of the transient outward current**
HVA	**high voltage-activated**
$I_{Ca,L}$	**L-type calcium current**
I_{Kr}	**rapid delayed rectifier potassium current**
$I_{Kv4.3}$	**Kv4.3-encoded current**
$I_{Kv1.4}$	**Kv1.4-encoded current**
I_{Ks}	**slow delayed rectifier potassium current**
I_{Na}	**sodium current**
I_{to}	**transient outward potassium current**

ICD	**implantable cardioverter-defibrillators**
LR1	**Luo-Rudy cell model**
LRd	**Luo-Rudy dynamic cell model**
LV	**left ventricle**
LVA	**low voltage-activated**
M	**midyocardial**
P2R	**phase-2 reentry**
RV	**right ventricle**
RVOT	**right ventricular outflow track**
SA	**sinoatrial**
SB	**switching behavior**
VF	**ventricular fibrillation**
VT	**ventricular tachycardia**

CHAPTER 1

INTRODUCTION

1.1 The cardiac system

1.1.1 The heart's function

The heart provides the circulation of uninterrupted blood supply in the body. Deoxygenated blood is collected in the right atrium (Figure 1.1) from the body via the superior and inferior vena cava. It is then pumped via the right ventricle (RV), into the lungs, where gas exchange occurs (carbon dioxide is released and oxygen is brought in). Oxygenated blood from the lungs is collected into the left atrium (Figure 1.1), and is pushed to the left ventricle (LV), which pumps it to the body via the aorta. The muscle wall surrounding the ventricles is thicker and sturdier than the atria, and the LV wall is thicker and sturdier than the RV wall because of the stronger force needed to push the blood through the systemic circulation.

1.1.2 The cardiac conduction system

The heart contains a conduction system aimed at fulfilling several goals. It must transmit electrical signals throughout the whole organ, with precise timing dependent on the cardiac region. The conduction system includes several parts [6]. The sinoatrial (SA) node generates electrical signals that result in an action potential (AP). The myocytes in the sinoatrial node have a direct connection with the atrial conduction fibers. Therefore, the action potential spreads immediately

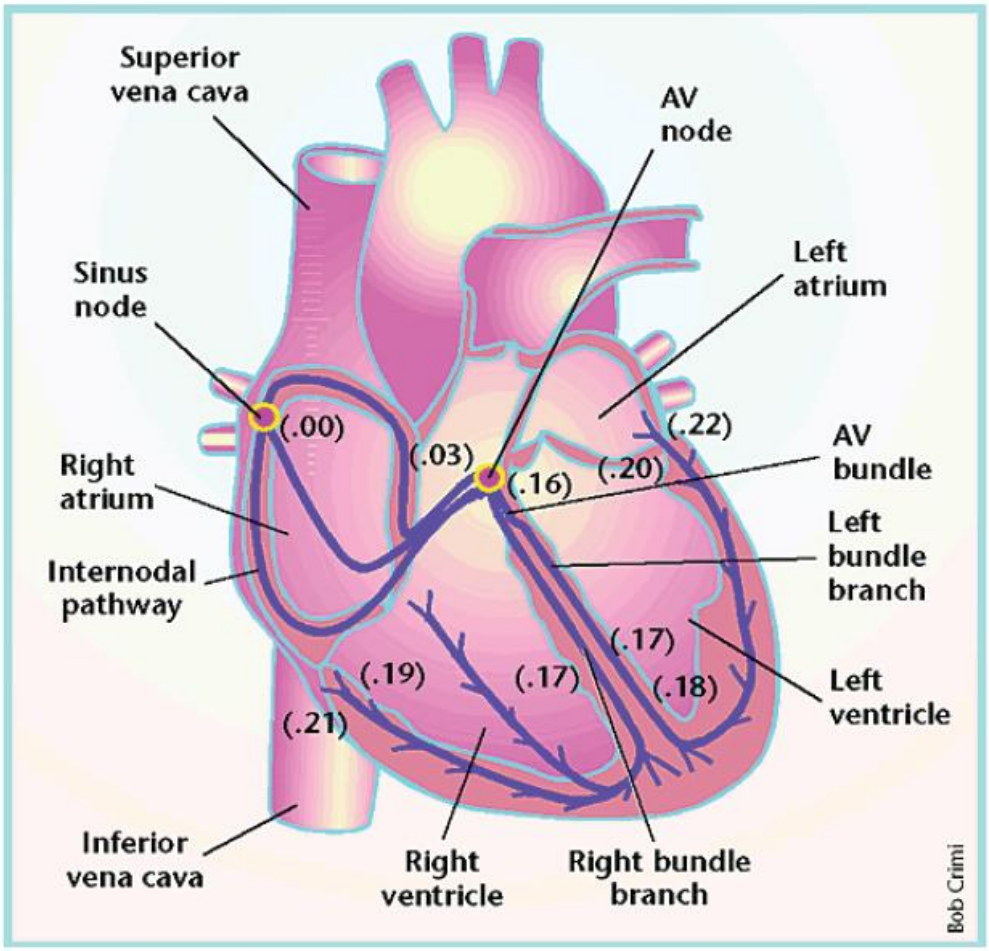

Figure 1.1: Cardiac structure and conduction system. The conductive system consists of the sinoatrial (SA) node, the atrio-ventricular (AV) node, and right and left Purkinje fiber bundles. Numbers represent activation time in milliseconds. Reproduced from reference [6].

into the atrial myocytes and throughout both atria. The three internodal pathways (Figure 1.1) facilitate faster propagation such that the conductive impulse arrives at the atrio-ventricular (AV) node within 30 ms. The signal then is delayed for about 130 ms in the AV node, allowing the atria to fill the ventricles. The Purkinje cells receive the signal and transmit it rapidly (at 200-400 cm/s), about 4-8 times faster than the normal ventricular myocardium rate of 50 cm/s. The full transmission through the Purkinje fiber system, with its left and right bundles, takes approximately 30 ms. This ensures timely blood ejection, where almost all portions of the ventricles contract simultaneously as the endocardial cells, and eventually the epicardial cells, become excited.

The electrical signal propagates between neighboring cells via gap junctions, which directly connect the cytoplasm of two cells. This conductive pathway allows electrical impulses to propagate between cells, so that the myocardium functions as a contractile unit. While normally beneficial, this property could be lethal. Therefore, these gap junctions can also block, facilitating isolation of damaged or dying tissue, as in a myocardial infarction [11].

1.2 The cardiac action potential

1.2.1 The ventricular action potential

A normal ventricular myocyte action potential is comprised of 5 phases: the action potential upstroke (phase 0), which is caused by a rapid influx of sodium ions, the sodium current I_{Na}; the rapid repolarization (phase 1) which is predominated by the transient outward current, I_{to}; the plateau or dome phase (phase 2) which is

predominated by an influx of calcium ions through the L-type calcium channels, $I_{Ca,L}$ and an outflow of potassium through the slow delayed rectifier potassium channels, I_{Ks}; final repolarization (phase 3) where potassium leaves the cell through the rapid delayed rectifier potassium channels, I_{Kr}; and diastolic potential (phase 4) which is predominated by an outflow of potassium through inward rectifier potassium channels, I_{K1}, bringing the membrane potential back to baseline (Figure 1.2.A.1).

Epicardial ventricular cells usually have APs that are of the *notch-and-dome* morphology (Figure 1.2.A.1). The formation of the dome phase is determined by the balance of membrane currents that play a role at the end of phase 1, mainly the sodium current, I_{Na}, and the transient outward current, I_{to}, and at the beginning of phase 2, the L-type calcium current, $I_{Ca,L}$. Failure of the dome to develop occurs when the outward current, mainly I_{to}, overwhelms the inward currents, I_{Na} and $I_{Ca,L}$, resulting in a marked abbreviation of the AP and the *loss-of-dome* morphology (Figure 1.2.A.2).

The above-mentioned notch-and-dome to loss-of-dome concept was demonstrated in a dynamic clamp experiment, using real-time variation of I_{to}, and showed its role in shaping the action potential morphology in left ventricle canine myocytes [7]. The dynamic clamp technique allows the injection of virtual membrane conductances, by calculating the corresponding current, into living cells in order to study its contribution to the cellular electrical behavior. In this particular study [7], left ventricle endocardial canine myocytes were studied using current-clamp mode. Simulated I_{to} current was calculated based on the measured instantaneous membrane voltage and a mathematical model describing $I_{to.}$ The

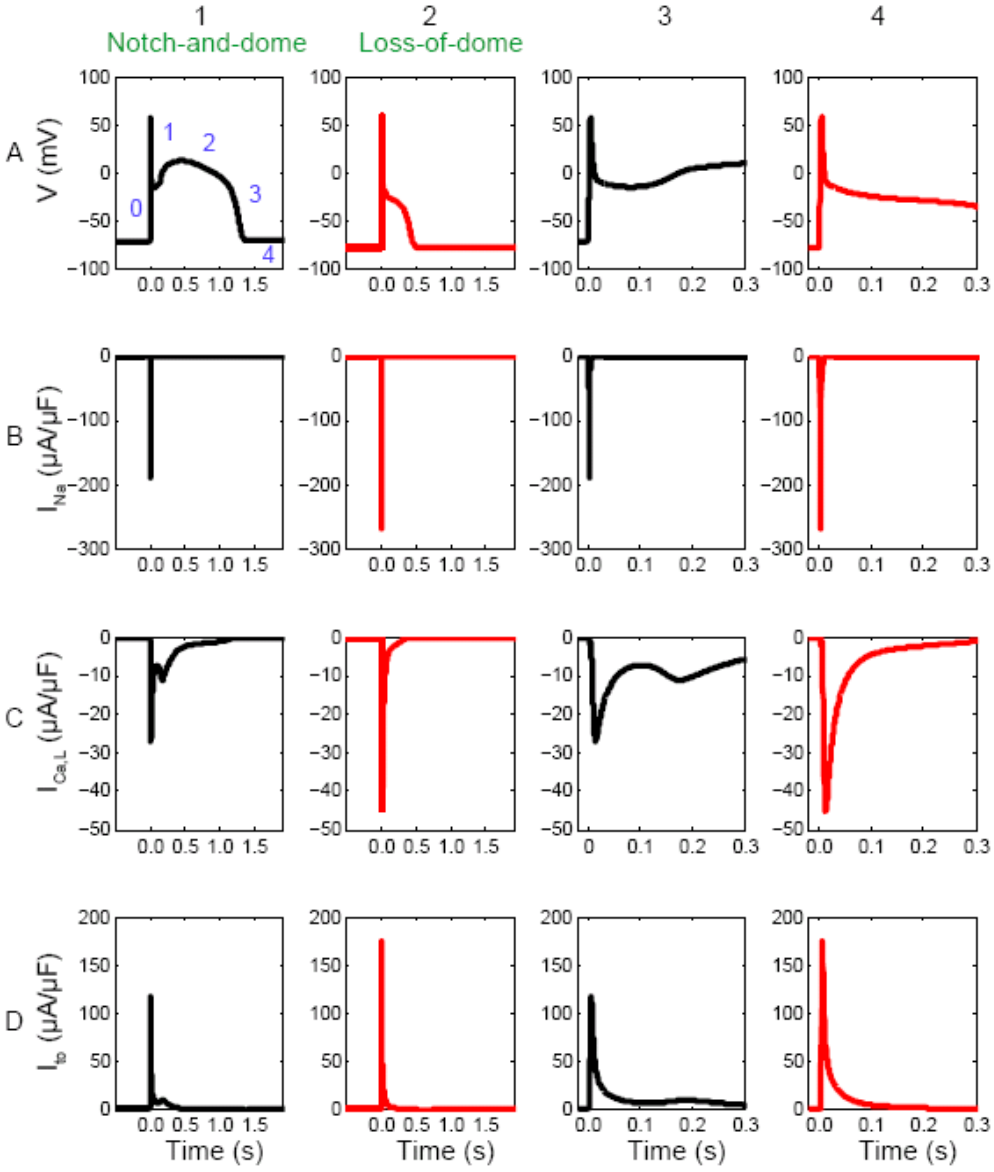

Figure 1.2: Simulated AP and selected currents using the modified LRd model (mathematical details are provided in Section 1.2.5). **A:** Membrane potential. **B:** Simulated I_{Na}. **C:** Simulated $I_{Ca,L}$ based on Miyoshi *et al* formalism [5]. **D:** I_{to} based on Dumaine *et al* formalism [10] **Column 1** shows notch-and-dome AP. **Column 3** shows its magnified view. **Colum 2** shows a loss-of-dome AP; its magnified view is in **column 4**. The different (0-4) AP phases are shown in panel 1A.

calculated current was injected into the endocardial cell (which natively has no significant I_{to}). Figure 1.3 shows that endocardial APs had no notch (control). However, increasing levels of injected I_{to} produced an increasingly deeper phase-1 notch and the notch-and-dome morphology. There were only minor effects on action potential duration (APD). The APDs responded to a further increase in the simulated I_{to}. They first exhibited moderate prolongation and then shortened dramatically as the dome of the AP was eliminated and the loss-of-dome morphology appeared.

A similar effect, where an increase in the outward current caused deepening of the notch of the canine ventricular AP, was shown in a mathematical study by Greenstein et al. [12]. In this model, I_{to} formalism was described as a combination of Kv4.3- and Kv1.4-encoded currents ($I_{Kv4.3}$ and $I_{Kv1.4}$, respectively). These two components were differentiated by their rate of recovery from inactivation, such that the $I_{Kv4.3}$, that had a fast recovery time constant, accounted for 77% and $I_{Kv1.4}$, with a slower recovery, accounted for the remainder 23%, based on experimental data. The I_{to} model was incorporated into the Winslow-Rice-Jafri mathematical model of the canine AP [13] and variations of the macroscopic conductances of $I_{Kv4.3}$, ($G_{Kv4.3}$) were studied. Few phases were identified. First, as $G_{Kv4.3}$ increased, phase-1 notch exhibited stronger repolarization with an unchanged notch-and-dome configuration, and no major effect on APD. Second, as $G_{Kv4.3}$ increased further, a threshold effect was evident, such that action potential morphology switched between the prolonged notch-and-dome morphology and the triangular loss-of-dome morphology.

The currents that are fundamental in setting the AP morphologies, the

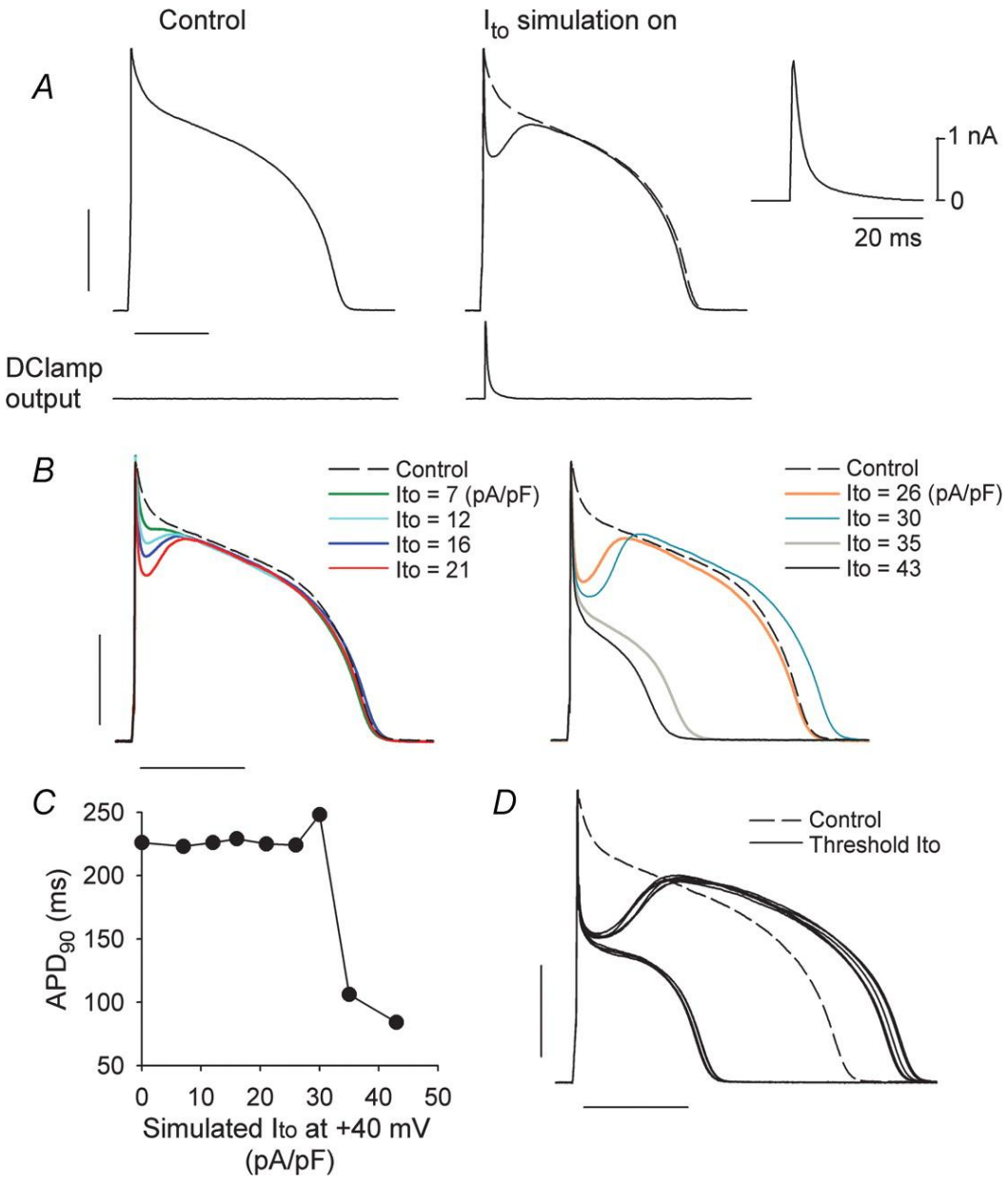

Figure 1.3: Dynamic clamp experiment of I_{to} simulation in canine endocardial myocytes. **A:** Left: AP recorded from an endocardial cell under control conditions where no I_{to} current was inserted; Right: AP recorded with the insertion of a simulated epicardial I_{to} (20 pA/pF at +40 mV). Bottom traces are the current output of the dynamic clamp for both recordings. Inset shows a magnified view of the current output. **B:** Endocardial APs resulted from the simulation of various densities of I_{to} in one cell. **C:** APDs of the cell recorded in B. **D:** Behavior of an endocardial cell when a threshold amount of I_{to} was inserted, causing the action potentials to alternate between a prolonged notch-and-dome morphology and a shortened loss-of-dome morphology; 12 consecutive traces are shown. Scale bars for the action potentials are 100 ms and 40 mV. Reproduced from reference [7].

notch-and-dome and the loss-of-dome, are I_{Na}, $I_{Ca,L}$ and I_{to}. It is the interplay between them that determines the AP morphology. Therefore, we will discuss them in detail below. Figure 1.2 displays the membrane voltage, together with I_{Na}, $I_{Ca,L}$ and I_{to} during a notch-and-dome and loss-of-dome AP morphologies.

1.2.2 The sodium current

I_{Na} is the voltage-gated Na^+ (Nav) encoded current. Upon membrane depolarization, it opens instantly, facilitating phase 0 of the AP in mammalian ventricular myocytes. Nav channels in different types of cardiac cells have similar properties [14]. Nav channel activation has a negative threshold of approximately -55 mV, and the activation and inactivation of these channels is voltage dependent [14].

1.2.3 L-type calcium current

There are two types of voltage-gated Ca^{2+} (Cav) currents. They are named high voltage-activated (HVA) and low voltage-activated (LVA) Cav channels. LVA Cav channels, also called T-type Ca^{2+} channels. These channels have a relatively hyperpolarized activation threshold of approximately -50 mV, and their activation and inactivation time constants are small. HVA Cav channels' activation threshold is approximately -20 mV, and their inactivation time is less than 100 ms. Multiple types of HVA channels exist. However, in the mammalian heart, there seems to be a universal expression of L-type HVA Cav currents [14]. Additionally, similarities exist between the properties and the densities of L-type Cav channel

currents in cells isolated from different regions of the myocardium. This suggests that the molecular basis of the underlying channels is the same [14].

In response to membrane depolarization, cardiac L-type Cav channels open later than the Nav channels. The calcium influx through these channels is the base of the plateau phase of the action potential (phase 2).

1.2.4 The transient outward current

Voltage-gated K^+ (Kv) channels stand at the basis of the repolarization of the mammalian myocardium action potential. Unlike Nav and Cav channels, electrophysiological and functional cardiac Kv channels notably vary when compared with sodium and calcium voltage-gated channels [14]. Generally, two classes of repolarizing cardiac Kv currents have been identified, which are different than each other in their kinetic properties and pharmacological responses: the transient outward K^+ currents (I_{to}) and the delayed outwardly rectifying K^+ currents [14]. When the membrane depolarizes to potentials greater than ~-30 mV, the transient currents (I_{to}) activate and inactivate rapidly. In ventricular cells, I_{to} is the base of phase 1 of the AP. Although the delayed rectifier currents activate at similar membrane potentials, there are the base of phase 3 of the AP due to their different kinetics [14].

Two transient outward currents, with distinct properties, have been found - $I_{to,1}$ and $I_{to,2}$. $I_{to,1}$ is a potassium current, blocked by 4-aminopyridine (4-AP) and extracellular-calcium independent where $I_{to,2}$ is primarily a Cl^- current, not responsive to 4-AP and is calcium dependent [14]. Human and Canine $I_{to,1}$ are

composed of Kv4.3- and Kv1.4- encoded currents, which have different kinetics of recovery from inactivation [12]. The Kv4.3-encoded current showed fast recovery from inactivation while the Kv1.4 current showed slow recovery. $I_{Kv4.3}$ accounts for about 77% and 89% of $I_{to,1}$ in canine [12] and humans [15] respectively. $I_{Kv1.4}$ accounts for the remainder.

I_{to} channel density was shown to be higher in the RV than the LV [16, 17] and canine myocytes dissected from the apical and the basal regions of the left ventricular free wall showed that current amplitude was double in the apex than in the base [18].

1.2.5 Single cell model of the action potential used in this project

A mathematical model of the cardiac ventricular action potential was developed by Luo and Rudy in 1994 (LRd) [19, 20] based on a previous model from 1991 (LR1) [21]. The LRd model accounts for dynamic changes in ionic concentrations and ionic fluxes, such as calcium current through the L-type channel, the Na^+-Ca^{2+} exchanger, Ca^{2+} release and uptake by the sarcoplasmic reticulum, and more. This model is of a mammalian ventricular action potential and is based mainly on guinea pig ventricular cell experimental data. One of its significant contributions is that it provides a basis for development of models for other types of ventricular cells of different species.

The model of I_{Na} in the LRd model incorporates fast activation and inactivation processes as well as a slow process of recovery from inactivation

reported in humans [19, 21]. The formalism of these parameters is based mainly on data from chicken embryo cardiac cells and provided a rate of depolarization (~300 V/s) which is realistic. The maximum conductance of I_{Na} (G_{Na}) provides an acceptable value of I_{Na} peak that equals ~380 μA/μF [19].

The L-type calcium current ($I_{Ca,L}$) may have a fundamental role in phase-2-reentry development, as it is the predominated current in the beginning of phase 2 of the AP. The computational description of $I_{Ca,L}$ originally introduced in the LRd model was based on atrial bullfrog single cell experiments [22]. This model appeared to poorly simulate the steepness of the slope of the upstroke of phase 2 and did not accurately represent the kinetics of I_{CaL} at a temperature of 37°C [5]. Therefore, a new mathematical model of the L-type Ca current was developed by Miyoshi et al., based on whole cell recordings of guinea pig ventricular myocytes [5]. We incorporated this model into the LRd model.

As described in Chapters 2-4, we used a model of I_{to1} developed by Dumaine et al. [10]. The model is a simplified representation of $I_{to,1}$ that does not account for its different components (i.e. $I_{Kv4.3}$ and $I_{Kv4.1}$), but does capture the overall dynamics. The modeled channel is composed of 4 voltage–dependent gates, 3 activation gates and 1 inactivation gate. Comparing the Dumaine model to several experimental studies of isolated canine ventricular myocytes shows that the Dumaine I_{to} overestimates I_{to}, but not by a great amount. Specifically, depending on the experimental study, Dumaine I_{to} I-V relationship was either less than 2-fold [23-25] or about 3-fold [16] larger than canine experimental data when corrected to RV/LV data. In addition, I_{to} diversity was shown experimentally to be broad [16, 23]. Specifically, I_{to} densities quantified for different individual canine

RV freewall epicardial myocytes ranged between 70% and 140% of the mean value [16].

1.3 The Brugada syndrome

The Brugada syndrome was classified as a distinct clinical entity in 1992, after which it received great attention. It was actively studied due to its high incidence and its association with sudden death in infants, children, and young adults [2]. The Brugada syndrome is defined by manifestation of ST segment elevation in the right precordial ECG leads V1-V3, located above the right ventricle, and a high incidence of sudden cardiac death in patients with apparent structurally normal hearts. However, it was shown recently that there might be a high prevalence of mild structural changes of the RV detected by cardiac MRI in Brugada patients [26]. These abnormalities include mild RV wall-motion abnormalities, outflow tract ejection fraction reduction, enlargement of the diameter and area of the inflow tract. Additionally, in many Brugada cases, in addition to the ST-segment elevation, apparent right bundle branch block is also present in the ECG [27]. It is difficult to assess the incidence rate of the Brugada syndrome because its ECG manifestation changes over time and is frequently hidden. It has been estimated that the syndrome is responsible for around 4-12% of all sudden cardiac deaths and 20% or more of sudden cardiac deaths in patients with hearts that are structurally normal [2]. Asian population incidence is high and is on the order of 0.05% [2].

1.3.1 Brugada syndrome diagnosis

Normally, the ST segment lies on the baseline. ST-segment abnormalities in the right precordial leads could be divided into three types of repolarization patterns (Figure 1.4). Type 1 is typified by a coved ST-segment elevation of 2 mm (0.2 mV) or more, followed by a negative T-wave. It is the only diagnostic of Brugada. The ECG manifestation of type 2 has a saddleback appearance with a high ST-segment elevation of 2 mm or more, followed by a trough, lying at least 1 mm above baseline, followed by either a positive or a biphasic T wave. The ECG of type 3 has either a saddleback or a coved manifestation with an ST-segment elevation of less than 1 mm. One may recognize these patterns appearing sequentially in the same patient or as a result of administration of specific drugs. If only types 2 and 3 appears during examination, it should not be a sufficient to Brugada syndrome diagnosis [2].

ST-segment elevation could be associated with benign pathophysiologic conditions as well as with malignant pathologies [2]. Distinguishing between the conditions may be difficult, particularly in cases where the ST-segment elevation is relatively small and when tests using sodium channel blockers (e.g. flecainide, pilsicainide and more) provide borderline results. For clinical diagnosis, patients undergo a continuous long-term ECG recording. A definitive diagnosis of Brugada syndrome can be achieved in the following cases [2]. First, when more than one right-precordial lead (V1-V3) manifest a Type 1 ST-segment elevation, either when sodium channel blockers were administered or not, together with at least one of the following conditions: (a) a documented ventricular fibrillation, (b) polymorphic ventricular tachycardia which terminate spontaneously, (c) a history

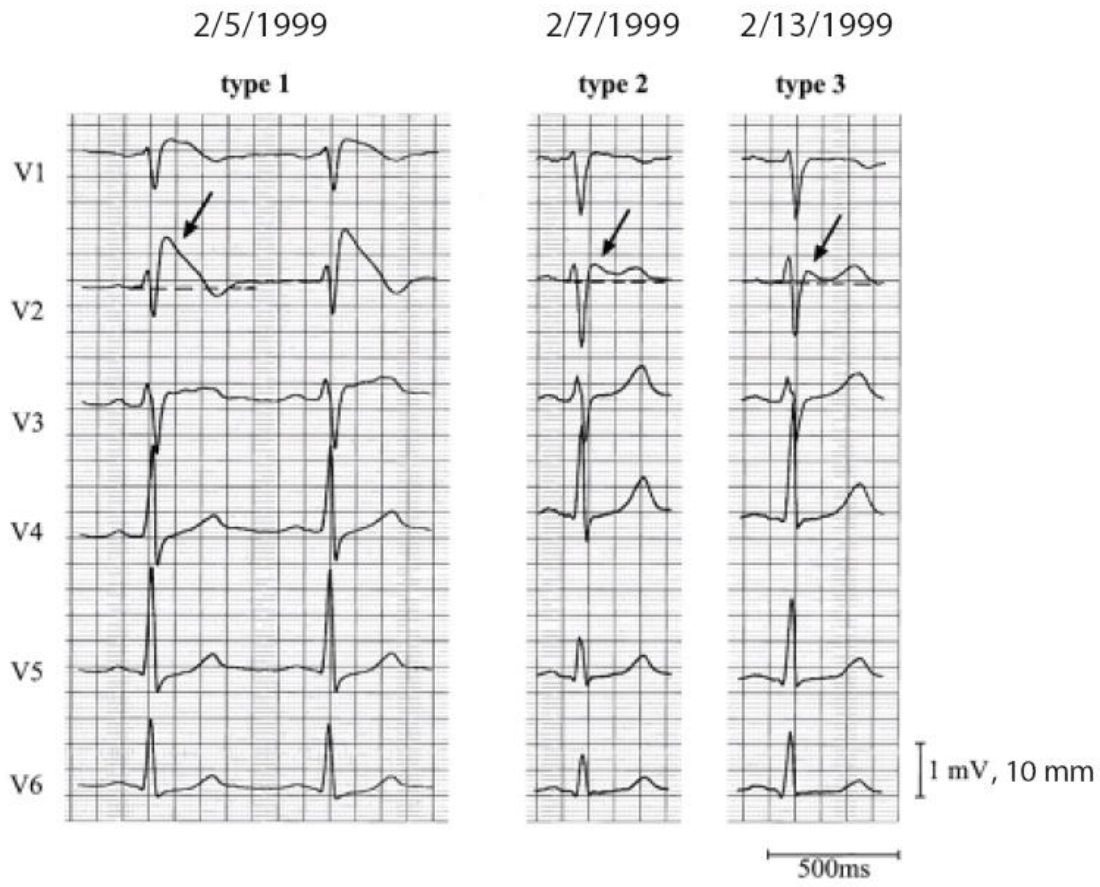

Figure 1.4: Precordial lead recordings of ECG Type 1, 2 and 3. The left panel shows a clear Type-1 ECG, which is diagnostic of the Brugada syndrome. The middle panel shows a saddleback ST segment elevation (Type 2) on 2/7/1999, two days thereafter. The right panel shows that the ST segment further normalized on 2/13/1999. Reproduced and modified from reference [8].

of sudden cardiac death (SCD) for relatives younger than 45 years, (d) coved-type ECGs in family members, (e) inducibility of ventricular tachycardia (VT) with programmed electrical stimulation, and (f) syncope. Second, when a Type 2 or Type 3 ST-segment elevation is shown in at least two right precordial leads under baseline conditions, and a diagnostic Type 1 pattern occurs post sodium-channel blocker administration. In addition, one should observe at least one of the abovementioned clinical criteria. Because the therapeutic alternatives are fairly limited (see below), diagnosis of the Brugada syndrome is done with extra caution.

1.3.2 Brugada syndrome at the cellular level

The main symptom of Brugada syndrome is ST elevation. A schematic representation of the hypothesized cellular explanation for ST-segment elevation is given in Figure 1.5. Under normal healthy conditions, the ST segment lies on the baseline (Figure 1.5.A). Under pathological conditions that cause an outward shift in the ionic balance at the end of phase-1, the I_{to}-mediated notch is accentuated in the epicardium but the morphology of the endocardial AP stays the same. This causes the inscription of the electrocardiographic J-wave (or an Osborn wave) and saddleback configuration (Figure 1.5.B). When the notch is accentuated further and the epicardial AP is prolonged, the repolarization order across the RV wall could be reversed. This manifests as a coved configuration with an inverted T wave on the ECG (Figure 1.5.C) typically observed in Brugada patients. This situation could be aggravated when the AP dome is abolished only at some epicardial sites (Figure 1.5.D), leading to phase-2 reentry (Figure 1.5.E) that could trigger ventricular tachycardia and ventricular fibrillation (VF).

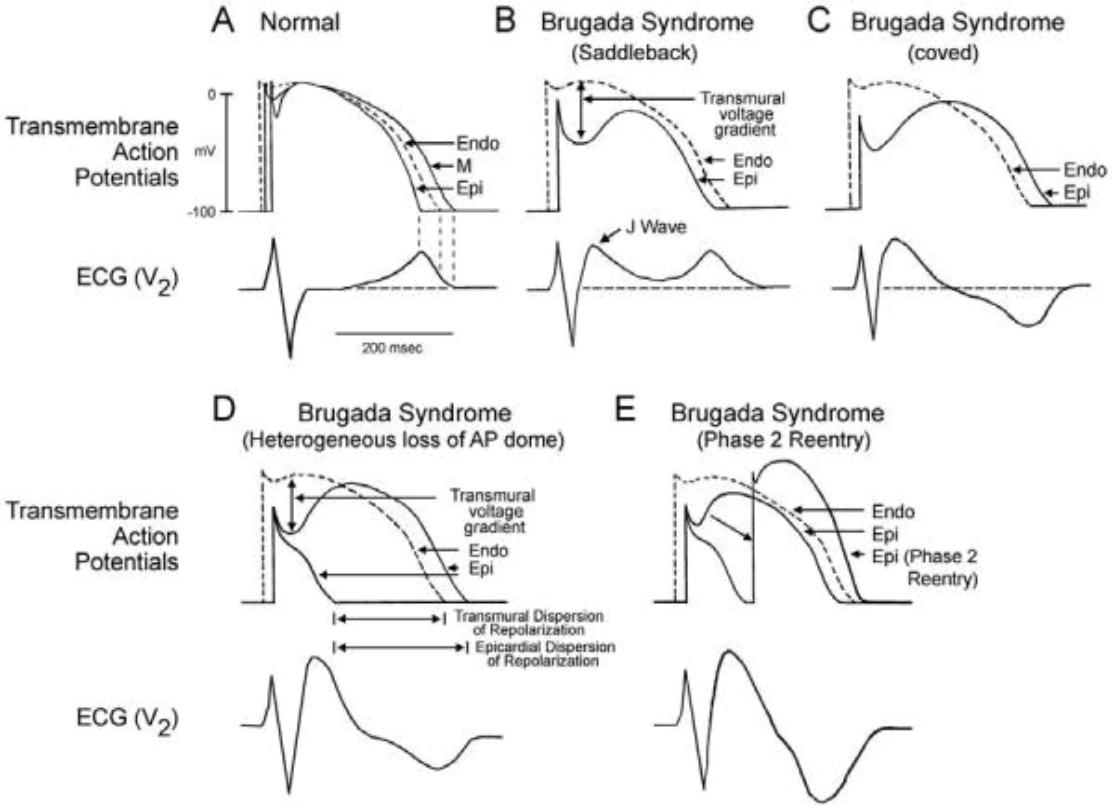

Figure 1.5: The changes in right ventricular epicardial action potential are schematically represented suggested to explain ECG manifestation of the Brugada syndrome. Reproduced from reference [2, 3].

1.3.3 Brugada syndrome genetic factors

Brugada Syndrome inheritance follows an autosomal dominant mode of transmission. SCN5A on chromosome 3, the gene encoding for the α-subunit of the cardiac sodium channel gene, was the first gene to be associated with the Brugada syndrome. Out of the approximately one hundred SCN5A mutations which were found to be linked to the syndrome (http://www.fsm.it/cardmoc/), about twenty have been studied in expression systems [2]. These demonstrated loss of function of I_{Na} due to either (1) reduced sodium channel expression; (2) voltage- and time-dependence I_{Na} activation and inactivation shift; or (3) a slower recovery from inactivation of the sodium channel. Only approximately 18-30% of Brugada syndrome patients were found to have a mutation in SCN5A. It is not yet known which of the SCN5A mutations, if any, is associated with a higher risk of arrhythmic events or SCD [2]. Yet, genetic testing could be justified for providing additional input to clinical diagnosis, for early detection (of patient's relatives at potential risk), and for studying genotype–phenotype relations.

In addition, some other mutations (e.g., in glycerol-3–phosphate dehydrogenase 1-like and SCN1B genes) have been associated with the Brugada syndrome and have been shown to result in loss of function of I_{Na} [28].

CACNA1C and CACNB2b encode the α- and β- subunits of the L-type current channel. Mutations in both of these genes are known to cause a loss of function secondary to a reduction of peak calcium current and have been associated with the Brugada syndrome [29]. In addition, a missense mutation (T11I) in CACNB2b was found to have an accelerated inactivation of L-type

calcium channel current responsible for the Brugada phenotype, while peak $I_{Ca,L}$ density was not significantly different [28].

1.3.4 Brugada mechanism

The ST-segment elevation associated with the Brugada syndrome is thought to be explained by either (1) a conduction delay within the RV wall or (2) early repolarization of the RV epicardial action potential (loss-of-dome) or both [2].

Supporting (1), a study by Petitprez et al [30] studied a Brugada mutation (C1850S) that was identified to decrease I_{Na} density and to accelerate I_{Na} inactivation. They found that the I_{to} density necessary to cause the loss-of-dome morphology was similar when modeling WT and C1850S mutant. However, the mutation slowed conduction and sometimes caused conduction blocks. Another study showed that two different Brugada mutations, Δ1479, and Δ1500, produced ST-segment elevation on the ECG only under reduced excitability conditions. Repolarization of the mutants versus WT took place at approximately the same time and therefore could not contribute much to the ST-Segment elevation manifestation. This strengthens the hypothesis that conduction delay might be the mechanism for ST-Segment elevation in Brugada patients.

A schematic illustration of (2) is depicted in Figure 1.6. A shift in the balance of ionic currents at the end of phase 1 or the beginning of phase 2 cause a loss of the AP dome at some epicardial sites. The dispersion of repolarization and refractoriness within the epicardium, as well as across the ventricular wall, provide a condition where the notch-and-dome morphology borders the loss-of-

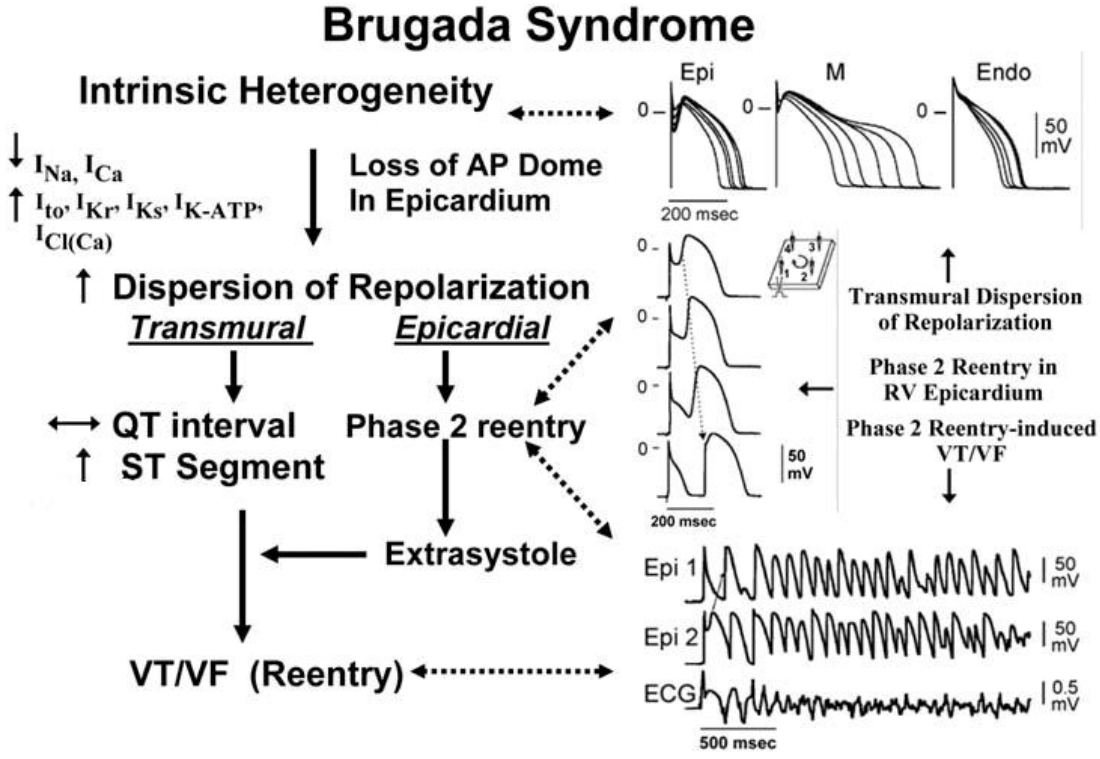

Figure 1.6: Proposed mechanism for the Brugada syndrome and its development into tachycardia (VT) or ventricular fibrillation (VF). Reproduced from reference [2].

dome morphology. This leads to the development of phase-2 reentry, which provides an ectopic beat (extrasystole) that could initiate VT/VF.

1.3.5 Therapy for the Brugada Syndrome

Brugada syndrome diagnosis has been improved impressively over the past decade. However, therapy progress has not been as remarkable [2]. Currently, the only proven therapeutic option available is an implantable cardioverter defibrillator (ICD). One study showed a 100% efficacy in stopping VF and preventing SCD [31]. However, serious complications, as unnecessary shocks initiated by the device, are still prevalent (28-36% rate) [32]. Since Brugada patients are much younger and more physically active than other ICD-implanted populations, inappropriate shocks are more common due to misclassified episodes of sinus tachycardia during physical activity. However, newer ICDs are better at sinus tachycardia classification. Another problem is that Brugada patients are also known to have more supraventricular arrhythmias, and inappropriate shocks may be introduced due to failure of the ICD to distinguish between atrial and ventricular arrhythmias [32]. Moreover, ICD treatment in children is problematic. Children are more susceptible to complications due to their smaller cardiac size, narrower vessels and also because the leads may be dislocated as the children grow [2]. Additionally, ICD cost might be unaffordable for patients residing in some regions of the world or lacking proper health insurance.

Other therapeutic options involve pharmacologic agents. One approach, is to partially block I_{to} [32]. Presently, I_{to}-specific blockers are not available for medical use. However, quinidine, which is an approved I_{Na} blocker, was proposed in 1999 as a pharmacological treatment for the disease [32]. In a small-scale study, in 22 out of 25 patients (88%), quinidine prevented VF initiation. Quinidine therapy could be a reasonable “bridge therapy” or an adjuvant treatment to ICD therapy. These data suggest that there is a strong need for a large, randomized, controlled clinical trial to assess quinidine’s effectiveness [32].

There are several alternative pharmacological treatment options for Brugada syndrome that include augmentation of early sodium or calcium currents, and/or blocking of potassium currents, all aimed to induce prolongation of the APD, hence eliminating the conditions for phase 2 reentry initiation. Of course, such approaches would introduce the possibility of drug-induced Long-QT syndrome. One example of such drugs is isoproterenol, which reduces vagal tone and therefore increases heart rate. These effects then contribute to reduction in the I_{to} current due to insufficient time for recovery from inactivation. In addition, isoproterenol increases the calcium current, contributing to the restoration of the action potential dome [33]. Another example is to use Dimethyl lithospermate B (dmLSB), which is an extract of Danshen (more details in Section 1.4.2). that cause gain of function to I_{Na} during phase 1 [34]. More invasive approaches include focal radiofrequency ablation to eradicate ventricular premature beats that trigger VT/VF. In one study [35], Brugada patients with episodes of VF or polymorphic ventricular tachycardia underwent ablation of the locations where premature beat locations were identified (peripheral right Purkinje conducting system or RVOT). Follow-up exam showed no recurrence of VF, syncope, or

sudden cardiac death in any patient. Although interesting, all these alternatives to ICD implantation treatment remain largely unexplored.

1.4 Phase-2 reentry

1.4.1 Reentry

Previously activated cardiac tissue is activated repeatedly when the activation wave, which did not subside naturally, reenters a previously excited region and reactivates it. This sets the basis for reentrant arrhythmias [36]. There are three types of reentrant arrhythmias: circus movement, reflection, and phase-2. Reflection reentry and phase-2 reentry are usually referred to as microreentry because their initiation is typically confined to small regions of tissue so it appears almost like a series of focal activity. In contrast, circus movement reentry is referred to as macroreentry and typically does not appear as focal activity. Circus movement reentry is the most common reentry [36]. Purkinje fibers having an unexcitable region showed reflection reentry [37], where the unexcited region seems to reflect back the anterograde conduction wave [37]. Circus movement reentry occurs when the activation pattern repeatedly circulates around an anatomical or functional obstacle in the heart [36].

Phase-2 reentry (P2R) is caused by conduction of electrotonic current from phase 2 of notch-and-dome AP sites to fully recovered sites of loss-of-dome APs, causing abnormal reexcitation. P2R could degenerate into ventricular fibrillation (VF) and cause sudden cardiac death [2]. P2R has been suggested to be one of

the mechanisms of malignant ventricular arrhythmias in humans who have electrical dysfunction but normal heart structure [38]. Specifically, P2R has been associated with genetic diseases such as Brugada syndrome [2, 39] and models of myocardial ischemia [40, 41]. Traditionally, susceptibility for P2R occurrence was thought to occur when the two AP morphologies, the notch-and-dome and the loss-of-dome are present in proximity. However, it was not clear what the mechanism that facilitates P2R initiation is.

1.4.2 Experimental phase-2 reentry research to date

P2R has been studied experimentally using models of Brugada syndrome and ischemia [42-44]. These models were used to cause ST-segment elevation, which is the ECG manifestation of these pathologies. One example is a study in which a novel therapeutic strategy for the Brugada syndrome was explored [34]. In this study multiple drugs were used separately. The investigators used Verapamil to block $I_{Ca,L}$, pinacidil for $I_{K\text{-}ATP}$ activation, and terfenadine to block both I_{Na} and $I_{Ca,L}$. They explored the use of dimethyl lithospermate B, which is a component extracted from Salvia miltiorrhiza (red sage) root, which selectively increases sodium current. A previous study [45] showed that dmLSB slowed I_{Na} inactivation, without changing persistent late I_{Na}. They hypothesized that loss of the epicardial AP dome will be prevented by this action of dmLSB, thus blocking development of phase-2 reentry and VT/VF in the Brugada syndrome. Each drug agent was used separately and induced a deeper epicardial AP notch, causing a more pronounced J wave, which is a positive ECG deflection between the QRS complex and the ST-segment. Drugs generated both local epicardial and transmural (between the shortest epicardial response and that of endocardium)

dispersion of repolarization, secondary to heterogeneous loss of the epicardial AP dome. Phase 2 reentry occurred in all models. Polymorphic VT occurred in 6 of 9 wedge preparations. In all preparations, Phase-2 reentry and all arrhythmic activity was eliminated once dmLSB (10 μmol/L) was added, suggesting that dmLSB is effective in eliminating ST-segment elevation, and warrants further study as a pharmacological therapy for Brugada patients.

Another study [44] used high-resolution optical mapping techniques in arterially perfused canine right ventricular wedges, comparing baseline to Brugada-ECG preparations made by terfenadine, pinacidil, and pilsicainide (I_{Na} blocker) [44]. P2R was displayed in 9 out of 10 of the preparations. The maximum gradient of repolarization region in the epicardium gave rise to 80% of P2R episodes, leading to polymorphic ventricular tachycardia or VF. The investigators found that a steep epicardial repolarization gradient triggered P2R extrasystoles in the Brugada-ECG condition, while the endocardium was not arythmogenic. These extrasystoles sometimes led to VF, in the presence of further depolarization and repolarization abnormalities.

Other studies used similar models of the Brugada syndrome [43, 46]. However, the purpose of the application of these drugs is to create a deliberate imbalance of ionic currents such that the outward current would overwhelm the inward currents in some areas of the tissue, resulting in ST-segment elevation, the ECG manifestation of Brugada. Therefore, the physiological relevance of those studies to pathological development of phase-2 reentry is unclear.

As discussed above, many mutations in the SCN5A gene, which encodes the sodium channel, have been reported [47], accounting for 18-30% of Brugada cases [2]. In addition, mutations in the L-type calcium channel have also been associated with the Brugada syndrome. However, the drug-based Brugada models were designed to simulate the Brugada phenotype and ECG manifestation, not the genotype. Therefore it is possible that arrhythmias in general, and particularly phase-2 reentry, may develop in these models without being representative of the actual pathological occurrence of P2R in patients.

1.4.3 P2R computational modeling research

In addition to experimental investigations of P2R, computational research has been performed to investigate the underlying mechanism of P2R; i.e., to isolate key factors that may contribute to P2R initiation.

Two such computational studies of P2R development, in epicardial one-dimensional cables, have been carried out by Miyoshi et al. [5, 48]. As mentioned above (in Section 1.2.5), they developed a new and more accurate mathematical model of the L-type calcium current and incorporated it into a modified Luo-Rudy model [5]. They simulated one-dimensional cables consisting of two distinct regions, each with a different level of G_{to} (the macroscopic conductance of I_{to}); i.e., the cables they studied had a discontinuity in G_{to}. P2R occurred for some G_{to} values [5]. In addition, they manipulated I_{Na} kinetics to identify what type of simulated mutation could be more arrhythmogenic and found that a reduced I_{Na} inactivation time constant, together with conduction disturbance, may cause P2R [48].

In another P2R computational study, the investigators analyzed how variations in I_{Na} inactivation and variations in G_{to} influence the probability of phase-2-reentry in epicardial tissue [49]. They used the Luo–Rudy model and introduced spatial dispersion in repolarization by splitting the fiber into discrete zones with different strength of I_{to}, as done previously by Miyoshi et al. [5, 48]. They found that even when decreasing I_{Na} inactivation time (i.e. faster inactivation), the percentage of reexcitations was not always increased monotonically. Instead, it created vulnerable windows, where reexcitation did not occur. Moreover, once L-type calcium current was augmented above a certain value, reexcitation disappeared. In addition, they stimulated two-dimensional epicardial tissue with increased I_{Na} inactivation and I_{to} heterogeneity, and showed the formation of reentry. They concluded that while I_{to} dispersion facilitates phase-2 reentry initiation, once sodium inactivation dynamics is altered, the probability of reexcitation changes inconsistently.

To summarize, three computational studies of P2R have been published (that we are aware of). All of them divided the cables/tissue into two regions that had two different distinct values of G_{to}. It is important to note that because there is no evidence of discontinuities in ion-channel expression in the RV and because discontinuities tend to cause rich dynamical results, the physiological relevance of those simulations and the degree to which their findings apply to P2R development is unclear. Therefore, in our studies of the epicardium (Chapters 2 and 4), G_{to} was varied in a continuous manner. We believe that this method is more realistic and therefore is likely to provide a better understanding of the mechanism of P2R development.

1.5 The ventricular wall

One of the important characteristics of the ventricular wall is its inherent electrophysiological heterogeneity. The ventricular wall is thought to be comprised of three distinct layers: the epicardium on the external surface of the heart, the midmyocardium, and the endocardium on the internal side (Figure 1.7). These layers have been found in dogs [50], humans [51] and guinea pigs [4]. Myocytes from each layer exhibit different action potential morphologies (Figure 1.8).

Epicardial and midmyocardial (M) action potentials possess a prominent notch, responsible for the notch-and-dome morphology, whereas the endocardial action potential has no notch [9]. The M-cells display the longest action potential duration (APD) relative to epicardial and endocardial ventricular cells [23, 52]. These cells also show greater sensitivity to interventions that prolong APD [9]. Changes in protein expression levels and/or electrophysiological function has been shown for the transient outward current [10, 53, 54], the late sodium current [55], and the slow components of the delayed rectifier current [9, 52, 56].

The delayed rectifier potassium current has two components, I_{Kr} (rapid) and I_{Ks} (slow), which play a central role in AP repolarization and therefore determine its duration. The transmural AP heterogeneity in repolarization and APD has been linked to heterogeneity in the relative densities of I_{Kr} and I_{Ks} [9]. I_{Kr} was not significantly different among isolated myocytes from the epicardium, midmyocardium and endocardium. In contrast, I_{Ks} level was significantly smaller in midmyocardial cells than in epicardial or endocardial cells. In addition, they demonstrated that the total current, consisting of the sum of I_{Kr} and I_{Ks}, was also

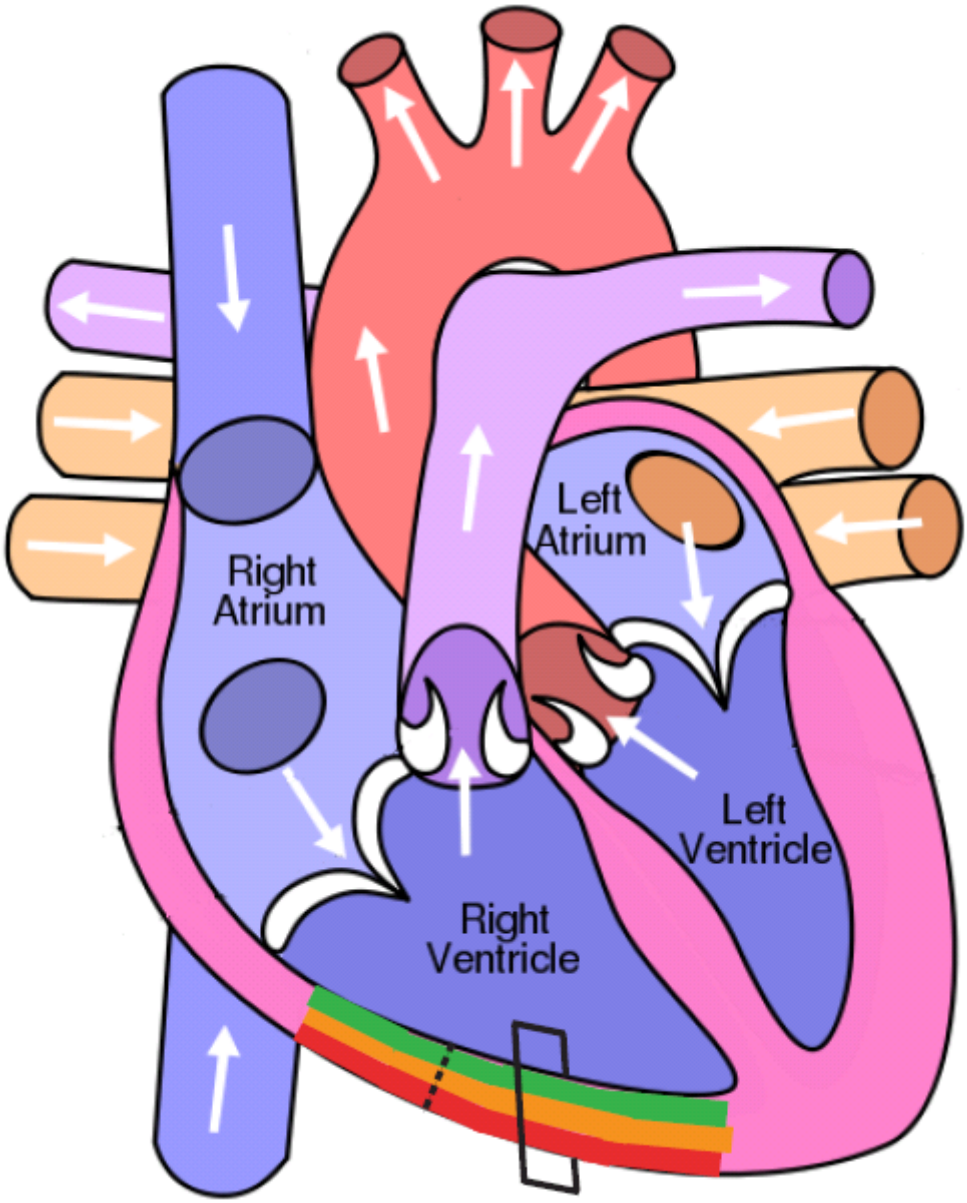

Figure 1.7: Diagram of the modeling orientations investigated in this study. Red, orange and green colors represent the RV epicardium (Research question 1; Section 1.6) midmyocardium and endocardial, respectively. Dashed line represents one-dimensional transmural cable (Research question 2; Section 1.6). Parallelogram represents two-dimensional transmural slice (Research question 3; Section 1.6). Reproduced and modified from reference [1] .

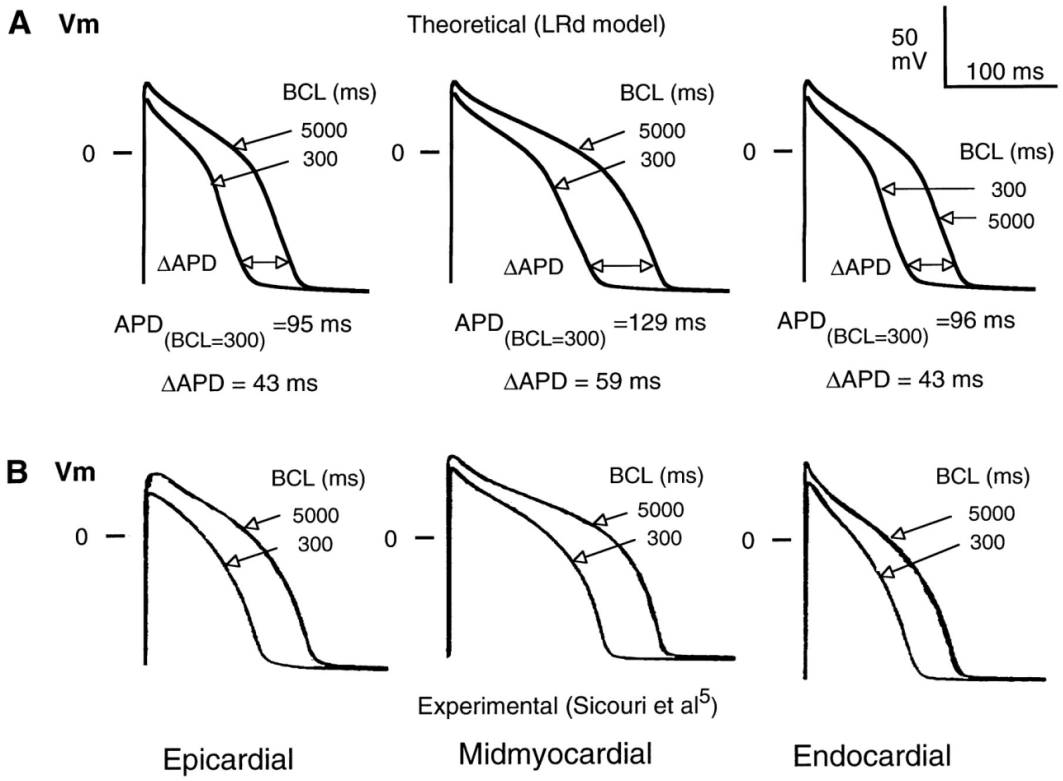

Figure 1.8: Action potentials at fast and slow pacing rates for different cell types (epicardial, midmyocardial and endocardial). **A:** Simulated cells using the LRd model incorporating difference levels of I_{Ks} density. **B:** experimentally recorded guinea pig APs from reference [4]. Reproduced from reference [9].

significantly greater in epicardial and endocardial myocytes than in cells from the M region [52].

The delayed rectifier potassium current has two components, I_{Kr} (rapid) and I_{Ks} (slow), which play a central role in AP repolarization and therefore determine its duration. The transmural AP heterogeneity in repolarization and APD has been linked to heterogeneity in the relative densities of I_{Kr} and I_{Ks} [9]. I_{Kr} was not significantly different among isolated myocytes from the epicardium, midmyocardium and endocardium. In contrast, I_{Ks} level was significantly smaller in midmyocardial cells than in epicardial or endocardial cells. In addition, they demonstrated that the total current, consisting of the sum of I_{Kr} and I_{Ks}, was also significantly greater in epicardial and endocardial myocytes than in cells from the M region [52].

In another study, human right ventricle myocytes were isolated from separated tissue of the subepicardium, midmyocardium and subendocardium of a replaced heart, during transplantation. Study of the transient outward current showed that I_{to} from subepicardial and midmyocardial origin was significantly greater than endocardial I_{to} [53].

Modeling the different-layer APs is usually based on such transmural differences. Figure 1.8 shows an example for such modeling using the LRd model, incorporating only I_{Kr}:I_{Ks} density difference (guinea pigs myocytes have no transient outward current). Compared with experimental data from left ventricular free wall guinea pig myocytes, the model produced similar APs in the different basic cycle lengths (BCL) presented in Figure 1.8.

The distribution and location of M-cells within the ventricular wall is controversial. Several studies showed prolonged action potentials for midmyocardial cells, as discussed before. However, a comprehensive study [57] reported that M-cell prolongation was not shown in three different settings: in-vivo data from patients undergoing coronary artery surgery [57, 58] and wedge preparations and Langendorff-perfused explanted human hearts [57]. The absence of AP prolongation in the midmyocardial area might be due to intercellular coupling smoothing the prolonged midmyocardial APD [57] or the possibility that M-cells may exist as circular islands embedded in the ventricular wall rather than being uniformly distributed within the midmyocardium [59].

The AP heterogeneity across the ventricular wall described above is the basis for our investigations of P2R development in the transmural direction (Chapters 3 and 4).

1.6 Thesis research questions

As discussed above, Phase-2 reentry occurs by conduction of electrotonic current from phase 2 of notch-and-dome action potential regions to fully recovered regions, causing abnormal reexcitation. It is generally thought that the existence of neighboring sites exhibiting the two different AP morphologies, the notch-and-dome and the loss-of-dome, is sufficient for local reexcitation and P2R development. However, this has not been demonstrated definitively. Furthermore,

the conditions that underlie phase-2 reentry initiation and the phase-2 reentry substrate are not clear. Therefore, we believe that a systematic study of P2R mechanism is needed.

Research question 1 (chapter 2): What is the mechanism of epicardial P2R? Could phase-2 reentry develop in epicardial tissue having no discontinuous ionic heterogeneity? Specifically,

a. Can P2R develop in one-dimensional cables having continuous gradients of ionic currents?
b. Can P2R develop in homogeneous one-dimensional cables?
c. What is the cellular mechanism that underlies phase-2 reentry initiation?
d. What is the mechanism for phase-2 reentry initiation in one-dimensional epicardial cables?

Research question 2 (chapter 3): What is the mechanism of transmural P2R? Could phase-2 reentry develop transmurally due to transmural changes in action potential morphology between the different layers that construct the ventricular wall? Specifically,

a. Could the prolonged midmyocardial AP neighboring the shorter epicardial AP be arrhythmogenic under certain conditions?
b. What is the degree of arrhythmogeneity provided by transmural differences compared to the epicardial arrhythmogeneity investigated in Chapter 2?

Research question 3 (chapter 4): What is the mechanism of transmural P2R in the context of epicardial heterogeneity? Specifically,

a. Is local development of P2R arrhythmogenic enough to expand to distant areas and reexcite previously excited regions?
b. Could sustained reentry result across the transmural wall due to P2R development?

REFERENCES

1. *Diagram of the human heart*, W. contributors, Editor. 2010, Wikipedia, The Free Encyclopedia.
2. Antzelevitch, C., et al., *Brugada syndrome: from cell to bedside.* Curr Probl Cardiol, 2005. **30**(1): p. 9-54.
3. contributors, W., *Diagram of the human heart*, W. contributors, Editor. 2010, Wikipedia, The Free Encyclopedia.
4. Sicouri, S., M. Quist, and C. Antzelevitch, *Evidence for the presence of M cells in the guinea pig ventricle.* J Cardiovasc Electrophysiol, 1996. **7**(6): p. 503-11.
5. Miyoshi, S., et al., *A mathematical model of phase 2 reentry: role of L-type Ca current.* Am J Physiol Heart Circ Physiol, 2003. **284**(4): p. H1285-94.
6. Robbins, J. and G.W. Dorn, 2nd, *Listening for hoof beats in heart beats.* Nat Med, 2000. **6**(9): p. 968-70.
7. Sun, X. and H.S. Wang, *Role of the transient outward current (Ito) in shaping canine ventricular action potential--a dynamic clamp study.* J Physiol, 2005. **564**(Pt 2): p. 411-9.
8. Wilde, A.A., et al., *Proposed diagnostic criteria for the Brugada syndrome: consensus report.* Circulation, 2002. **106**(19): p. 2514-9.
9. Viswanathan, P.C., R.M. Shaw, and Y. Rudy, *Effects of IKr and IKs heterogeneity on action potential duration and its rate dependence: a simulation study.* Circulation, 1999. **99**(18): p. 2466-74.
10. Dumaine, R., et al., *Ionic mechanisms responsible for the electrocardiographic phenotype of the Brugada syndrome are temperature dependent.* Circ Res, 1999. **85**(9): p. 803-9.

11. Miura, T., et al., *Protective role of gap junctions in preconditioning against myocardial infarction.* Am J Physiol Heart Circ Physiol, 2004. **286**(1): p. H214-21.

12. Greenstein, J.L., et al., *Role of the calcium-independent transient outward current I(to1) in shaping action potential morphology and duration.* Circ Res, 2000. **87**(11): p. 1026-33.

13. Winslow, R.L., et al., *Mechanisms of altered excitation-contraction coupling in canine tachycardia-induced heart failure, II: model studies.* Circ Res, 1999. **84**(5): p. 571-86.

14. Nerbonne, J.M. and R.S. Kass, *Molecular physiology of cardiac repolarization.* Physiol Rev, 2005. **85**(4): p. 1205-53.

15. Iyer, V., R. Mazhari, and R.L. Winslow, *A computational model of the human left-ventricular epicardial myocyte.* Biophys J, 2004. **87**(3): p. 1507-25.

16. Di Diego, J.M., Z.Q. Sun, and C. Antzelevitch, *I(to) and action potential notch are smaller in left vs. right canine ventricular epicardium.* Am J Physiol, 1996. **271**(2 Pt 2): p. H548-61.

17. Volders, P.G., et al., *Repolarizing K+ currents ITO1 and IKs are larger in right than left canine ventricular midmyocardium.* Circulation, 1999. **99**(2): p. 206-10.

18. Szentadrassy, N., et al., *Apico-basal inhomogeneity in distribution of ion channels in canine and human ventricular myocardium.* Cardiovasc Res, 2005. **65**(4): p. 851-60.

19. Luo, C.H. and Y. Rudy, *A dynamic model of the cardiac ventricular action potential. I. Simulations of ionic currents and concentration changes.* Circ Res, 1994. **74**(6): p. 1071-96.

20. Luo, C.H. and Y. Rudy, *A dynamic model of the cardiac ventricular action potential. II. Afterdepolarizations, triggered activity, and potentiation.* Circ Res, 1994. **74**(6): p. 1097-113.

21. Luo, C.H. and Y. Rudy, *A model of the ventricular cardiac action potential. Depolarization, repolarization, and their interaction.* Circ Res, 1991. **68**(6): p. 1501-26.

22. Rasmusson, R.L., et al., *A mathematical model of electrophysiological activity in a bullfrog atrial cell.* Am J Physiol, 1990. **259**(2 Pt 2): p. H370-89.

23. Liu, D.W., G.A. Gintant, and C. Antzelevitch, *Ionic bases for electrophysiological distinctions among epicardial, midmyocardial, and endocardial myocytes from the free wall of the canine left ventricle.* Circ Res, 1993. **72**(3): p. 671-87.

24. Di Diego, J.M., et al., *Ionic and cellular basis for the predominance of the Brugada syndrome phenotype in males.* Circulation, 2002. **106**(15): p. 2004-11.

25. Calloe, K., et al., *A transient outward potassium current activator recapitulates the electrocardiographic manifestations of Brugada syndrome*. Cardiovasc Res, 2009. **81**(4): p. 686-94.

26. Catalano, O., et al., *Magnetic resonance investigations in Brugada syndrome reveal unexpectedly high rate of structural abnormalities.* Eur Heart J, 2009. **30**(18): p. 2241-8.

27. Zipes, D. and J. Jalife, *Cardiac Electrophysiology: From Cell to Bedside*. Third ed. 1999: Saunders.

28. Cordeiro, J.M., et al., *Accelerated inactivation of the L-type calcium current due to a mutation in CACNB2b underlies Brugada syndrome.* J Mol Cell Cardiol, 2009. **46**(5): p. 695-703.

29. Antzelevitch, C., et al., *Loss-of-function mutations in the cardiac calcium channel underlie a new clinical entity characterized by ST-segment elevation, short QT intervals, and sudden cardiac death.* Circulation, 2007. **115**(4): p. 442-9.

30. Petitprez, S., et al., *Analyses of a novel SCN5A mutation (C1850S): conduction vs. repolarization disorder hypotheses in the Brugada syndrome.* Cardiovasc Res, 2008. **78**(3): p. 494-504.

31. Brugada, J., R. Brugada, and P. Brugada, *Determinants of sudden cardiac death in individuals with the electrocardiographic pattern of Brugada syndrome and no previous cardiac arrest.* Circulation, 2003. **108**(25): p. 3092-6.

32. Antzelevitch, C. and E. Nof, *Brugada syndrome: recent advances and controversies.* Curr Cardiol Rep, 2008. **10**(5): p. 376-83.

33. Marquez, M.F., et al., *Ionic basis of pharmacological therapy in Brugada syndrome.* J Cardiovasc Electrophysiol, 2007. **18**(2): p. 234-40.

34. Fish, J.M., et al., *Dimethyl lithospermate B, an extract of Danshen, suppresses arrhythmogenesis associated with the Brugada syndrome.* Circulation, 2006. **113**(11): p. 1393-400.

35. Haissaguerre, M., et al., *Mapping and ablation of ventricular fibrillation associated with long-QT and Brugada syndromes.* Circulation, 2003. **108**(8): p. 925-8.

36. Jordan, P.N. and D.J. Christini, *Therapies for ventricular cardiac arrhythmias.* Crit Rev Biomed Eng, 2005. **33**(6): p. 557-604.

37. Antzelevitch, C., *Clinical application of new concepts of parasystole, reflection, and tachycardia.* Cardiol Clin, 1983. **1**(1): p. 39-50.

38. Brugada, P. and J. Brugada, *Right bundle branch block, persistent ST segment elevation and sudden cardiac death: a distinct clinical and electrocardiographic syndrome. A multicenter report.* J Am Coll Cardiol, 1992. **20**(6): p. 1391-6.

39. Antzelevitch, C. and G.X. Yan, *Cellular and ionic mechanisms responsible for the Brugada syndrome.* J Electrocardiol, 2000. **33 Suppl**: p. 33-9.

40. Lukas, A. and C. Antzelevitch, *Phase 2 reentry as a mechanism of initiation of circus movement reentry in canine epicardium exposed to simulated ischemia.* Cardiovasc Res, 1996. **32**(3): p. 593-603.

41. Di Diego, J.M., J.M. Fish, and C. Antzelevitch, *Brugada syndrome and ischemia-induced ST-segment elevation. Similarities and differences.* J Electrocardiol, 2005. **38**(4 Suppl): p. 14-7.

42. Fish, J.M. and C. Antzelevitch, *Cellular mechanism and arrhythmogenic potential of T-wave alternans in the Brugada syndrome.* J Cardiovasc Electrophysiol, 2008. **19**(3): p. 301-8.

43. Kimura, M., et al., *Mechanism of ST elevation and ventricular arrhythmias in an experimental Brugada syndrome model.* Circulation, 2004. **109**(1): p. 125-31.

44. Aiba, T., et al., *Cellular basis for trigger and maintenance of ventricular fibrillation in the Brugada syndrome model: high-resolution optical mapping study.* J Am Coll Cardiol, 2006. **47**(10): p. 2074-85.

45. Yoon, J.Y., et al., *A novel Na+ channel agonist, dimethyl lithospermate B, slows Na+ current inactivation and increases action potential duration in isolated rat ventricular myocytes.* Br J Pharmacol, 2004. **143**(6): p. 765-73.

46. Fish, J.M. and C. Antzelevitch, *Role of sodium and calcium channel block in unmasking the Brugada syndrome.* Heart Rhythm, 2004. **1**(2): p. 210-7.

47. Zimmer, T. and R. Surber, *SCN5A channelopathies--an update on mutations and mechanisms.* Prog Biophys Mol Biol, 2008. **98**(2-3): p. 120-36.

48. Miyoshi, S., et al., *Link between SCN5A mutation and the Brugada syndrome ECG phenotype: simulation study.* Circ J, 2005. **69**(5): p. 567-75.

49. Cantalapiedra, I.R., et al., *Reexcitation mechanisms in epicardial tissue: role of I(to) density heterogeneities and I(Na) inactivation kinetics.* J Theor Biol, 2009. **259**(4): p. 850-9.

50. Sicouri, S. and C. Antzelevitch, *A subpopulation of cells with unique electrophysiological properties in the deep subepicardium of the canine ventricle. The M cell.* Circ Res, 1991. **68**(6): p. 1729-41.

51. Drouin, E., et al., *Electrophysiologic characteristics of cells spanning the left ventricular wall of human heart: evidence for presence of M cells.* J Am Coll Cardiol, 1995. **26**(1): p. 185-92.

52. Liu, D.W. and C. Antzelevitch, *Characteristics of the delayed rectifier current (IKr and IKs) in canine ventricular epicardial, midmyocardial, and endocardial myocytes. A weaker IKs contributes to the longer action potential of the M cell.* Circ Res, 1995. **76**(3): p. 351-65.

53. Li, G.R., et al., *Transmural heterogeneity of action potentials and Ito1 in myocytes isolated from the human right ventricle.* Am J Physiol, 1998. **275**(2 Pt 2): p. H369-77.

54. Wettwer, E., et al., *Transient outward current in human ventricular myocytes of subepicardial and subendocardial origin.* Circ Res, 1994. **75**(3): p. 473-82.

55. Zygmunt, A.C., et al., *Larger late sodium conductance in M cells contributes to electrical heterogeneity in canine ventricle.* Am J Physiol Heart Circ Physiol, 2001. **281**(2): p. H689-97.

56. Viswanathan, P.C. and Y. Rudy, *Cellular arrhythmogenic effects of congenital and acquired long-QT syndrome in the heterogeneous myocardium.* Circulation, 2000. **101**(10): p. 1192-8.

57. Conrath, C.E., et al., *Intercellular coupling through gap junctions masks M cells in the human heart.* Cardiovasc Res, 2004. **62**(2): p. 407-14.

58. Taggart, P., et al., *Transmural repolarisation in the left ventricle in humans during normoxia and ischaemia.* Cardiovasc Res, 2001. **50**(3): p. 454-62.

59. Akar, F.G., et al., *Unique topographical distribution of M cells underlies reentrant mechanism of torsade de pointes in the long-QT syndrome.* Circulation, 2002. **105**(10): p. 1247-53.

CHAPTER 2

INSTABILITY IN ACTION POTENTIAL MORPHOLOGY UNDERLIES PHASE 2 REENTRY: A MATHEMATICAL MODELING STUDY*

2.1 Abstract

BACKGROUND Phase-2 reentry (P2R) occurs when electrotonic current propagates from sites of normal notch-and-dome action potentials (AP) to loss-of-dome abbreviated AP sites, causing abnormal reexcitation. It is thought that the existence of two neighboring regions exhibiting these two different AP morphologies is sufficient for local re-excitation and P2R development.

OBJECTIVE The purpose of this study was to investigate the mechanism of P2R development in simulated epicardial tissues having no gradient or continuous gradients of ionic currents that affect phase 2.

METHODS Single-cell simulations of Luo-Rudy dynamic model cells were performed. To simulate epicardial ionic heterogeneity, the outward current that predominates phase-1, I_{to}, was perturbed using changes in its macroscopic conductance (G_{to}). In addition, one-dimensional fiber simulations were used to investigate the spatiotemporal phenomenon of P2R.

* Modified and reproduced from Maoz, A., T. Krogh-Madsen, and D.J. Christini, *Instability in action potential morphology underlies phase 2 reentry: a mathematical modeling study.* Heart Rhythm, 2009. **6**(6): p. 813-22.

RESULTS In single-cell simulations, at the end of phase 1 of the AP, when the inward current overwhelmed the outward current (low to normal G_{to} values), notch-and-dome action potentials were produced. When the outward current overwhelmed the inward current (high G_{to} values), abbreviated loss-of-dome action potentials were produced. However, intermediate values of G_{to} caused cells to switch intermittently between the two morphologies during constant pacing. P2R occurred in homogeneous and heterogeneous cable simulations, but only when a mass of cells manifested the unstable "switching" behavior.

CONCLUSION It appears that a main factor underlying P2R is not the presence of two different stable morphologies in adjacent regions, but rather unstable switching AP morphology within a significant subset of cells.

2.2 Introduction

Epicardial myocytes typically have a notch-and-dome action-potential (AP) morphology with a large phase-1 notch and a domed phase 2. Under certain conditions, regions of cells undergo dramatic action potential shortening due to loss of the dome phase. If such regions border normal, non-abbreviated regions, a potentially arrhythmogenic substrate is formed. In such a substrate, electrotonic current propagates from depolarized regions undergoing dome phase into repolarized loss-of-dome regions. This may lead to the improper reactivation of loss-of-dome sites, known as phase-2 reentry (P2R) [2, 3]. If sufficiently large and ill-timed, the secondary activation associated with P2R may initiate ventricular fibrillation and cause sudden cardiac death [2, 4]. Indeed, P2R has been

proposed as a mechanism for triggering lethal arrhythmias in individuals with structurally normal hearts who have electrical dysfunction. In particular, P2R has been suggested to underlie arrhythmogenesis in two main disease categories: genetic diseases such as the Brugada syndrome [2, 4] and myocardial ischemia [3].

At the cellular level, the formation of the dome phase (phase 2) is determined by the balance of membrane currents that play a role at the end of the rapid repolarization phase (phase 1), mainly the transient outward current (I_{to}) and the sodium current (I_{Na}), and the current that dominates the beginning of the dome phase, the L-type calcium current ($I_{Ca,L}$) [2-5]. Failure of the dome to develop occurs when the outward current I_{to} overwhelms the inward currents I_{Na} and $I_{Ca,L}$, resulting in a marked abbreviation of the AP. Hence, loss of the dome phase is facilitated by an increase in I_{to} or a decrease in $I_{Ca,L}$ or I_{Na}. Indeed, experimental evidence shows a correlation between increased I_{to} density and the prominence of phase-1 notch in canine epicardial cells [6, 7] and in guinea pig cardiomyocytes fused with cells expressing I_{to} [8]. In a dynamic-clamp study, introduction of a virtual I_{to} into isolated endocardial canine myocytes (having low intrinsic I_{to}) revealed a threshold effect of action potential duration (APD) on I_{to} amplitude: small levels of I_{to} produced a spike-and-dome morphology, whereas large levels produced loss-of-dome [6].

In tissue, the leading hypothesis for the development of P2R in the epicardial direction (Figure 1.7, epicardium), is the presence of intrinsic heterogeneity in ionic channel density, which facilitates the loss of the AP dome in some regions but not others [3, 9, 10]. This hypothesis has been tested using

heterogeneity in I_{to} channel density in previous simulation studies [11, 12]. In these studies, the simulated tissue was divided into two distinct regions, each with a discrete level of G_{to} (the macroscopic conductance of I_{to}). However, the physiological relevance of those simulations and the degree to which their findings apply to epicardial P2R development in the right ventricle (RV) is unclear given that there is no evidence of discontinuities in ion-channel expression in the RV epicardium. In addition, relative to the smoothing that occurs with a continuous transition region, such a discontinuity exaggerates the P2R-causing electrotonic current between distinct regions. Thus P2R may be more likely in the presence of such artificial discontinuities.

Thus, here we investigate the mechanism of P2R development in simulated tissue with continuous (including zero) gradients in ion-channel expression along the epicardial direction (Figure 1.7, epicardium). In real tissue, these heterogeneities might include perturbations in I_{to}, $I_{Ca,L}$ and I_{Na} channel density. In this study, we investigated variation in G_{to}, as it has been suggested that gradients of G_{to} exist in the RV epicardium [3, 13, 14] and because the RV is a prime suspect for P2R occurrence [2, 4, 10, 15, 16]. That being said, we believe that the dynamics we observe may stem from the dynamics of any of the ionic currents affecting the notch and/or dome. In contrast to the prevailing hypothesis, our study suggests that two neighboring regions exhibiting the two different AP morphologies (notch-and-dome versus loss-of-dome) is not sufficient for P2R development. Rather, we found that instability of the AP dome when I_{to} is near the loss-of-dome threshold plays a critical role.

2.3 Methods

2.3.1 Computational Model and Methods

We used the Luo-Rudy dynamic (LRd) [17] with the L-type Ca^{2+} current formalism developed by Miyoshi et al.[11] and the transient outward current (I_{to}) formalism developed by Dumaine et al [18]. For cable simulations, a variety of G_{to} gradients were applied along the cable, all of which were continuous and within plausible physiological range. Simulated cables were composed of 300 grid points representing 3 cm RV epicardial fibers. Square-wave stimuli (200 mA, 0.5 ms duration, basic cycle length (BCL) of 1000 ms) were applied to the first 5 cells. To minimize model transients, we ran single-cell simulations for each G_{to} value for 311 beats (i.e., 311 s), saved all system variables (gating variables, concentrations and transmembrane potential) and used those as initial conditions for the corresponding cable simulations. Each cable simulation ran for 17 beats. The forward Euler method with a time step of Δt=0.005 ms was used to integrate dV/dt, while the gating variables were computed from their analytic expressions [19]. For the fiber simulations, a space step of Δx=0.01 cm was used, with a diffusion coefficient of D=0.0007 cm^2/ms, resulting in conduction velocity ~50 cm/s. CV was computed at all locations along the cable from the upstroke occurrence times (crossing of -65 mV) at points separated by five grid points.

2.3.2 G_{to} values

While there is some evidence of heterogeneity in I_{to} expression in the RV, [3, 13, 14] the precise apical-basal gradient of I_{to} along the epicardial RV is not known.

However, in the canine left ventricle (LV), I_{to} current density in the apex is twice as large as in the base, consistent with the finding of a shorter APD in the apex [20]. Additionally, average peak I_{to} density is significantly greater (155% in one study [21], 220% in another [18]) in the canine RV epicardium than in the LV epicardium, correlating with a deeper phase-1 notch in the RV [7]. These higher levels of I_{to} make the RV much more vulnerable than the LV to loss-of-dome, which could lead to dispersion of APD and P2R.

The nominal value in the Dumaine model for G_{to} of 0.5 mS/µF is for the LV [18]. We used 1.1 mS/µF for the RV which is 220% of 0.5 mS/µF. To construct a plausible G_{to} gradient along the RV, we used G_{to} values up to 2.2 mS/µF, which is based on the 1:2 gradient found along the LV epicardium [20]. We expanded the range to extreme values and explored the range of 0.0 to 2.4 mS/µF.

2.3.3 G_{to} Gradients

Several sets of simulations having various G_{to} gradients were applied to the cable. As the in situ G_{to} gradient is unknown, and likely varies among individuals and species, various gradients were chosen to provide insight into plausible substrates for P2R and to help rule out the possibility that our findings would be specific to a certain type of gradient. Hence, to investigate the dependence of P2R on the underlying heterogeneity, we used linear gradients, piece-wise linear gradients, and Boltzmann function gradients. The Boltzmann gradient function was:

$$G_{to}(x) = \frac{G_{to,proximal} - G_{to,distal}}{1 + e^{(x - x_{1/2})/s}} + G_{to,distal} \qquad \text{(Eq. 2.1)}$$

where x is the cell number along the cable, ($1 \leq x \leq 300$), $x_{1/2}=150$ and $s=5$. $G_{to,proximal}$ and $G_{to,distal}$ represent G_{to} values of the proximal and distal ends of the cable, respectively.

2.3.4 P2R Detection

P2R was detected automatically using a custom algorithm that distinguished two distinct action potentials from a single action potential comprised of an upstroke followed by a deep notch and a dome. For each cell and for each beat, the maximum and minimum membrane potentials defined the AP range. Next, two thresholds were calculated: the depolarizing threshold, equal to 95% of the AP range above baseline and the repolarizing threshold, equal to 5% of that range above baseline. P2R was defined as two upstrokes occurring as a response to one stimulus, both of which cross the depolarizing threshold, separated by full repolarization below the repolarizing threshold.

2.4 Results

2.4.1 Single-cell simulations

We first carried out single-cell simulations to investigate G_{to} dependence and to determine the threshold value between the notch-and-dome and the loss-of-dome morphologies. While low and normal values of G_{to} produced the notch-and-dome morphology, high values of G_{to} produced abbreviated APs with loss-of-dome morphology. Interestingly, intermediate values of G_{to} caused cells to switch intermittently between two morphologies, prolonged notch-and-dome morphology and loss-of-dome morphology. This “switching” behavior is shown in Figure 2.1.

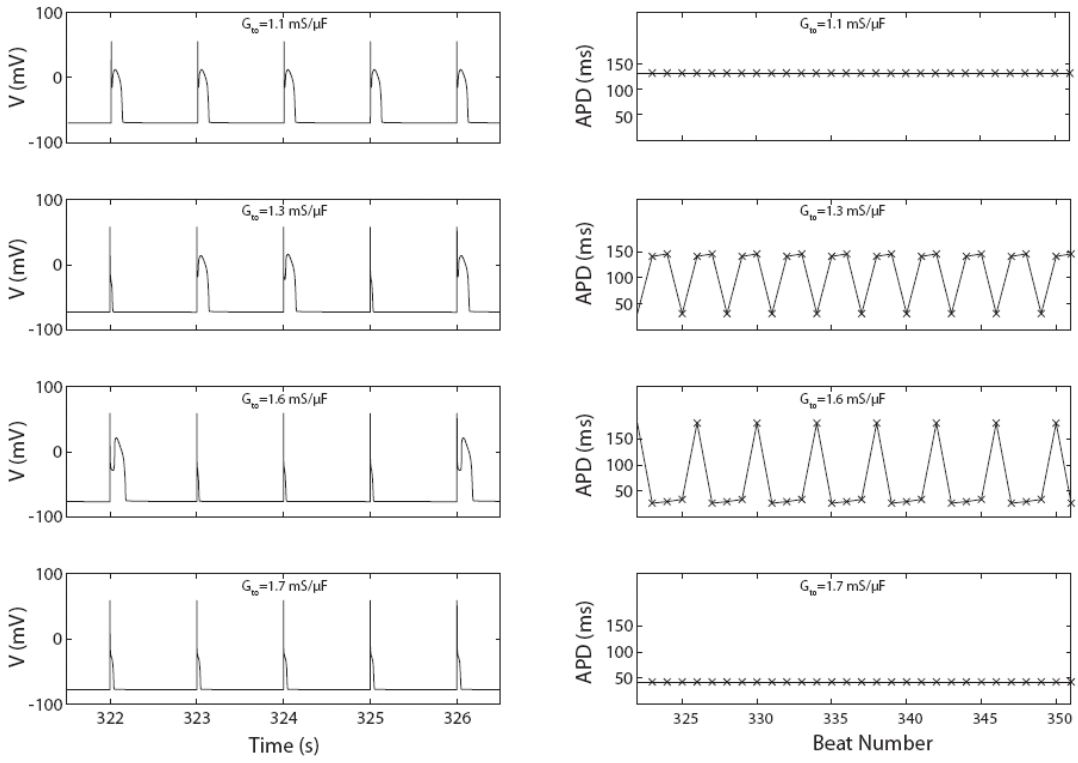

Figure 2.1: Single-cell simulations for selected G_{to} values showing AP morphologies (left) and APDs (right). **A**: With sufficiently small G_{to}, all morphologies are notch-and-dome. **C, E**: For intermediate G_{to}, some APs have prolonged notch-and-dome morphology while others have loss-of-dome morphology. **G**: G_{to} is sufficiently large, all morphologies are loss-of-dome. **B**, **D**, **F**, **H** display corresponding APDs. Reproduced from reference [1].

All cells having G_{to} values in the range of 1.3 to 1.6 mS/µF displayed APs with both morphologies. The frequency of prolonged morphology versus that of abbreviated morphology varied depending on the G_{to} value, with more long APs occurring when G_{to} was closer to 1.3 mS/µF and more short APs occurring when G_{to} was closer to 1.6 mS/µF. Notably, similar switching between these two morphologies has been observed experimentally in canine myocytes, when G_{to} was set to the transition level between the two morphologies [6].

2.4.2 Cable simulations

Figure 2.2 demonstrates various behaviors observed in this study, in two cable simulations with different G_{to} distributions. Panel A shows the APs along a cable for the 9th beat of a simulation where the APs of the proximal end of the cable had a stable notch-and-dome morphology, while APs at the distal end had a stable loss-of-dome morphology. In the middle of the cable, the dome became progressively shorter until it disappeared, thereby transforming to the loss-of-dome morphology. Panel B shows this gradual decrease in APD along the cable leading up to a small jump corresponding to the loss-of-dome.

Figure 2.2D shows the APs along a cable for the 9th beat of a different simulation. Here, the APs at the proximal end of the cable had a stable notch-and-dome morphology. The APs at the distal end of the cable had the loss-of-dome morphology but because the G_{to} value here was within the switching behavior range (Figure 2.1), this morphology was not stable. Near the middle of the cable, the dome phase, and therefore the APD, were prolonged (which may be due to

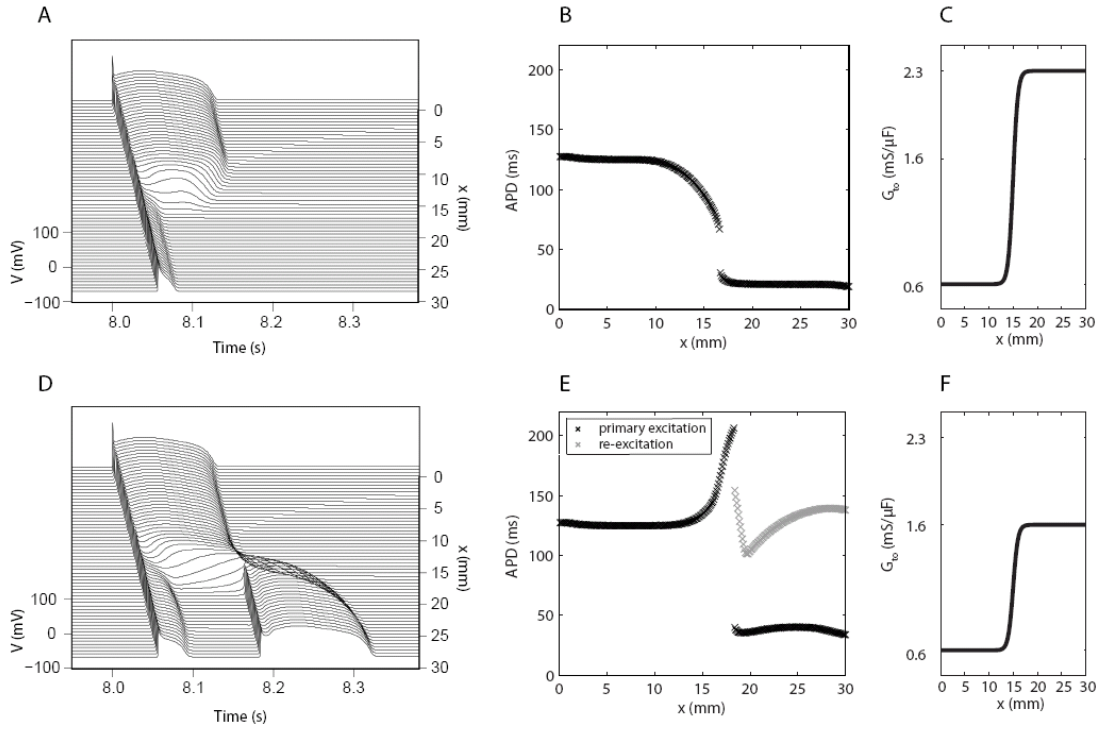

Figure 2.2: Results of two cable simulations. G_{to} distributions along the cables are based on a Boltzmann function (**C, F**). **A**: APs along a cable for a single beat from a simulation with $G_{to,proximal}$=0.6 mS/µF and $G_{to,distal}$=2.3 mS/µF. **D**: APs along a cable for a single beat from a simulation with $G_{to,proximal}$=0.6 mS/µF and $G_{to,distal}$= 1.6 mS/µF. **B,E**: corresponding APDs along the cable. x represents the distance along the cable, with x=0 representing the proximal (stimulation) end. Reproduced from reference [1].

local dynamics [6] or due to electrotonic current that diffused backward from the distal end of the cable, or both). At cells where the notch was sufficiently deep (x>18 mm), full repolarization occurred, creating a situation where a prolonged phase-2 was adjacent to repolarized cells. As shown in the figure, the repolarized area was re-excited by the depolarized dome and P2R occurred. APD prolongation that occurred just proximal to the loss-of-dome (clearly seen in E), occurred in all simulations that manifested P2R, suggesting that this behavior is one of the hallmarks of P2R occurrence. Interestingly, APD prolongation has also been observed experimentally in single cells as G_{to} approached the threshold [6].

In Figure 2.3, linear-gradient results are depicted. Panel A shows results of simulations using G_{to} values that started from $G_{to,proximal}$ = 2.0 mS/μF and systematically decreased linearly to various values of $G_{to,distal}$ (2.0-0.0 mS/μF). For cables with $G_{to} \geq 1.7$ mS/μF along the entire length ($G_{to,distal} \geq 1.7$ mS/μF), P2R did not occur at all, or occurred only in the first beats of the simulation. But when a significant portion of cells along the cable (12%, $G_{to,distal} \leq 1.6$ mS/μF) had G_{to} values within the switching range (1.25-1.65 mS/μF), P2R did occur. When $G_{to,distal} \leq 1.5$ mS/μF, such that a larger percentage of cells had G_{to} in the switching range (≥ 20%), P2R occurred in over 30% of beats. In panel C, another set of linearly decreasing simulation results is shown. Here, $G_{to,proximal}$ varied between 2.0 and 0.0 mS/μF while $G_{to,distal}$ remained constant and equal to 0.0 mS/μF. Again, where only a small portion of the cells (up to 16%, $G_{to,proximal} \leq 1.5$ mS/μF) were within the switching range, there was no P2R. However, when a greater percentage of cells (22%, $G_{to,proximal} \geq 1.6$ mS/μF) had G_{to} within the switching range, P2R did occur. As this percentage increased further (23%,

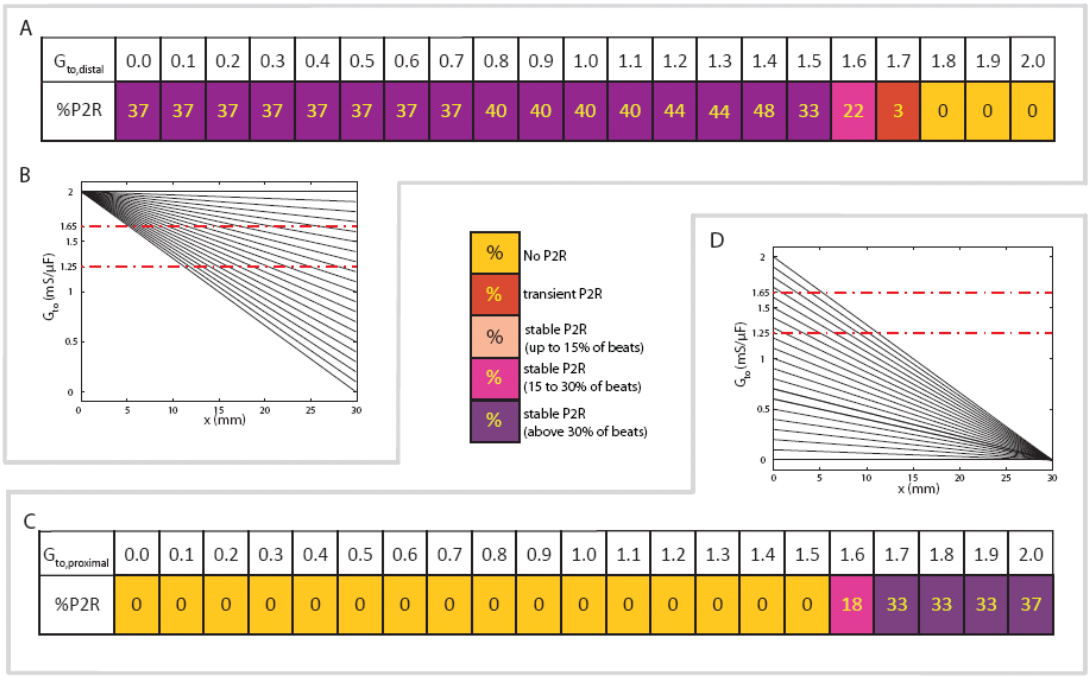

Figure 2.3: Simulation results for linearly decreasing gradients of G_{to}. **A**: Simulations started at $G_{to,proximal}$ = 2.0 mS/µF. First row indicates $G_{to,distal}$. Second row indicates the percentage of beats that manifested P2R. Yellow represents simulations in which P2R did not occur and red represents simulations where P2R occurred only transiently. Three levels of pink/purple represent simulations where P2R happened in less than 15%, 15%-30% and more than 30% of the beats, respectively. **B**: G_{to} distributions for simulations in **A**. Dashed red line marks switching behavior range. x represents distance along the cable. **C**: Results of a set of linearly decreasing G_{to} gradients shown in **D**. Reproduced from reference [1].

$G_{to,proximal}$ ≥1.7 mS/μF) the system became very arrhythmogenic and P2R occurred in more than 30% of the beats.

In Figure 2.4, simulation results for piece-wise linear gradients are shown. The results in panel A are from cables in which the G_{to} distribution was divided into 3 portions: the first portion had a linear gradient starting from 2.0 mS/μF, the middle portion of the cable had a constant value and the distal portion again had a linear gradient starting from the constant value down to 0.5 mS/μF (Figure 2.4B). P2R occurred for all tested gradients, which all had cells within the switching behavior range. In panel C, results for increasing piece-wise linear gradients are depicted. For both the decreasing (A) and increasing gradients (C), P2R was most frequent when the constant of the distribution was within the switching behavior range, supporting the hypothesis that P2R is correlated to switching behavior.

Figure 2.5A shows a summary of the results obtained when systematically varying $G_{to,proximal}$ and $G_{to,distal}$ according to a Boltzmann distribution (Eq. 1). This G_{to} allocation provided continuous gradients having two main G_{to} values for the cable, $G_{to,proximal}$ and $G_{to,distal}$, such that the number of cells that are not assigned these values is small (~6%, Figure 2.5B) . The P2R occurrence results demonstrated a plus-sign shape. As expected, there was no P2R when $G_{to,proximal}$ and $G_{to,distal}$ were both either large (≥1.8 mS/μF causing the short AP morphology everywhere, upper right of Figure 2.5A) or small (≤1.2 mS/μF causing the long AP morphology everywhere, lower left of Figure 5A). When the G_{to} values were very different, and both far from the switching behavior region, P2R occurred mostly transiently (upper left and lower right). P2R occurrence was greatest when either

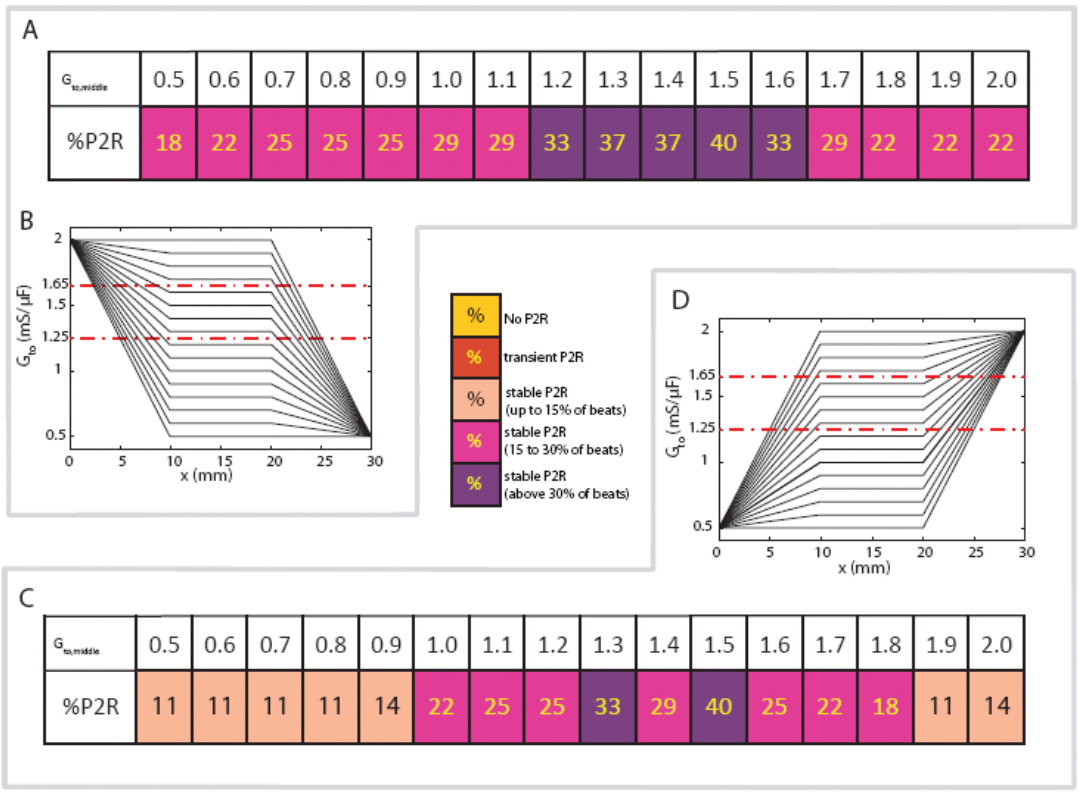

Figure 2.4: Simulation results for piece-wise linear gradients. Same colour code as for Figure 3. **A:** First row indicates the G_{to} value of the middle portion of the gradients shown in **B**. Second row shows the percentages of beats in each simulation that manifested P2R. **C**: Results of a set of increasing piece-wise linear gradients, as shown in **D**.

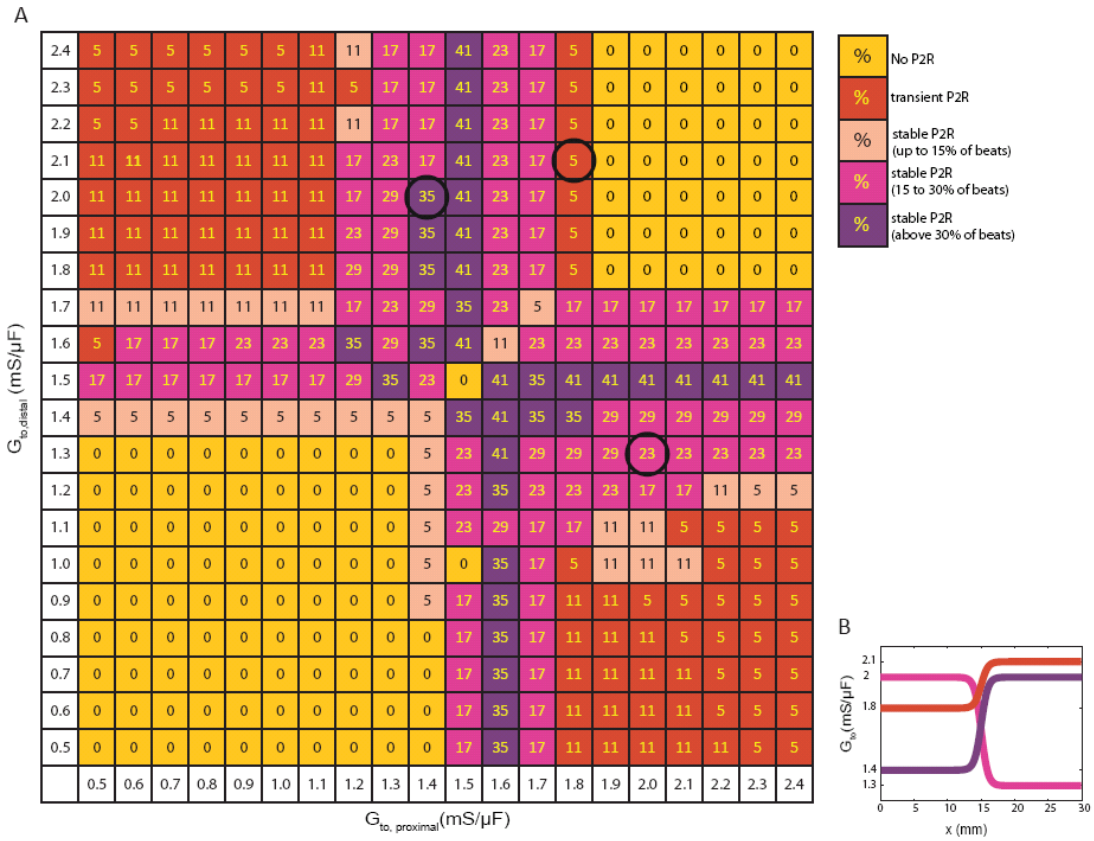

Figure 2.5: Simulation results from Boltzmann gradients. Same colour code as for Figure 3. **A**: Percentages of beats that manifested P2R. Each simulation is identified by its $G_{to,proximal}$ (x-axis) and $G_{to,distal}$ (y-axis) values such that the G_{to} distribution between follows a Boltzmann function. **B:** Three sample Boltzmann G_{to} distributions. These distributions correspond to the circled results in A. Reproduced from reference [1].

$G_{to,proximal}$ or $G_{to,distal}$ were within the range 1.4-1.6 mS/μF which is within the switching behavior range. In that case, P2R occurred in almost all simulations regardless of the value of G_{to} on the other end side of the cable.

Interestingly, P2R also occurred in homogenous cables when their G_{to} was within or near the switching range (middle portion of lower-left to upper-right diagonal). Here, P2R occurred in fewer beats because the APs along the cable often tended to switch together such that the two morphologies were not often present along the cable for the same beat (see also Figure 2.6A). Notably, in homogeneous cables P2R occurred only anterogradely. The increased depolarizing current due to the stimulus caused notch-and-dome morphology at the proximal end, whereas the loss-of-dome morphology persisted distally where the inherent depolarizing current was below the notch-and-dome threshold. Thus, for homogenous tissue with G_{to} in the switching regime, small heterogeneities, either dynamical as in this case (i.e., pacing induced) or structural (i.e., due to small normal anatomical variability), can lead to P2R.

Figure 2.6 depicts two representative forms of P2R. In panel A, anterograde P2R is shown. The cable is homogeneous, having G_{to}=1.6 mS/μF. As 1.6 mS/μF is within the switching behavior range, the cells manifested the two AP morphologies. In the first beat that is displayed (3^{rd} beat of the simulation), all cells had the long morphology, while in the second and third beats (4^{th} and 5^{th} beats of the simulation) all cells manifested the short morphology. However, on the fourth beat (6^{th} beat of the simulation) the dynamics were spatially heterogeneous and the proximal cells demonstrated the notch-and-dome morphology while the distal cells demonstrated the loss-of-dome morphology,

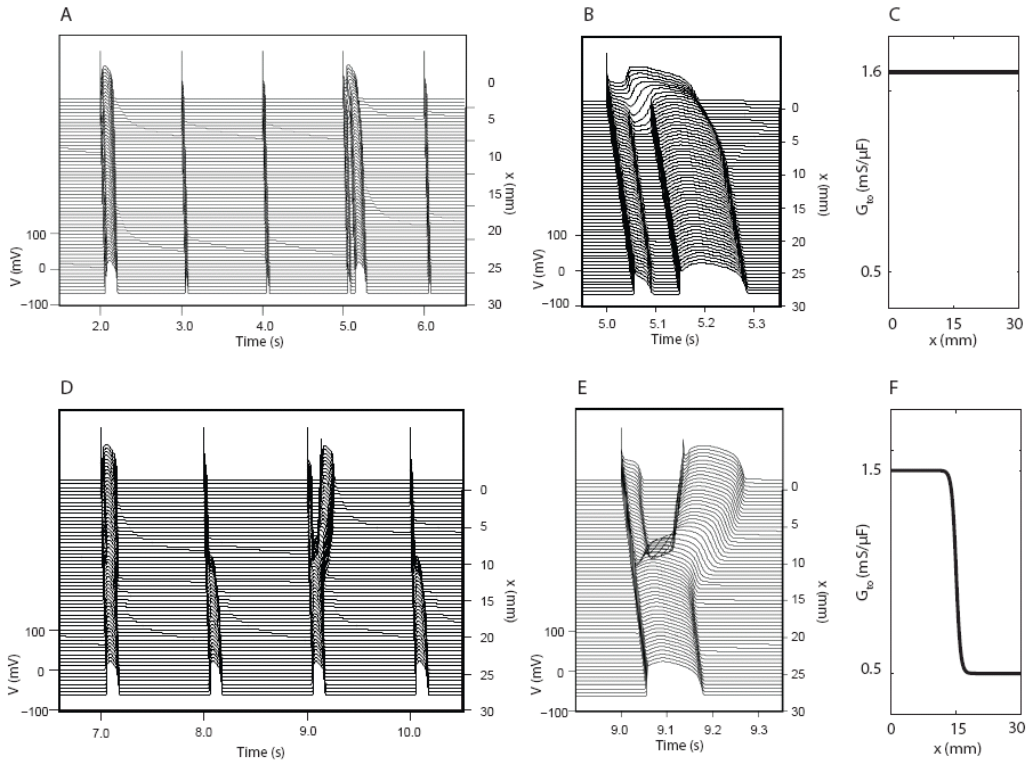

Figure 2.6: Examples of P2R manifestation. **A:** Anterograde P2R in a homogeneous cable having G_{to}=1.6 mS/µF. **B:** A close-up of the fourth beat from **A**. **D**: Retrograde P2R from a Boltzmann-gradient simulation of a heterogeneous cable having $G_{to,proximal}$=1.5 mS/µF and $G_{to,distal}$=0.5 mS/µF. **E**: A close-up of the third beat from D. **C, F**: G_{to} distribution along the cable. Reproduced from reference [1].

leading to P2R. Figure 2.6B shows a close-up of this anterograde P2R. Thus, even in a cable with uniform G_{to} levels, a spatially non-uniform arrhythmogenic substrate and P2R may occur.

P2R could also occur retrogradely, as shown in a heterogeneous cable having $G_{to,proximal}$=1.5 mS/µF and $G_{to,distal}$=0.5 mS/µF (Figure 2.6D). For the distal portion of the cable there was always a stable dome. In the proximal portion of the cable, where G_{to} was within the switching behavior range, the AP morphology changed between notch-and-dome morphology and loss-of-dome. In the third beat that is presented (10^{th} beat of the simulation), an arrhythmogenic condition developed when the proximal end had the short morphology and current from the dome region propagated retrogradely. A close-up of this retrograde P2R is shown in E.

To quantify the relationship between cells in the switching region and P2R occurrence, we calculated:

$$\Delta G_{to} = \sum_{x=1}^{300} |G_{to}(x) - G_{to}^{*}|, \qquad \text{(Eq. 2.2)}$$

where x is the cell number along the cable and G_{to}^{*}= 1.45 mS/µF is the center of the single-cell switching range (1.25-1.65 mS/µF). We binned the results into 9 bins according to their ΔG_{to}. For each bin we calculated the percentage of the simulations manifesting non-transient P2R. In general, we found that as ΔG_{to} decreased, the percentage of simulations exhibiting P2R increased (Figure 2.7).

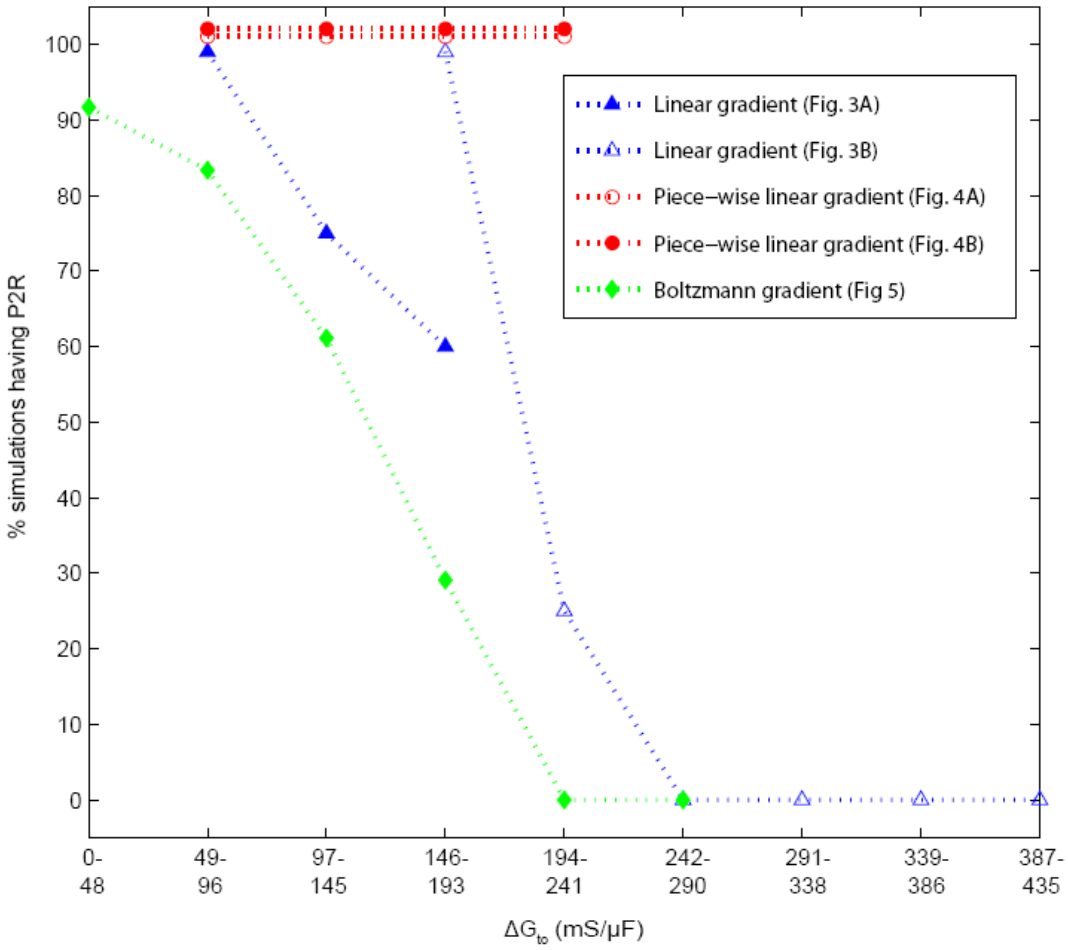

Figure 2.7: Relationship between the percentage of simulations manifested P2R and ΔG_{to}. The different types of gradients are indicated by different symbols: linear (Figure 3A), blue triangles; linear (Figure 3B), blue triangles; piece-wise linear (Figure 4A), red circles; piece-wise linear (Figure 4B), red circles; Boltzmann (Figure 5), green diamonds. Reproduced from reference [1].

For all simulations, CV was in the range of 49-54 cm/sec, and was dependent on G_{to} values. For individual simulations, CV values varied (as much as the 49-54 cm/sec range) along the cable as a function of G_{to}. Importantly, there was no difference in spatial CV profile between beats in a given simulation; i.e., the spatial CV profile was the same whether or not P2R occurred. Thus, there was no correlation between CV and P2R occurrence.

2.5 Discussion

Our results show that spontaneous notch-and-dome to/from loss-of-dome switching behavior at the single-cell level is likely to lead to P2R initiation in this model. This suggests a very different mechanism of P2R, than the “neighboring regions of different morphology”-hypothesis, as neighboring regions of cells with different morphologies was not, in itself, sufficient for stable P2R. Moreover, P2R happened even in homogeneous cables in the absence of any ionic gradient, suggesting that an intrinsic ionic gradient is not necessary for P2R development.

Similar switching behavior between the notch-and-dome and the loss-of-dome has been observed in other contexts. For example, patterns of 2:1 (dome, no dome) and 3:1 (dome, no dome, no dome) rhythms have been observed in ischemic canine epicardial tissue [22] and reproduced in simulations in which the underlying ionic mechanism was an interplay between $I_{Ca,L}$ and I_{to} [23]. 2:1 patterns also occurred in a computational study of the Y1795H SCN5A Brugada syndrome mutation due to partial block of I_{Na} [24]. Finally, switching behavior between action potentials with and without early afterdepolarizations have

developed in canine ventricular myocytes with isoproterenol [25] and in simulated ventricular cells with partial I_{Ks} block [26].

2.5.1 Ionic mechanisms underlying action potential morphology variation

The ionic mechanisms for the different AP morphologies are illuminated in Figure 2.8. In contrast to the notch-and-dome morphology (A-D; blue), the loss-of-dome morphology (A-D; green), had a higher G_{to} that led to a higher I_{to} peak (B; green arrow). This in turn repolarized the membrane further (A; green arrow) and closed the d-gates completely (C; green arrow) such that the calcium current was not reactivated (D; green arrow) and no dome was formed.

The prolonged AP (A-D; red) occurs for intermediate G_{to} values, where a very fine balance between inward and outward current at the end of phase 1 leads to a prolongation of the notch prior to the dome, thus extending the APD. In contrast to the notch-and-dome morphology, the prolonged morphology had higher G_{to} and higher I_{to} peak (B; red arrow). This resulted in increased membrane repolarization (A; red arrow) and more closing of the d-gates (A; red arrow). The small fraction of d-gates that remained open facilitated a delayed $I_{Ca,L}$ reactivation (D; red asterisk), which delayed the dome phase and extended the APD.

Panels E-I show data from two consecutive beats for G_{to}=1.3 mS/µF. For the first beat (green), the extracellular calcium concentration ($[Ca^{2+}]_o$) was lower (H; green arrow), resulting in reduced $I_{Ca,L}$ driving force ($\overline{I_{Ca,L}}$) (I; green arrow) and $I_{Ca,L}$ peak (F; green arrow). This caused further repolarization and complete

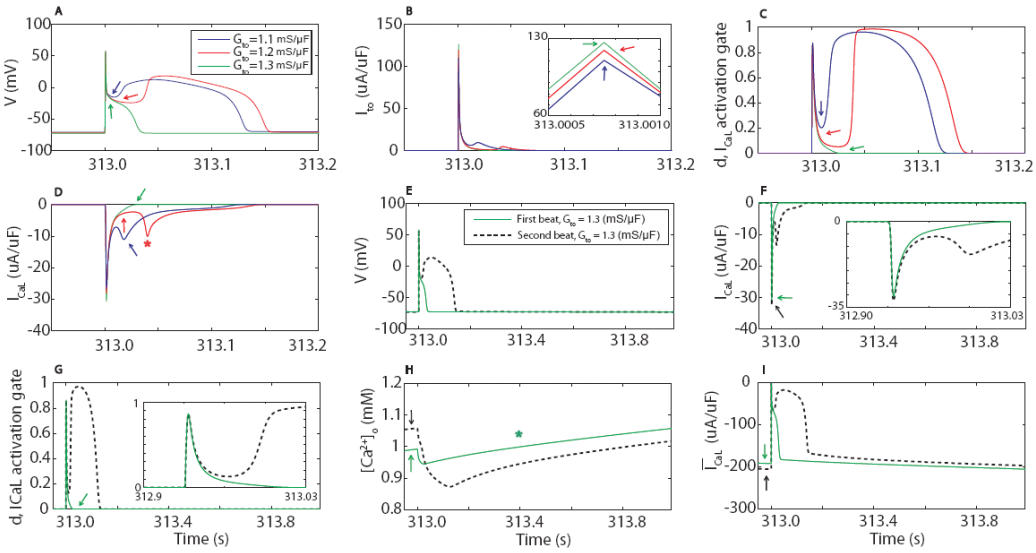

Figure 2.8: The cellular mechanism for the three different AP morphologies. **A-D**: Attributes of the three distinct morphologies having G_{to}=1.1, 1.2 and 1.3 mS/μF. **E-I**: Attributes of the switching behavior for G_{to}=1.3 mS/μF. Reproduced from reference [1].

closing of the d-gates (G; green arrow). Consequently, no dome was formed. This lack of reactivation of $I_{Ca,L}$ means that $[Ca^{2+}]_o$ was less decreased during the AP (H; green asterisk) and the next AP (E-I; dashed) started off with an increased $[Ca^{2+}]_o$ and conditions favorable for dome formation.

2.5.2 Phase-2 Reentry Cellular Mechanism

The cellular mechanism for P2R is investigated in Figure 2.9. Panel A shows two consecutive beats, with P2R occurring in the second one. Cell 130 G_{to} (1.482 mS/µF) was within the switching behavior range and therefore its AP was unstable (B; red). The second beat manifested a prolonged notch-and-dome morphology due to high $[Ca^{2+}]_0$ (C; arrow at Time= 4.0 s shows higher $[Ca^{2+}]_0$ than arrow at Time=3.0 s; see also Figure 2.7H). This prolonged morphology bordered a loss-of-dome morphology (i.e. B; blue) facilitating retrograde current propagation and P2R as seen by the AP at Time=4.2 s at cell 40. This loss-of-dome morphology was due to a larger value of G_{to} (1.4975 mS/µF), resulting in an increased I_{to} in cell 120 versus cell 130. P2R occurred due to the electrotonic current propagating retrogradely (D; blue arrow) and not due to $I_{Ca,L}$ (E; blue arrow) or any other depolarizing current (data not shown). This example is representative of all other simulations in which P2R was initiated, including homogenous cables.

2.5.3 Clinical Relevance

We note that there is an ongoing debate regarding the occurrence of P2R in Brugada syndrome patients [4, 15, 27-29]. Phase-2 reentry has been

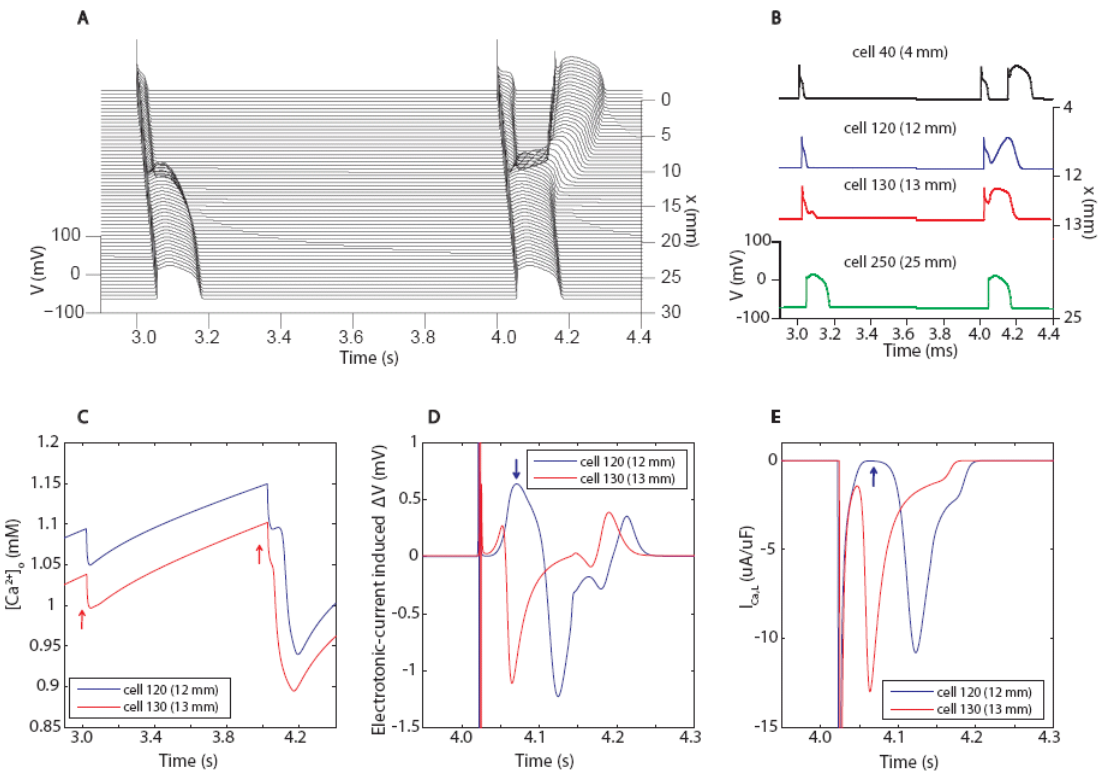

Figure 2.9: Cellular explanation of P2R in a heterogeneous cable having a Boltzmann gradient with $G_{to,proximal}$=1.5 mS/µF and $G_{to,distal}$=0.5 mS/µF. A: APs along the cable. B: APs in four different locations. C: Extracellular calcium concentration along the two beats of cells 120 and 130. Arrows point to the beginning of both beats. D: Electrotonic-current induced ΔV calculated as: $\Delta V_i = V_{i+1} + V_{i-1} - 2 * V_i$, where i indicates the cell number. E: $I_{Ca,L}$ of cells 120 and 130.

demonstrated not only in animal experimental models [10, 29, 30] but was also assessed in a human study of Brugada patients with implantable cardioverter-defibrillators (ICD) [31]. In this case, there was evidence that P2R was the underlying mechanism of ventricular extrasystoles, ventricular tachycardia and VF. In contrast, it has been suggested that the dispersion of repolarization potentially causing P2R may not be present in Brugada patients, and that conduction slowing and/or conduction block is the arrhythmogenic mechanism causing VF [27, 28]. Our study does not attempt to address such issues, but rather establishes conditions sufficient for the occurrence of P2R.

2.5.4 P2R Directionality

Future studies of P2R might address directionality in P2R development. The ventricular wall is highly heterogeneous, being comprised of three layers (the epicardium, the midmyocardium and the endocardium), each characterized by different electrophysiological properties [32, 33]. P2R has been proposed to occur in two orientations, either along the epicardium, as investigated in our study, or transmurally. The development of P2R transmurally could be due to the discontinuities in ionic properties of the distinct layers, together with a large epicardial I_{to}. An extension of our simulations to a 3-dimensional slab of tissue could provide insight into this. Having said that, we believe the transition from epicardial single-cell simulations to one-dimensional epicardial fiber simulations likely illuminates the fundamental system dynamics and reveals the basic mechanism of the P2R arrhythmogenicity substrate.

2.5.5 Study limitations

First, as mentioned above, all currents affecting the notch-and-dome (e.g., $I_{Ca,L}$ and I_{Na}) may contribute to P2R; investigation of balances/gradients of all such currents should be investigated in the future. Second, because the exact range and gradient characteristics of G_{to} in the RV are unknown, we chose to investigate a rather broad range of G_{to} values, as well as several different G_{to} gradient types. It is therefore likely that some of our gradients/ranges are unphysiological. Importantly, our findings suggest that the type of gradient, or even whether a gradient exists, is not fundamental for the initiation of P2R. Instead, we showed that an unstable AP in a subset of cells is a sufficient and promoting factor for P2R development. Third, our study investigated only one ventricular model and only one BCL (1000 ms; chosen because most Brugada-related episodes occur during rest). Further studies are needed to address rate- and model- dependence. Fourth, simulations of pathological conditions such as ischemia or the Brugada syndrome, in which P2R is hypothesized to occur, were not included. Given that these conditions alter ionic current balances in ways that favour loss-of-dome, they could potentially shift the switching behavior range toward more physiological values of G_{to}.

2.6 Conclusions

We conclude that an important factor facilitating P2R in this model is not the presence of two different morphologies in adjacent cells (as previously hypothesized), but rather a switching AP morphology caused by an ionic-current

imbalance within a significant subset of cells. With such instability, cells can switch intermittently between notch-and-dome and loss-of-dome morphologies, which can trigger P2R. Hence, our findings suggest that such switching behavior may be one of the bases for P2R development in cardiac tissue.

R**ERERENCES**

1. Maoz, A., T. Krogh-Madsen, and D.J. Christini, *Instability in action potential morphology underlies phase 2 reentry: a mathematical modeling study.* Heart Rhythm, 2009. **6**(6): p. 813-22.
2. Antzelevitch, C. and G.X. Yan, *Cellular and ionic mechanisms responsible for the Brugada syndrome.* J Electrocardiol, 2000. **33 Suppl**: p. 33-9.
3. Lukas, A. and C. Antzelevitch, *Phase 2 reentry as a mechanism of initiation of circus movement reentry in canine epicardium exposed to simulated ischemia.* Cardiovasc Res, 1996. **32**(3): p. 593-603.
4. Antzelevitch, C., et al., *Brugada syndrome: from cell to bedside.* Curr Probl Cardiol, 2005. **30**(1): p. 9-54.
5. Greenstein, J.L., et al., *Role of the calcium-independent transient outward current I(to1) in shaping action potential morphology and duration.* Circ Res, 2000. **87**(11): p. 1026-33.
6. Sun, X. and H.S. Wang, *Role of the transient outward current (Ito) in shaping canine ventricular action potential--a dynamic clamp study.* J Physiol, 2005. **564**(Pt 2): p. 411-9.
7. Di Diego, J.M., Z.Q. Sun, and C. Antzelevitch, *I(to) and action potential notch are smaller in left vs. right canine ventricular epicardium.* Am J Physiol, 1996. **271**(2 Pt 2): p. H548-61.
8. Hoppe, U.C., et al., *Manipulation of cellular excitability by cell fusion: effects of rapid introduction of transient outward K+ current on the guinea pig action potential.* Circ Res, 1999. **84**(8): p. 964-72.
9. Krishnan, S.C. and C. Antzelevitch, *Flecainide-induced arrhythmia in canine ventricular epicardium. Phase 2 reentry?* Circulation, 1993. **87**(2): p. 562-72.

10. Aiba, T., et al., *Cellular basis for trigger and maintenance of ventricular fibrillation in the Brugada syndrome model: high-resolution optical mapping study.* J Am Coll Cardiol, 2006. **47**(10): p. 2074-85.
11. Miyoshi, S., et al., *A mathematical model of phase 2 reentry: role of L-type Ca current.* Am J Physiol Heart Circ Physiol, 2003. **284**(4): p. H1285-94.
12. Miyoshi, S., et al., *Link between SCN5A mutation and the Brugada syndrome ECG phenotype: simulation study.* Circ J, 2005. **69**(5): p. 567-75.
13. Oudit, G.Y., et al., *The molecular physiology of the cardiac transient outward potassium current (I(to)) in normal and diseased myocardium.* J Mol Cell Cardiol, 2001. **33**(5): p. 851-72.
14. Morita, H., et al., *Differences in arrhythmogenicity between the canine right ventricular outflow tract and anteroinferior right ventricle in a model of Brugada syndrome.* Heart Rhythm, 2007. **4**(1): p. 66-74.
15. Morita, H., et al., *Repolarization heterogeneity in the right ventricular outflow tract: correlation with ventricular arrhythmias in Brugada patients and in an in vitro canine Brugada model.* Heart Rhythm, 2008. **5**(5): p. 725-33.
16. Di Diego, J.M., J.M. Fish, and C. Antzelevitch, *Brugada syndrome and ischemia-induced ST-segment elevation. Similarities and differences.* J Electrocardiol, 2005. **38**(4 Suppl): p. 14-7.
17. Luo, C.H. and Y. Rudy, *A dynamic model of the cardiac ventricular action potential. I. Simulations of ionic currents and concentration changes.* Circ Res, 1994. **74**(6): p. 1071-96.
18. Dumaine, R., et al., *Ionic mechanisms responsible for the electrocardiographic phenotype of the Brugada syndrome are temperature dependent.* Circ Res, 1999. **85**(9): p. 803-9.

19. Rush, S. and H. Larsen, *A practical algorithm for solving dynamic membrane equations.* IEEE Trans Biomed Eng, 1978. **25**(4): p. 389-92.

20. Szentadrassy, N., et al., *Apico-basal inhomogeneity in distribution of ion channels in canine and human ventricular myocardium.* Cardiovasc Res, 2005. **65**(4): p. 851-60.

21. Volders, P.G., et al., *Repolarizing K+ currents ITO1 and IKs are larger in right than left canine ventricular midmyocardium.* Circulation, 1999. **99**(2): p. 206-10.

22. Lukas, A. and C. Antzelevitch, *Differences in the electrophysiological response of canine ventricular epicardium and endocardium to ischemia. Role of the transient outward current.* Circulation, 1993. **88**(6): p. 2903-15.

23. Hopenfeld, B., *Mechanism for action potential alternans: the interplay between L-type calcium current and transient outward current.* Heart Rhythm, 2006. **3**(3): p. 345-52.

24. Vecchietti, S., et al., *In silico assessment of Y1795C and Y1795H SCN5A mutations: implication for inherited arrhythmogenic syndromes.* Am J Physiol Heart Circ Physiol, 2007. **292**(1): p. H56-65.

25. Priori, S.G. and P.B. Corr, *Mechanisms underlying early and delayed afterdepolarizations induced by catecholamines.* Am J Physiol, 1990. **258**(6 Pt 2): p. H1796-805.

26. Lerma, C., Krogh-Madsen, T., Guevara, M.R., Glass, L., *Stochastic Aspects of Cardiac Arrhythmias.* J. Stat. Phys., 2007. **128**: p. 347-374.

27. Petitprez, S., et al., *Analyses of a novel SCN5A mutation (C1850S): conduction vs. repolarization disorder hypotheses in the Brugada syndrome.* Cardiovasc Res, 2008. **78**(3): p. 494-504.

28. Zhang, Z.S., et al., *Sodium channel kinetic changes that produce Brugada syndrome or progressive cardiac conduction system disease.* Am J Physiol Heart Circ Physiol, 2007. **292**(1): p. H399-407.

29. Fish, J.M. and C. Antzelevitch, *Cellular mechanism and arrhythmogenic potential of T-wave alternans in the Brugada syndrome.* J Cardiovasc Electrophysiol, 2008. **19**(3): p. 301-8.

30. Kimura, M., et al., *Mechanism of ST elevation and ventricular arrhythmias in an experimental Brugada syndrome model.* Circulation, 2004. **109**(1): p. 125-31.

31. Bloch Thomsen, P.E., et al., *Phase 2 reentry in man.* Heart Rhythm, 2005. **2**(8): p. 797-803.

32. Sicouri, S. and C. Antzelevitch, *A subpopulation of cells with unique electrophysiological properties in the deep subepicardium of the canine ventricle. The M cell.* Circ Res, 1991. **68**(6): p. 1729-41.

33. Drouin, E., et al., *Electrophysiologic characteristics of cells spanning the left ventricular wall of human heart: evidence for presence of M cells.* J Am Coll Cardiol, 1995. **26**(1): p. 185-92.

CHAPTER 3

STUDYING PHASE-2 REENTRY MECHANISM IN THE TRANSMURAL DIRECTION

3.1 Abstract

BACKGROUND Phase-2 reentry (P2R) is caused by conduction of electrotonic current from phase 2 of notch-and-dome action potential sites to fully recovered sites, causing abnormal reexcitation. It is postulated that in addition to apicobasal potential differences, as studied in Chapter 2, transmural electrophysiological heterogeneities may contribute to phase-2 reentry initiation.

OBJECTIVE The purpose of the work described in this chapter was to investigate whether P2R could develop in the transmural direction and to illuminate the underlying factors for transmural P2R initiation.

METHODS The Luo-Rudy dynamic model was modified to simulate cells from the endocardium, midmyocardium and epicardium. In the epicardium, to represent hypothesized intrinsic right ventricular ionic heterogeneity, a range of the transient outward current conductances, G_{to}, was investigated; i.e., we investigated transmural cables where the epicardial end was representative of a range of apical to basal locations. One-dimensional cables were composed of the three transmural layers and were used to systematically investigate P2R.

RESULTS P2R occurred in one-dimensional cable simulations where epicardial action potentials manifested unstable AP morphology behavior in which cells switched intermittently between notch-and-dome and loss-of-dome morphologies.

CONCLUSION P2R can occur in the transmural direction and is facilitated by the switching AP morphology behavior in the epicardium.

3.2 Introduction

As discussed in Chapter 2, phase-2 reentry (P2R) is caused by conduction of electrotonic current from phase 2 of notch-and-dome action potential (AP) sites to fully recovered sites, causing abnormal reexcitation. AP heterogeneity consisting of the two AP morphologies, the notch-and-dome and the loss-of-dome regions is required for P2R development. As the balance between the depolarizing and repolarizing currents at the end of phase 1 or the beginning of phase 2 determines the dome formation, regions having intrinsically high levels of repolarizing current like I_{to} are more susceptible for loss-of-dome morphology development and are natural candidates for studying P2R initiation. Indeed, P2R has been associated with the right ventricle (RV) [1, 2] and the right ventricular outflow track (RVOT) [3].

P2R has been studied experimentally using models of Brugada syndrome [2, 4, 5]. These models try to mimic Brugada using drugs such as sodium channel blockers (e.g. Pilsicainide) [4, 5], sodium and calcium blockers (e.g. Terfenadine, Verapamil) [2, 5, 6] and I-K_{ATP} augmenters (e.g. Pinacidil) [4-6]. The drugs are

used to create a deliberate imbalance of ionic currents such that ST-segment elevation, the ECG manifestation of Brugada, appears on the ECG. Hence, the physiological relevance of those studies to pathological development of phase-2 reentry is unclear. Many mutations in the SCN5A gene that encodes the sodium channel have been reported [7], accounting for 18-30% of Brugada cases [8]. In addition, mutations in the L-type calcium channel have been also associated with the Brugada syndrome [9]. However, the drug-based Brugada models were designed to simulate the Brugada phenotype and ECG manifestation, not the genotype. Therefore it is possible that arrhythmias in general and particularly phase-2 reentry may be more likely to develop in these models.

In-silico studies that have investigated P2R [10-12], including ours (Chapter 2), focused on the RV epicardium (Figure 1.7, epicardium) due to its high expression level of I_{to} channels. We found that an important factor facilitating epicardial P2R is a switching AP morphology caused by an ionic-current imbalance. With such instability, cells can switch intermittently between notch-and-dome and loss-of-dome morphologies, which can trigger P2R. Yet, activation and repolarization are known to have a transmural component [13, 14]. Because of such heterogeneity, it has been hypothesized that P2R can occur due to transmural electrophysiological heterogeneities [4, 6]. Therefore, a study that investigates the transmural direction (Figure 1.7, dashed line) would help in form the complete understanding of phase-2 reentry substrate and mechanism. Therefore, this present study focuses on P2R development in the transmural direction using one-dimensional simulations.

The ventricular wall is thought to be comprised of three distinct layers: the epicardium, the midmyocardium, and the endocardium (Figure 1.7). These layers have been found in dogs [15], humans [16] and guinea pigs [17]. Myocytes from each layer exhibit different action potential morphologies. Epicardial and midmyocardial (M) cells action potentials possess a prominent notch, responsible for the notch-and-dome morphology, while the endocardial action potential has no notch [18]. The M-cells display the longest action potential duration (APD) relative to epicardial and endocardial ventricular cells [19, 20]. These cells are also the most sensitive to pharmacological interventions that prolong the AP [18]. Transmural variability of protein expression and/or electrophysiological function have been specifically reported for I_{to} [21] and the slow activating component of the delayed rectifier K^+ current (I_{Ks}) [18, 20, 22].

The purpose of this study was to investigate the mechanism of P2R development in the transmural direction in one-dimensional simulations to illuminate the factors underlying transmural P2R initiation. We found that the intrinsic heterogeneity within the ventricular wall (discontinuous gradients in the macroscopic conductances of the transient outward and the delayed rectifier potassium currents), together with the switching behavior in the epicardium, could produce P2R in the transmural direction and abnormal AP propagation.

3.3 Methods

3.3.1 Computational Model and Methods

We used a modified version of the Luo-Rudy dynamic (LRd) model [23]. The L-type calcium current formalism composed by Miyoshi et al [10] and the transient outward current (I_{to}) formalism composed by Dumaine et al [24] were incorporated into the model. The forward Euler method with a time step of Δt=0.005 ms was used to integrate dV/dt and the ionic concentrations, while the gating variables were computed from their analytic expressions [25] . Square-wave stimuli of 200 mA and 0.5 ms duration were applied to excite the cells at a pacing cycle length of 1000 ms.

3.3.1 Single-cell simulations

Because the ventricular wall is composed of three distinct cell types: epicardial, M-cells, and endocardial cells, we first modelled each cell type individually. G_{to} values in each layer ($G_{to,endo}$, $G_{to,mcell}$ and $G_{to,epi}$) were chosen based on transmural experimental data. As in our previous work, the nominal RV epicardial G_{to} value was set to 1.1 mS/µF [24]. The midmyocardial and endocardial G_{to} values were set to $G_{to,mcell}$ = 0.935 mS/µF and $G_{to,endo}$ = 0.0 mS/µF based on experimental studies [21, 24, 26] and similar to the $G_{to,mcell}$ to $G_{to,epi}$ ratio used by Gima et al [27].

The M-cells display longer APDs, relative to endocardial or epicardial APDs, in guinea pigs [17], humans[16] and dogs [20, 28]. The prolongation of the

M-cell AP has been attributed to a decrease in I_{Ks} in canine myocytes [20]. To account for that, we multiplied the delayed rectifier current by a scaling parameter, M_G_K. M_G_K was set to 1.0 for endocardial and epicardial cells and 0.24 for midmyocardial cells based on experimental data [20].

These adjustments for the epicardium, midmyocardium and endocardium produced midmyocardial APD of 137% longer than the epicardial APD in steady state, consistent with APD experimental data that showed an increase of 125-140% [16, 17, 20, 28].

3.3.2 Epicardial G_{to} values

In the RV epicardium there is some evidence of heterogeneity in G_{to} expression [29]; however, the precise G_{to} expression distribution is not known. The canine epicardial LV has been shown to display twice as large I_{to} expression level in the apex than in the base [30]. Additionally, average peak G_{to} density is significantly greater in the canine RV epicardium than in the LV epicardium [29, 31], correlating with a deeper phase 1 notch in the RV [29]. Based on these studies, and the wild type value of RV epicardial G_{to} of 1.1 mS/µF, we explored the epicardial G_{to} range from $G_{to,epi}$=0.0 to 2.9 mS/µF.

3.3.3 One-dimensional cable simulations

Simulated transmural cables were composed of 165 LRd connected cells representing 1.65 cm fiber. Transmural cables were composed of endocardial (cells 1 to 60), midmyocardial (M-cells, cells 61 to 105), and epicardial (cells 106 to 165) cells [27]. Each cell type was modelled incorporating the heterogeneities

of ion channel densities described above. For each cable $G_{to,epi}$ was set to a value between 0.0 and 2.9 mS/μF. Connectivity between the cells was simulated using homogeneous gap junction modeling (g_j = 1.73 μS) for all cells, except for a 5-fold decrease at the M-to-epicardium transition region (cells 104-107) due to a dramatic increase of tissue resistivity that has been observed in the canine ventricular wall in about 10% of the epicardium between the deep sub-epicardium and epicardium [28]. Stimuli were applied to the five end cells, either of the endocardium to simulate normal propagation or of the epicardium to simulate epicardial ectopic activity. As described in Chapter 2, to minimize model transients, we ran single-cell simulations for an endocardial cell, an M-cell, and each epicardial cell ($0 \leq G_{to,epi} \leq 2.9$ mS/μF) for 500 excitations (i.e. 500 s), saved all system variables (gating variables, concentrations, transmembrane potential) and used those as initial conditions for the corresponding cable simulations. Each cable simulation ran for 30 beats. A space step of $\Delta x = 0.01$ cm was used. When analysing the data, we distinguished between transient and stable P2R. Transient P2R was defined as P2R that occurred only in the first beats of the simulation, whereas stable P2R was defined as later occurrences of P2R. Conduction velocity (CV) was calculated in cells 16 to 150. CV, computed from the upstroke occurrence times crossing of -65 mV, was ~52.0 cm/s.

3.3.4 P2R Detection

P2R was detected automatically using a custom algorithm that distinguished between a single AP comprised of an upstroke followed by a deep notch and dome (not P2R) and a morphology of two distinct action potentials (P2R) [1].

3.4 Results

3.4.1 One-dimensional cable simulations

Figure 3.1 shows a few typical transmural cable simulations. While the endocardium and the midmyocardium always produced notch-and-dome action potentials due to a fixed, small G_{to} value, the AP morphology in the epicardium varied between simulations according to its G_{to} value. Hence, as expected, low and normal values of epicardial G_{to} produced the normal notch-and-dome morphology in the epicardium (panel A(1)) and high values of epicardial G_{to} produced abbreviated APs with the loss-of-dome morphology (panel A(4)), because the outward current (I_{to}) overwhelmed the inward currents (I_{Na} and $I_{Ca,L}$). However, when the epicardial G_{to} was between 1.3 and 1.6 mS/μF (panels A(2) and A(3)), the epicardium displayed both the loss-of-dome and notch-and-dome morphologies, where the APs switched intermittently between the two morphologies. Panel B shows the G_{to} distribution for each subplot of A. These results fully correlate with the switching behaviour (SB) that was defined for single cells in Chapter 2. The SB range is defined as the range of G_{to} values where APs switch morphologies ($1.25 \leq G_{to} \leq 1.65$ mS/μF). The frequency of prolonged morphology in the epicardium versus that of abbreviated morphology varied depending on the G_{to} value, with more long APs occurring when $G_{to,epi}$ was closer to 1.3 mS/μF and more short epicardial APs occurring when $G_{to,epi}$ was closer to 1.6 mS/μF. Notably, similar switching between these two morphologies was observed in single cells in dynamic clamp experiments when the G_{to} value of the transition level between the two morphologies was “injected” into canine myocytes

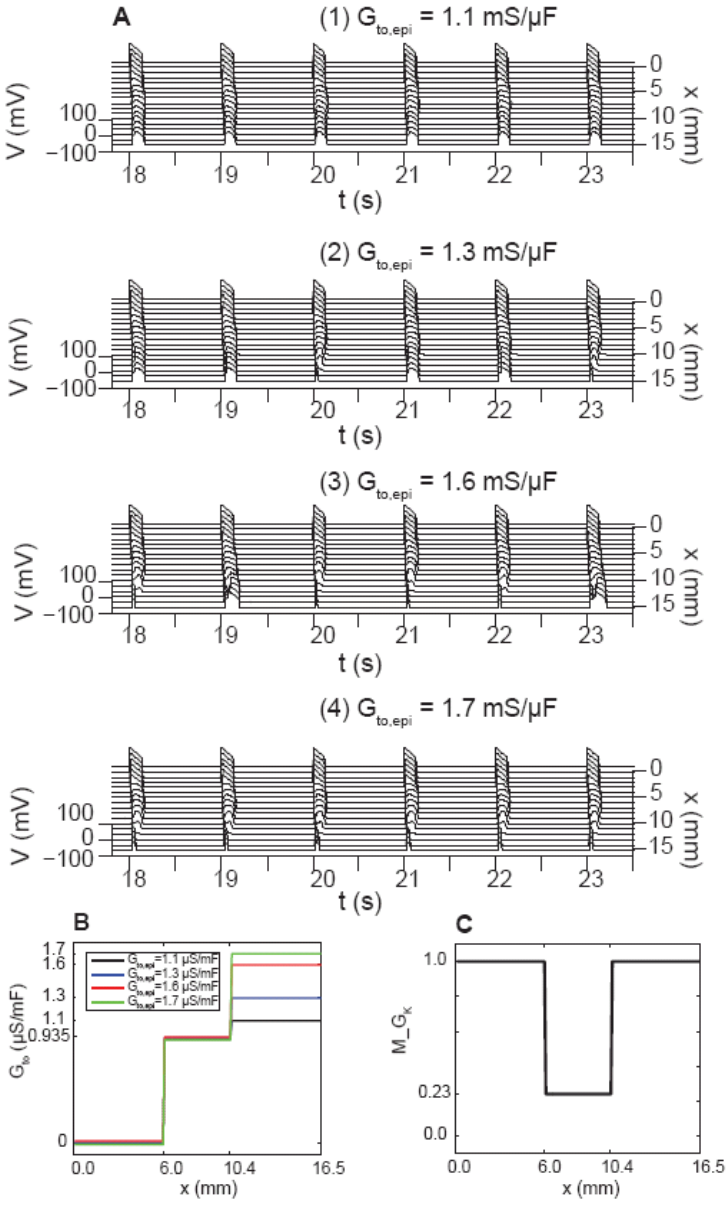

Figure 3.1 A: Transmural cable simulations with endocardial stimulation and selected epicardial G_{to} values ($G_{to,endo}$=0.0 and $G_{to,mcell}$= 0.935 mS/μF). (1) When $G_{to,epi}$ was sufficiently small, all epicardial APs were notch-and-dome. (2),(3) For intermediate $G_{to,epi}$ levels, epicardial APs switched between the prolonged AP notch-and-dome morphology and the abbreviated loss-of-dome morphology. (4) High $G_{to,epi}$ values produced only the loss-of-dome morphology in the epicardium. **B:** G_{to} values along the cable consisting of three layers: endocardium x<6 mm, midmyocardium 6≤x≤10.4 mm and epicardium x>10.4 mm. **C:** M_G_K for the three different layers as in (B). M_G_K=1.0 in the endocardium and epicardium. M_G_K=0.238684 in the midmyocardium.

[32]. In addition, single-cell simulations reported in Chapter 2 showed the same effect.

3.4.2 Endocardial excitation

In order to reach a better understanding regarding the mechanism underlying P2R in the transmural direction, we carried out simulations in which we systematically changed the epicardial G_{to} value. Figure 3.2 displays results of cable simulations where $G_{to,epi}$ was varied between 0.0 and 2.9 mS/μF. In the figure, for each simulation, the percentage of beats in which P2R occurred is presented. Figure 3.2A displays the results where endocardial stimulation was applied to the cables. When $G_{to,epi}$ was less than the SB range ($G_{to,epi}$ < 1.3 mS/μF) P2R did not occur, because the epicardium manifested only the notch-and-dome morphology (which bordered the same morphology in the midmyocardium). An example of a cable having such dynamics is shown in Figure 3.3A. Figure 3.3A(1) displays a cable simulation of the wild-type case, where $G_{to,epi}$=1.1 mS/μF. The prolongation of the AP in the midmyocardium is noticeable, while the epicardium displayed only notch-and-dome APs. Figure 3.3A(2) shows a magnified view of the last beat of the simulation. Figure 3.3A(3) shows the APDs along the cable, depicting the prolongation of the midmyocardial AP.

For cables with $G_{to,epi}$≥2.0 mS/μF, P2R did not occur or occurred only transiently (Figure 3.2A). Figure 3.3C depicts a representative simulation. Figure 3.3C(1) shows results of a cable simulation with $G_{to,epi}$ = 2.0 mS/μF. The epicardium displayed only the loss-of-dome morphology. The APs in the

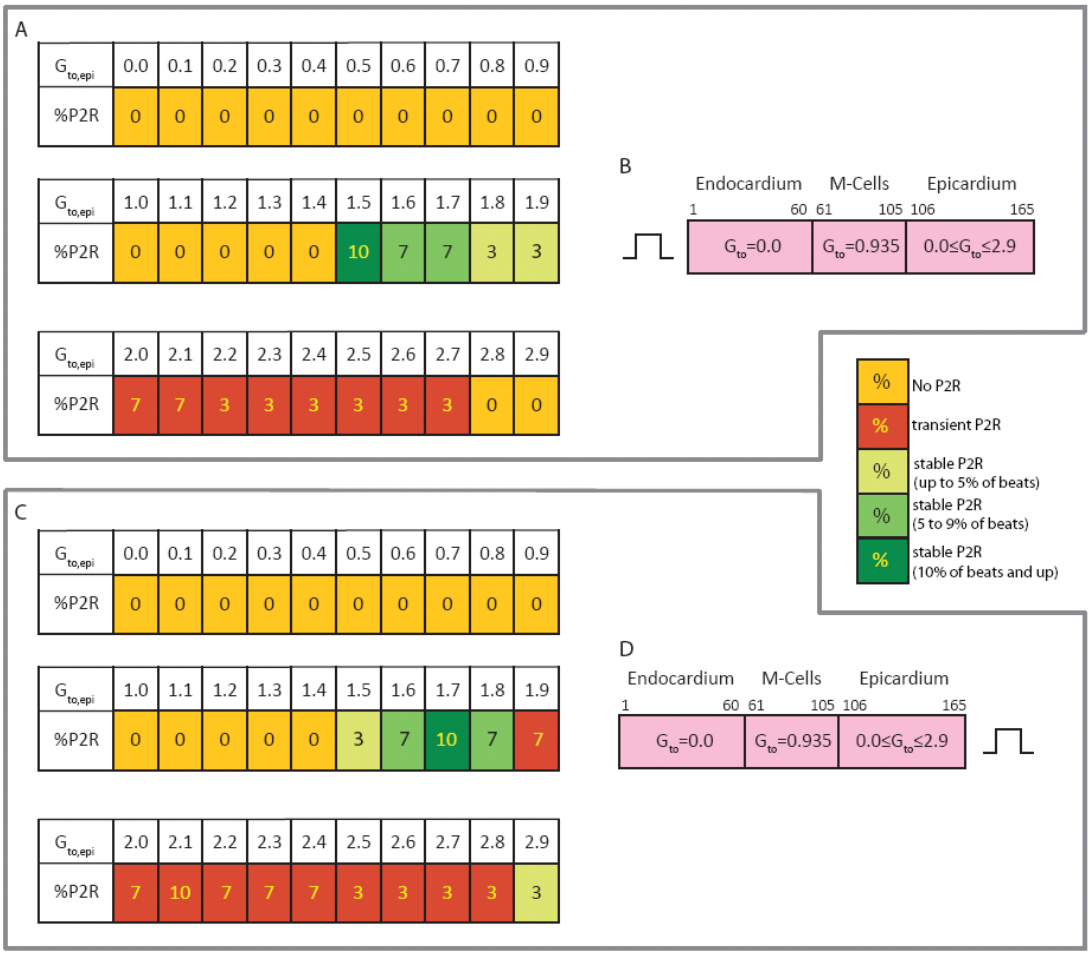

Figure 3.2 Simulation results for transmural cables where epicardial G_{to} was varied systematically between 0.0 and 2.0 mS/µF. **A:** Stimulation was applied at the endocardium. First row indicates $G_{to,epi}$. Second row indicates the percentage of beats that manifested phase-2 reentry. Yellow represents simulations in which phase-2 reentry did not occur and red represents simulations where phase-2 reentry occurred only transiently. Three shades of green colors represent simulations where phase-2 reentry happened in less than 5%, 5%-9%, and more than 9% of the beats, respectively. **B:** Schematic representation of the transmural cables. G_{to} values in each layer are shown. **C:** Results of another set of transmural cable simulations where the stimuli were given in the epicardium. **D:** Schematic representation of the transmural cables.

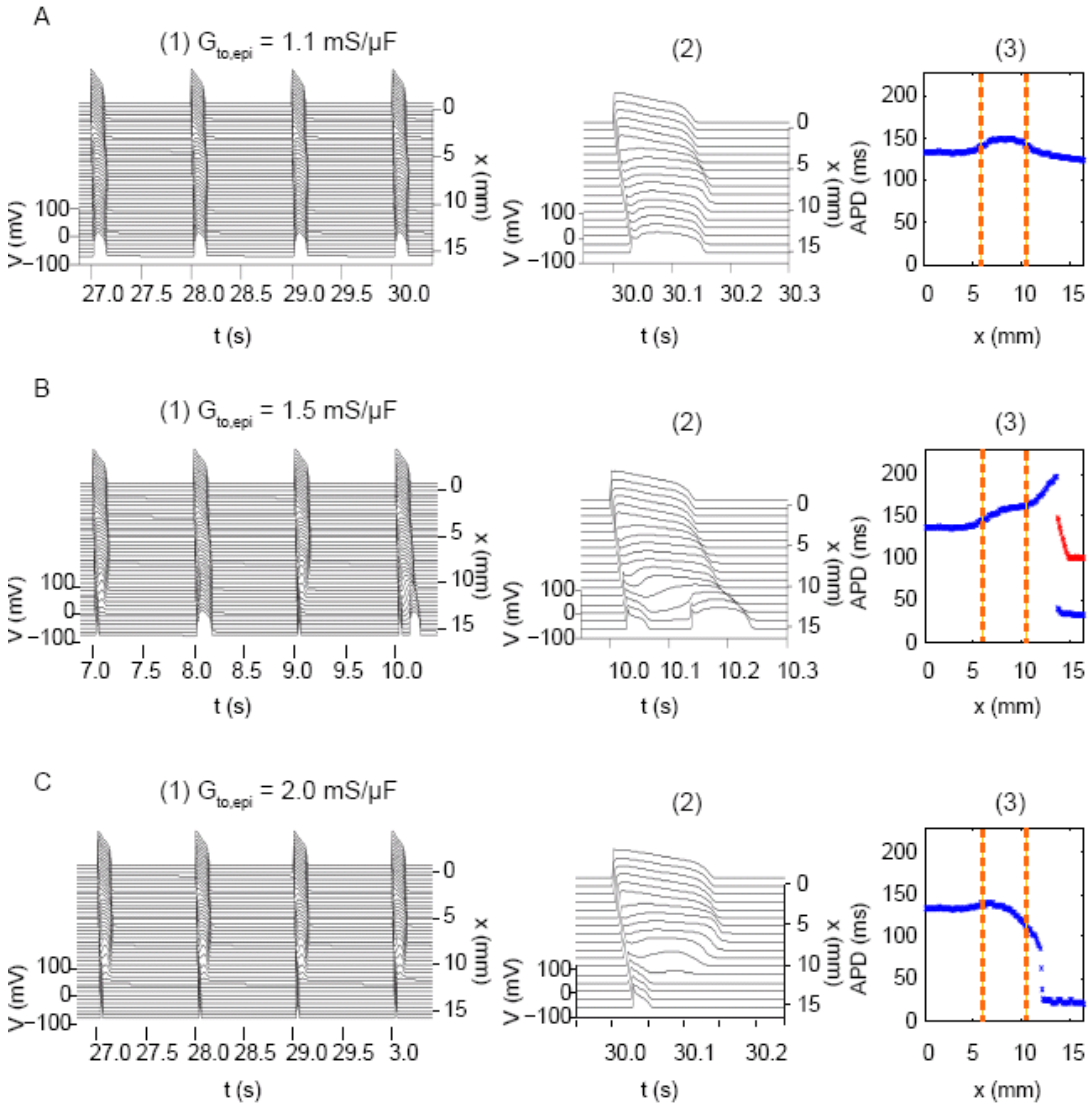

Figure 3.3 Endocardially stimulated transmural cable simulations. First column displays a few beats for each simulation. Second column displays a magnified view of one of the beats from the first column. APD along the cable is presented in the third column; dashed lines represent the border between the different layers. **A:** $G_{to,epi}$=1.1 mS/µF, all APs along the cable are of the notch-and-dome morphology. No phase-2 reentry occurred. **B:** $G_{to,epi}$=1.5 mS/µF caused alternating epicardial AP morphology. Phase-2 reentry occurred on the 10th beat of the simulation. **C:** $G_{to,epi}$ = 2.0 mS/µF, epicardial APs are loss-of-dome. No phase-2 reentry occurred.

midmyocardium-epicardium transition zone changed gradually between the midmyocardial notch-and-dome APs and the epicardial loss-of-dome APs (Figure 3.3C(2)). Epicardial APs were short and stable. Figure 3.3C(3) shows the gradual decrease in APD along the cable.

Stable P2R occurred only for simulations in which $G_{to,epi}$ was within or close to the SB range ($1.5<=G_{to,epi}<=1.9$ mS/μF), as seen in Figure 3.2A. In these simulations the epicardium manifested the notch-and-dome morphology in some beats and the loss-of-dome morphology in others. Figure 3.3B(1) shows an example where $G_{to,epi}=1.5$ mS/μF. The epicardium manifested both morphologies (notch-and-dome at t=7.0, 9.0 s and the loss-of-dome at t=8.0 s). However, on the 10^{th} beat of the simulation (Figure 3.3B(2)), P2R occurred, with the beginning of the epicardium (where it borders the midmyocardium) manifesting a prolonged notch-and-dome morphology and the end of the epicardium (where the end of the cable is) manifesting the loss-of-dome morphology. The prolonged notch-and-dome morphology in the beginning of the epicardium was likely due both to intrinsic electrophysiological behavior (due to $G_{to,epi}$ within the SB range) and electrotonic current propagating down/up the cable. This created a deeper notch that delayed the dome phase. When the AP propagated down the cable, the notch became deeper until the outward current (i.e. I_{to}) overwhelmed the inward currents (i.e., I_{Na} and $I_{Ca,L}$), at which point a loss-of-dome morphology occurred. This loss-of-dome created a situation where the prolonged morphology bordered the abbreviated morphology and provided a substrate for P2R development. Next, phase-2 current from the beginning of the epicardium propagated down the cable, reexcited the epicardium and caused phase-2 reentry.

3.4.3 Epicardial excitation

Simulations where the cable was excited from its epicardial end are summarized in Figure 3.2C. The results are similar to the endocardial stimulation results (Figure 3.2A). P2R did not occur when $G_{to,epi}$ was below the SB range ($G_{to,epi}$ < 1.3 mS/µF). P2R happened transiently for larger values of $G_{to,epi}$ (1.9≤$G_{to,epi}$≤2.8 mS/µF).

Stable P2R occurred when $G_{to,epi}$ was within or close to the SB range (1.5≤$G_{to,epi}$≤1.8 mS/µF). A detailed example is shown in Figure 3.4A. Since $G_{to,epi}$ was within the SB range ($G_{to,epi}$=1.6 mS/µF), different APs manifested either the notch-and-dome (t=10.0 s) or the loss-of-dome (t=11.0, 12.0 s) morphology in the epicardium. At t=13.0 s the epicardium manifested the loss-of-dome morphology at the end of the cable. When it reached the epicardium-midmyocardium transition zone, the AP morphology changed to notch-and-dome due to electrotonic current arriving from the midmyocardium. This created a situation where the two morphologies bordered each other, such that current from the dome phase of the long morphology propagated back down the cable and reexcited the epicardium.

In addition to the P2R that occurred when $G_{to,epi}$ was in or close to the SB range, there was one outlier occurrence of P2R. Figure 3.4B(1) shows some beats of a cable simulation with $G_{to,epi}$=2.9 mS/µF. Reentry occurred on the second beat of the simulation (Figure 3.4B(2)). The epicardial stimulation and the short epicardial APD (due to high $G_{to,epi}$) facilitated fast full recovery in the area of the epicardium that manifested the loss-of-dome morphology. Therefore

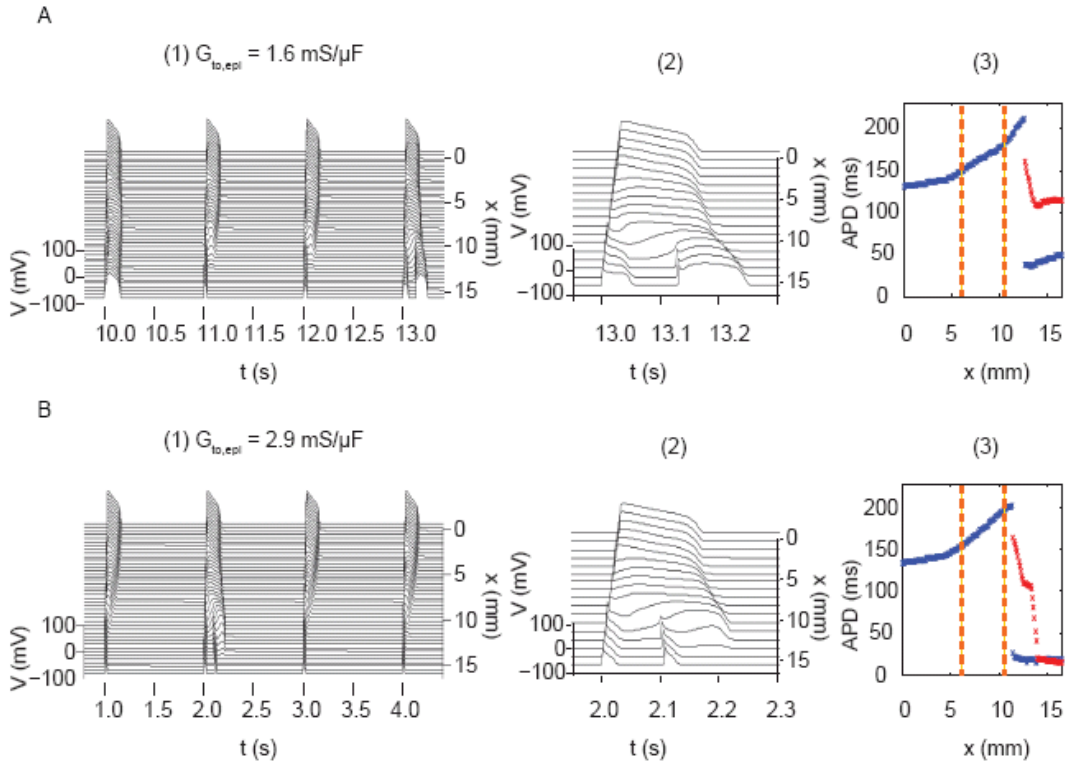

Figure 3.4 Epicardially stimulated transmural cable simulations. First column displays a few beats for each simulation. Second column displays a magnified view of one of the beats from the first row. APD along the cable is presented in the third column; dashed lines represent the border between the different layers. **A:** $G_{to,epi}$=1.6 mS/µF, $G_{to,epi}$ was within the SB range, therefore epicardial APs alternated. P2R occurred on the 13th beat. **B:** $G_{to,epi}$=2.9 mS/µF. P2R occurred on the 2nd beat.

reexcitation occurred at the epicardium closer to the midmyocardium (cell 108 in Figure 3.4B(3) versus cell 125 in Figure 3.4A(3)). Further prolongation of the midmyocardial APs may have been facilitated by retrograde current originating from P2R occurrence. Due to high $G_{to,epi}$ values, both the primary excitation and re-excitation manifested the loss-of-dome morphology.

3.5 Discussion

We found that P2R in the transmural direction is strongly facilitated by epicardial switching behavior, in which epicardial cells spontaneously switch between the notch-and-dome and loss-of-dome AP morphologies. Such behavior creates the substrate in which the epicardium could manifest both AP morphologies in the same beat; the prolonged notch-and-dome at the M-cell border (due to high midmyocardial electrotonic current) and the loss-of-dome morphology at the end of the epicardium (due to intrinsic properties). This creates a condition where the notch-and-dome morphology borders the loss-of-dome morphology and could therefore trigger phase-2 reentry. Moreover, we found that, typically, the existence of the two morphologies, the long notch-and-dome in the midmyocardium and the abbreviated loss-of-dome in the epicardium, was not sufficient by itself to trigger P2R (i.e., without switching instability).

Dispersion of repolarization in the epicardium has been previously attributed to be an arrhythmogenic risk factor. Alternating loss of the epicardial AP dome produced P2R in a Brugada model used in an investigation of T-wave alternans [2]. In addition, epicardial dispersion of repolarization was shown to be

the primary factor that induced P2R in studies of the canine RV [5] and in canine RVOT [3]. Also, in a recent modeling study, we found that switching behavior in the epicardium was found to be a key factor in P2R development in the epicardium [1].

3.5.1 Transmural phase-2 reentry mechanism

While the endocardium and the midmyocardium always manifested notch-and-dome AP morphologies, the epicardial AP morphology varied between simulations according to its G_{to} value. In all cables, P2R originated from the epicardium if both morphologies were present concurrently. This facilitated a condition within the epicardium where a prolonged notch-and-dome morphology bordered the loss-of-dome morphology. In such a case, phase-2 reentry occurred due to electrotonic current that propagated from phase 2 of the prolonged morphology to recovered tissue. This held true for either endocardial or epicardial stimulation.

The cellular explanation for the prolonged morphology in the midmyocardial side of the epicardium is consistent with the mechanism of APD prolongation and P2R in epicardial cables [1]. Specifically, the prolongation of the AP in this particular region of the cable was due to high electrotonic current propagating from the midmyocardium, combined with high extracellular calcium concentration ($[Ca^{2+}]_o$). The high extracellular calcium concentration facilitated the prolonged notch (and therefore prolonged APD) by increasing $I_{Ca,L}$. $[Ca^{2+}]_o$ changed during the simulation since it was highly dependent on AP morphology. During a notch-and-dome morphology, Ca^{2+} enters the cell

throughout the dome phase; thus, $[Ca^{2+}]_o$ decreases. However, during the loss-of-dome AP, $[Ca^{2+}]_o$ does not decrease much, facilitating an increased driving force for $I_{Ca,L}$ in the beginning of the next beat and creating prolonged morphology [1]. Therefore, the prolonged morphology in the beginning of the epicardium occurred only intermittently, according to its dependence on both $[Ca^{2+}]_o$ and the electrotonic current.

3.5.2 M-cell distribution

The distribution and location of the M-cells in the myocardium is controversial and a topic of several recent studies. In canine left and right ventricles, M-cell zones appeared within the mid-wall region in various thicknesses [15, 33, 34]. In some experiments, areas of M cell were interrupted by areas of cells manifesting AP with shorter APD and in other experiments, M cell regions has the appearance of circular islands [34]. Additionally, evidence has suggested that the anatomical distribution of M cell regions within the ventricular wall is not restricted only to midmyocardial layers [34]. Given this animal data, there has been great interest in investigating M cells in human hearts. However, in vivo data from patients undergoing coronary artery surgery showed no prolongation of the midmyocardial APD [35]. Furthermore, Langendorff-perfused explanted human hearts displayed no midmyocardial APD peak [35]. Also, explanted human wedge preparations showed no indication of a significant transmural dispersion of repolarization [35]. The absence of M-cell evidence to date in the human heart might be because M cells do not exist in the human heart, or that they are electrophysiologically hidden due to intercellular coupling smoothing the M-cell APD [35]. In a different study of the human ventricular wall [16], however, three cell subtypes were identified,

providing evidence of M-cell APD inhomogeneity in normal human hearts. In this study, the midmyocardial APD was prolonged in about 100 ms relative to epicardial and endocardial APD [16]. It is difficult to reconcile the significant differences in findings between these studies; one possibility is that they might be due to differences in experimental methods e.g. anesthetic drug usage that blocks late I_{Na} and therefore preferentially abbreviates the action potential of the M cells and reduces transmural heterogeneities [36].

3.5.3 P2R incidence in the transmural direction versus the epicardial direction

It is worthwhile to compare the incidence of P2R in the transmural (this chapter) and epicardial (Chapter 2) directions. The simulations in each direction were executed in an analogous manner, including usage of the same single cell model, similar initial conditions, and epicardial G_{to} values. The major differences between the simulations were threefold. First, epicardial cable models consisted of 300 grid points while transmural simulations had 165 grid points. Second, the macroscopic conductance of I_{Ks} was reduced in the midmyocardium of transmural simulations while in epicardial simulations it remained constant throughout the cables. Third, epicardial cable simulations were composed of continuous gradients of G_{to} based on linear, piece-wise linear, and Boltzmann function distributions, while transmural cable simulations had inherent (i.e., based on experimentally quantified values) G_{to} discontinuities between the endocardium, midmyocardium and epicardium. Despite these differences, here we present a qualitative comparison between transmural and epicardial P2R occurrences.

When comparing endocardially excited transmural cable simulations to epicardial cable simulations, it is most informative to examine the simulations with G_{to} values based on a Boltzmann distribution with $G_{to,proximal}$ = 0.5 mS/µF. The reason is that in both simulations sets (Figure 3.2.A and Figure 2.5.A), the beginning of the cable APs had the long morphology and the end of the cable APs were a function of the G_{to} value. In both sets, P2R did not happen when G_{to} at the end of the cable ($G_{to,epi}$ in transmural simulations and $G_{to,distal}$ in epicardial simulations) was below the switching behavior range. Also, when G_{to} at the end of the cable was high, P2R happened only transiently in both sets. When G_{to} was within the SB range or close to it, P2R happened in both types of simulations. The rate of P2R occurrences was similar in both directions.

When comparing epicardially excited transmural cable simulations to epicardial cable simulations, we believe that the epicardial cable simulations having G_{to} values based on a Boltzmann distribution with $G_{to,distall}$=0.5 mS/µF are the most relevant. Qualitatively, the results are similar between the two sets of simulations and are also similar to the previous comparison. However, when G_{to} at the beginning of the cable was within or close to the SB range, the rate at which P2R happened in the epicardial direction was higher than the rate of P2R occurrences in the corresponding transmural simulations. This may be due to differences in AP morphology at the cable ends in each set and the reduction in the conductance in the M-to-epicardium transition region (only in the transmural simulations).

3.5.4 Study limitations

First, as the precise location and distribution of M cells within the ventricular wall in the right ventricle is still unknown, modeling of the midmyocardium homogenously as composed only of M cells is an oversimplification of the system. Second, because the exact range of epicardial G_{to} in the RV is unknown, a broad range of G_{to} values was used. Third, we investigated only one ventricular model and one basic cycle length (1000 ms; chosen because most Brugada related episodes occur during rest). Further studies are needed to address rate and model dependence. When G_{to} expression pattern data of the RV epicardium become available, they could be integrated into the model. Despite these limitations, we believe that this study of the transmural direction, together with our previous study investigating the epicardial direction, shed light on the underlying dynamics and offer insight into the basic mechanism of phase-2 reentry arrhythmogeneity.

3.6 Conclusion

We found that P2R can occur in the transmural direction and is facilitated both by the presence of different AP morphologies in distinct transmural layers and by the switching AP morphology in the epicardium, where cells switch intermittently between the notch-and-dome and loss-of-dome morphologies and trigger phase-2 reentry. These findings are consistent with our previous results regarding P2R in the epicardial direction. Accordingly, our findings suggest that such switching

behavior may be one of the bases for the development of phase-2 reentry in cardiac tissue.

REFERENCES

1. Maoz, A., T. Krogh-Madsen, and D.J. Christini, *Instability in action potential morphology underlies phase 2 reentry: a mathematical modeling study.* Heart Rhythm, 2009. **6**(6): p. 813-22.
2. Fish, J.M. and C. Antzelevitch, *Cellular mechanism and arrhythmogenic potential of T-wave alternans in the Brugada syndrome.* J Cardiovasc Electrophysiol, 2008. **19**(3): p. 301-8.
3. Morita, H., et al., *Repolarization heterogeneity in the right ventricular outflow tract: correlation with ventricular arrhythmias in Brugada patients and in an in vitro canine Brugada model.* Heart Rhythm, 2008. **5**(5): p. 725-33.
4. Kimura, M., et al., *Mechanism of ST elevation and ventricular arrhythmias in an experimental Brugada syndrome model.* Circulation, 2004. **109**(1): p. 125-31.
5. Aiba, T., et al., *Cellular basis for trigger and maintenance of ventricular fibrillation in the Brugada syndrome model: high-resolution optical mapping study.* J Am Coll Cardiol, 2006. **47**(10): p. 2074-85.
6. Fish, J.M., et al., *Dimethyl lithospermate B, an extract of Danshen, suppresses arrhythmogenesis associated with the Brugada syndrome.* Circulation, 2006. **113**(11): p. 1393-400.
7. Zimmer, T. and R. Surber, *SCN5A channelopathies--an update on mutations and mechanisms.* Prog Biophys Mol Biol, 2008. **98**(2-3): p. 120-36.
8. Antzelevitch, C., et al., *Brugada syndrome: from cell to bedside.* Curr Probl Cardiol, 2005. **30**(1): p. 9-54.

9. Cordeiro, J.M., et al., *Accelerated inactivation of the L-type calcium current due to a mutation in CACNB2b underlies Brugada syndrome.* J Mol Cell Cardiol, 2009. **46**(5): p. 695-703.

10. Miyoshi, S., et al., *A mathematical model of phase 2 reentry: role of L-type Ca current.* Am J Physiol Heart Circ Physiol, 2003. **284**(4): p. H1285-94.

11. Miyoshi, S., et al., *Link between SCN5A mutation and the Brugada syndrome ECG phenotype: simulation study.* Circ J, 2005. **69**(5): p. 567-75.

12. Petitprez, S., et al., *Analyses of a novel SCN5A mutation (C1850S): conduction vs. repolarization disorder hypotheses in the Brugada syndrome.* Cardiovasc Res, 2008. **78**(3): p. 494-504.

13. Ramanathan, C., et al., *Activation and repolarization of the normal human heart under complete physiological conditions.* Proc Natl Acad Sci U S A, 2006. **103**(16): p. 6309-14.

14. Durrer, D., et al., *Total excitation of the isolated human heart.* Circulation, 1970. **41**(6): p. 899-912.

15. Sicouri, S. and C. Antzelevitch, *A subpopulation of cells with unique electrophysiological properties in the deep subepicardium of the canine ventricle. The M cell.* Circ Res, 1991. **68**(6): p. 1729-41.

16. Drouin, E., et al., *Electrophysiologic characteristics of cells spanning the left ventricular wall of human heart: evidence for presence of M cells.* J Am Coll Cardiol, 1995. **26**(1): p. 185-92.

17. Sicouri, S., M. Quist, and C. Antzelevitch, *Evidence for the presence of M cells in the guinea pig ventricle.* J Cardiovasc Electrophysiol, 1996. **7**(6): p. 503-11.

18. Viswanathan, P.C., R.M. Shaw, and Y. Rudy, *Effects of IKr and IKs heterogeneity on action potential duration and its rate dependence: a simulation study.* Circulation, 1999. **99**(18): p. 2466-74.

19. Liu, D.W., G.A. Gintant, and C. Antzelevitch, *Ionic bases for electrophysiological distinctions among epicardial, midmyocardial, and endocardial myocytes from the free wall of the canine left ventricle.* Circ Res, 1993. **72**(3): p. 671-87.

20. Liu, D.W. and C. Antzelevitch, *Characteristics of the delayed rectifier current (IKr and IKs) in canine ventricular epicardial, midmyocardial, and endocardial myocytes. A weaker IKs contributes to the longer action potential of the M cell.* Circ Res, 1995. **76**(3): p. 351-65.

21. Li, G.R., et al., *Transmural heterogeneity of action potentials and Ito1 in myocytes isolated from the human right ventricle.* Am J Physiol, 1998. **275**(2 Pt 2): p. H369-77.

22. Viswanathan, P.C. and Y. Rudy, *Cellular arrhythmogenic effects of congenital and acquired long-QT syndrome in the heterogeneous myocardium.* Circulation, 2000. **101**(10): p. 1192-8.

23. Luo, C.H. and Y. Rudy, *A dynamic model of the cardiac ventricular action potential. I. Simulations of ionic currents and concentration changes.* Circ Res, 1994. **74**(6): p. 1071-96.

24. Dumaine, R., et al., *Ionic mechanisms responsible for the electrocardiographic phenotype of the Brugada syndrome are temperature dependent.* Circ Res, 1999. **85**(9): p. 803-9.

25. Rush, S. and H. Larsen, *A practical algorithm for solving dynamic membrane equations.* IEEE Trans Biomed Eng, 1978. **25**(4): p. 389-92.

26. Wettwer, E., et al., *Transient outward current in human ventricular myocytes of subepicardial and subendocardial origin.* Circ Res, 1994. **75**(3): p. 473-82.

27. Gima, K. and Y. Rudy, *Ionic current basis of electrocardiographic waveforms: a model study.* Circ Res, 2002. **90**(8): p. 889-96.

28. Yan, G.X., W. Shimizu, and C. Antzelevitch, *Characteristics and distribution of M cells in arterially perfused canine left ventricular wedge preparations.* Circulation, 1998. **98**(18): p. 1921-7.

29. Di Diego, J.M., Z.Q. Sun, and C. Antzelevitch, *I(to) and action potential notch are smaller in left vs. right canine ventricular epicardium.* Am J Physiol, 1996. **271**(2 Pt 2): p. H548-61.

30. Szentadrassy, N., et al., *Apico-basal inhomogeneity in distribution of ion channels in canine and human ventricular myocardium.* Cardiovasc Res, 2005. **65**(4): p. 851-60.

31. Volders, P.G., et al., *Repolarizing K+ currents ITO1 and IKs are larger in right than left canine ventricular midmyocardium.* Circulation, 1999. **99**(2): p. 206-10.

32. Sun, X. and H.S. Wang, *Role of the transient outward current (Ito) in shaping canine ventricular action potential--a dynamic clamp study.* J Physiol, 2005. **564**(Pt 2): p. 411-9.

33. Yang, X.C., P. Zhou, and C.L. Li, *Electrical heterogeneity of canine right ventricular transient outward potassium currents.* Chin Med J (Engl), 2004. **117**(4): p. 528-31.

34. Akar, F.G., et al., *Unique topographical distribution of M cells underlies reentrant mechanism of torsade de pointes in the long-QT syndrome.* Circulation, 2002. **105**(10): p. 1247-53.

35. Conrath, C.E., et al., *Intercellular coupling through gap junctions masks M cells in the human heart.* Cardiovasc Res, 2004. **62**(2): p. 407-14.

36. Antzelevitch, C. and J. Fish, *Electrical heterogeneity within the ventricular wall.* Basic Res Cardiol, 2001. **96**(6): p. 517-27.

CHAPTER 4

PHASE-2 REENTRY DEVELOPMENT IN TWO-DIMENSIONAL TRANSMURAL TISSUE

4.1 Abstract

BACKGROUND Phase-2 reentry (P2R) is a local arrhythmogenic phenomenon where phase-2 electrotonic current propagates from a notch-and-dome action potential region to a loss-of-dome action potential region. It is hypothesised that P2R can occur both along the epicardium layer or transmurally through the ventricular wall. However little is known about the initiation and development of P2R in two-dimensional transmural tissue.

OBJECTIVE The purpose of the work described in this chapter was to investigate P2R development in two-dimensional transmural tissues and to explore whether P2R expands and creates macroscopic reentry.

METHODS The Luo-Rudy dynamic model was modified to simulate action potentials originating from the endocardium, midmyocardium and epicardium. Two-dimensional tissues were composed of 300x165 grid points representing a 3 cm length of tissue along the endocardium, midmyocardium and epicardium and 1.65 cm in the transmural direction. To represent hypothesized intrinsic right ventricular ionic heterogeneity, different linear G_{to} gradients were investigated.

RESULTS We found that P2R could be arrhythmogenic in two-dimensional tissue and could approximately double the time from excitation to full repolarization relative to normal propagation.

CONCLUSION P2R can cause abnormal propagation and reentry in two-dimensional transmural tissues. A notable increase in P2R incidence in two-dimensional transmural simulations compared to one-dimensional epicardial and transmural simulations was demonstrated.

4.2 Introduction

Phase-2 reentry (P2R) is a local arrhythmogenic phenomenon where phase-2 electrotonic current propagates from a notch-and-dome action potential region to a loss-of-dome action potential region. P2R has demonstrated to occur along the epicardium layer [1-4] or transmurally through the ventricular wall [5] as described in chapter 2. However, little is known about the initiation and development of P2R in two-dimensional transmural tissues.

Computational studies of one-dimensional epicardial and transmural P2R, as presented in Chapters 2 and 3, showed the contribution of the switching behavior to P2R initiation. P2R developed when action potentials (APs) with a delayed notch (and therefore a prolonged notch-and-dome morphology) bordered APs with the loss of dome morphology. The prolonged notch-and-dome morphology was facilitated by the switching behavior that produced two AP morphologies, the prolonged notch-and-dome morphology and the loss-of-dome

morphology, intermittently. In addition, the loss-of-dome morphology was facilitated by an imbalance of the ionic currents active at the end of phase-1 or the beginning of phase-2 of the AP such that the outward currents overwhelm the inward currents. Both epicardial and transmural P2R studies showed that instability within the epicardium played an important role in P2R initiation consistent with other P2R studies [6-8] . This instability in the epicardium was dependent on the intrinsic properties of epicardial cells as well as on electrotonic current propagating either from the midmyocardium in the transmural case or from other epicardial regions as in the epicardial case.

Experimental studies of P2R have been performed with three-dimensional right ventricular canine tissues perfused with Tyrode's solution containing drug combinations to experimentally mimic ST-segment elevation, the Brugada syndrome phenotype [6, 7]. In both of these studies, high-resolution optical mapping techniques were applied to the endocardial and epicardial surfaces to measure its electrical activity and provide the ability to detect electrical heterogeneity of APs on the two surfaces. However, because the transmural direction was not mapped, no insights regarding the transmural contribution to the initiation of P2R or the propagation of P2R between the two surfaces could be offered.

The purpose of the work described in this chapter was to investigate the mechanism of P2R development in the transmural direction in two-dimensional transmural simulations (Figure 1.7, parallelogram**)** and to explore whether P2R local excitation would die out in two-dimensional tissue or be sufficiently arrhythmogenic to trigger macroscopic reentry. We hypothesized that P2R can

disrupt normal propagation in two-dimensional tissue. We found that P2R could degenerate into macroscopic reentry when occurring on a two-dimensional tissue, creating spiral waves and prolonging the time of tissue excitation. The switching behavior where APs switch intermittently between a prolonged notch-and-dome morphology and loss-of-dome morphology facilitated the reentry initiation.

4.3 Methods

4.3.1 Computational Model and Methods

We used a modified version of the Luo-Rudy dynamic (LRd) model [9] with the L-type calcium current formalism composed by Miyoshi et al [3] and the transient outward current (I_{to}) formalism composed by Dumaine et al [10] similar to the methods described in Chapters 2 and 3. The forward Euler method with a time step of Δt=0.005 ms was used to integrate dV/dt and the ionic concentrations, while the gating variables were computed from their analytic expressions [11] .

Simulations of two-dimensional sheets were composed of 300x165 grid points representing a 3 cm length of tissue along the endocardium, midmyocardium and epicardium and 1.65 cm in the transmural direction (see Figure 4.1D). The endocardium consisted of all cells in rows 1-60, the midmyocardium consisted of rows 61-105 and the epicardium accounted for rows 106-165. Each cell type (epicardial, M-cells, and endocardial) was modelled individually using the same methods described in chapter 3. Briefly, G_{to} values in the endocardium and midmyocardium, $G_{to,endo}$, $G_{to,mcell}$, were 0.0 and 0.935

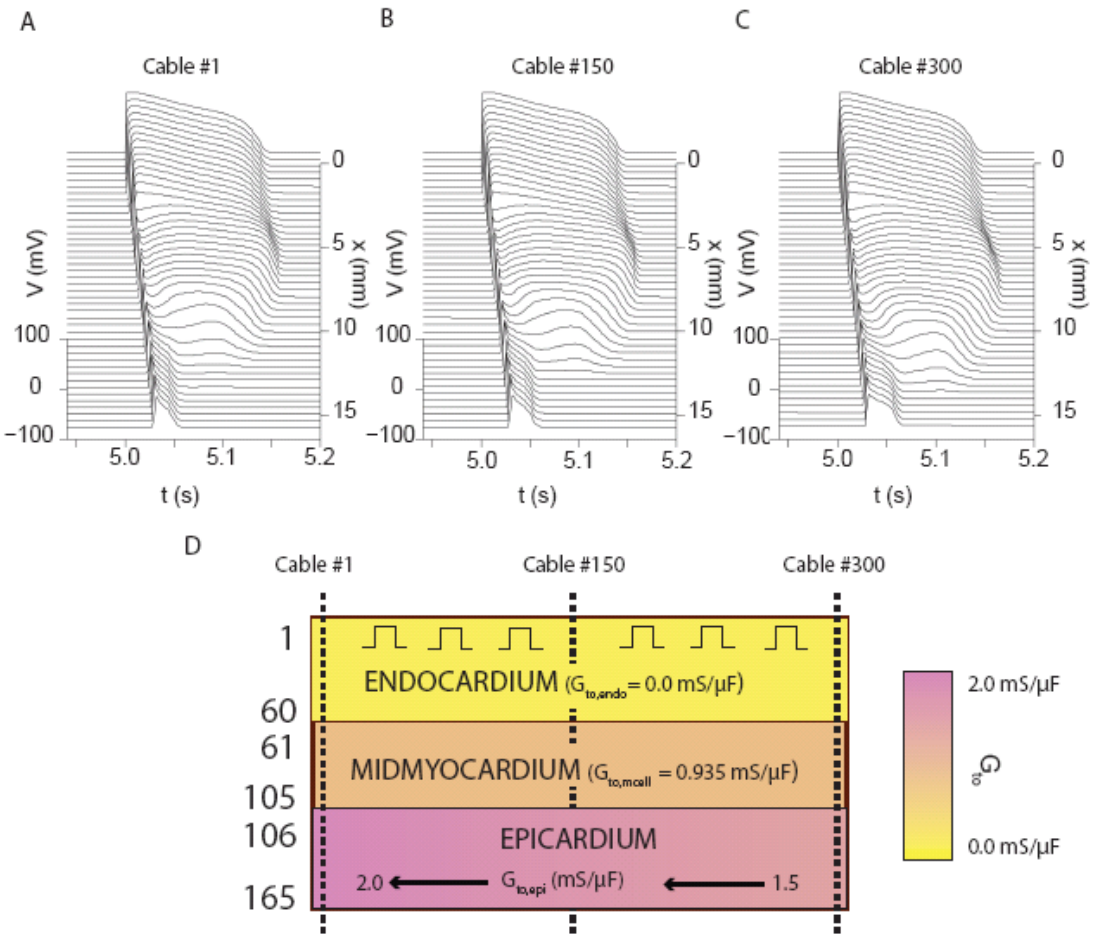

Figure 4.1 APs along virtual cables extracted from the two dimensional simulation in Figure 4.1. Cable locations are as shown in Figure 4.1A, first panel. **A:** AP along cable #1. Notch-and-dome morphology occurred in endocardium and midmyocardium. Loss-of-dome morphology occurred in epicardium due to large G_{to} ($G_{to,epi}$ = 2.0 mS/μF). **B:** AP along cable #150 ($G_{to,epi}$ = 1.75 mS/μF). **C:** AP along cable #300. ($G_{to,epi}$ = 1.5 mS/μF). Epicardial AP is loss-of-dome but longer than that of panel B due to smaller $G_{to,epi}$. **D:** Schematic representation of the 2D tissue. Epicardial G_{to} linear gradient between 1.5 to 2.0 mS/μF is shown. Schematic representations of cable locations are shown by dashed vertical lines.

mS/μF, respectively. Nominal epicardial G_{to}, $G_{to,epi}$, was 1.1 mS/μF. The delayed rectifier's scaling parameter, M_G_K, was 1.0 for endocardial and epicardial cells and 0.24 for midmyocardial cells. Initial condition files were based on single-cell simulations of 500 s. Diffusion was isotropic. Square-wave stimuli of 200 mA and 0.5 ms duration were applied along the endocardium (columns 1-300) to the first five rows (rows 1-5, as shown in Figure 4.1D). Simulation duration was 10 s (10 beats) at a pacing cycle length of 1000 ms. To break the symmetry, continuous ionic epicardial gradients were introduced to the tissue. Specifically, we explored two different epicardial linear G_{to} gradients. One from 1.5 to 2.0 mS/μF and one from 0.0 to 2.0 mS/μF representing plausible G_{to} gradients in the RV. Two-dimensional simulations were coded in C++ and parallelized using OpenMP.

4.4 Results

4.4.1 Linear epicardial G_{to} gradient from 1.5 to 2.0 mS/μF

Two-dimensional simulations, having epicardial G_{to} values distributed linearly from 1.5 to 2.0 mS/μF, were run for 10 beats. Abnormal propagation occurred at some beats of the simulation (1^{st}, 2^{nd}, 6^{th} and the 10^{th}), while the reminder of the beats manifested normal propagation.

Figure 4.2A displays snapshots of membrane potentials of the 5^{th} beat of the simulation, for which regular propagation occurred. The stimulus was delivered at t=5.0 s. At t=5.002 s, the beginning of the endocardium was

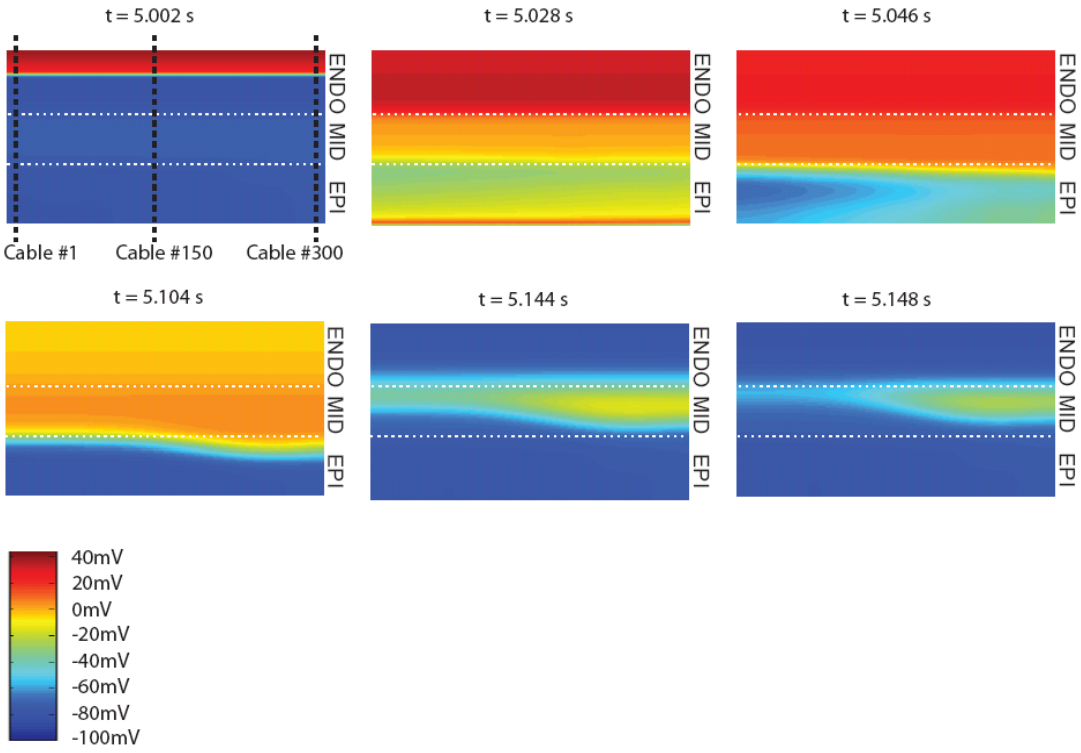

Figure 4.2 Membrane potential snapshots from the 5th beat of a representative two-dimensional tissue simulation. Vertical dashed lines in upper left panel show schematic representation of cables depicted in Figure 4.2. Horizontal dotted lines delineate transmural layers: ENDO (endocardium), MID (midmyocardium) and EPI (epicardium).

depolarized (red) and most of the tissue was not yet excited (blue), as the wavefront propagated from the endocardium toward the midmyocardium and epicardium. At t=5.028 s, the propagation reached the end of the epicardium and the midmyocardium displayed the notch (orange and green colors). The epicardium had shorter loss-of-dome APs, while the endocardium and the midmyocardium had notch-and-dome APs (Figure 4.1A-C). Therefore, the membrane voltage in the epicardium repolarized before the endocardium and midmyocardium (t=5.046 s). Because the epicardium of cable #1 (Figures 4.1) had a higher $G_{to,epi}$ value ($G_{to,epi}$ = 2.0 mS/μF) than the epicardial G_{to} value of cable #300 ($G_{to,epi}$ = 1.5 mS/μF), cable #1 manifested a shorter epicardial AP than cable #300. Hence, repolarization of the epicardium started from the direction of cable #1 (Figure 4.2, t=5.046 s), continuing toward cable #300. Next, the endocardium and midmyocardium began to repolarize (Figure 4.2, t=5.104 s) until full repolarization of the endocardium occurred, by t=5.144 s. Because the midmyocardium had the longest APs (Figure 4.1C), full repolarization occurred there last. At t=5.148 s the midmyocardium was almost fully repolarized. Complete repolarization occurred by t=5.162 s.

Figure 4.3 depicts snapshots of the next AP propagation, which was abnormal. Excitation started normally from the endocardium at t=6.0 s. At t=6.028 s, the propagating AP reached the end of the epicardium, while the midmyocardium APs were of the notch-and-dome morphology type (green and orange colors). Similar to the previous beat, due to the epicardial G_{to} gradient, at t=6.046 s, the epicardium repolarized starting from cable #1. Figure 4.4 shows the APs along four representative virtual cables of the simulation. At this point in time the epicardial APs were loss-of-dome for all cables between cable #1 and cable

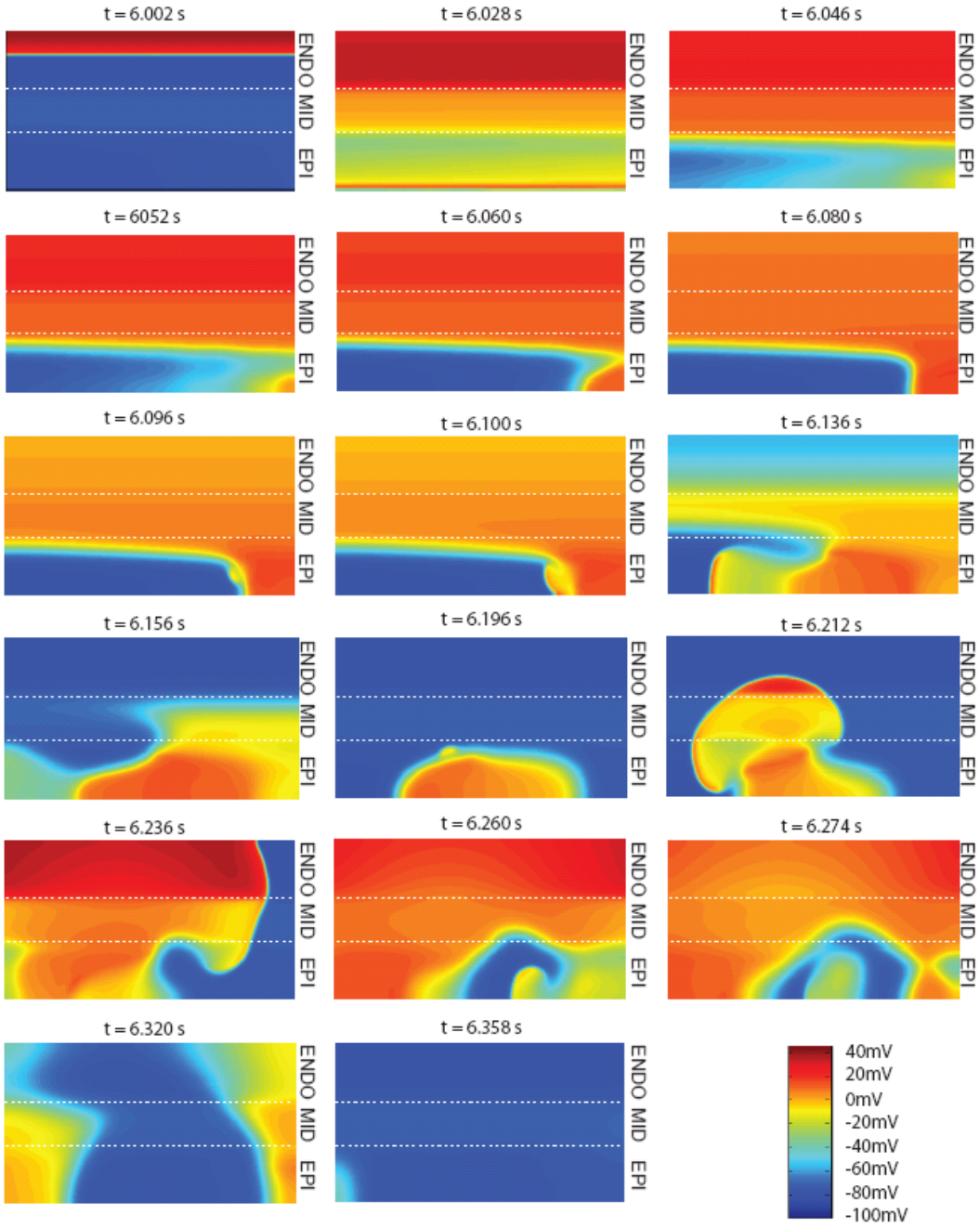

Figure 4.3 Membrane potential snapshots from the 6th beat of a two-dimensional tissue simulation with epicardial G_{to} linear gradient from 1.5 to 2.0 mS/µF. Membrane potential shows abnormal AP propagation and prolongation of excitation. Dashed lines delineate transmural layers: ENDO (endocardium), MID (midmyocardium) and EPI (epicardium).

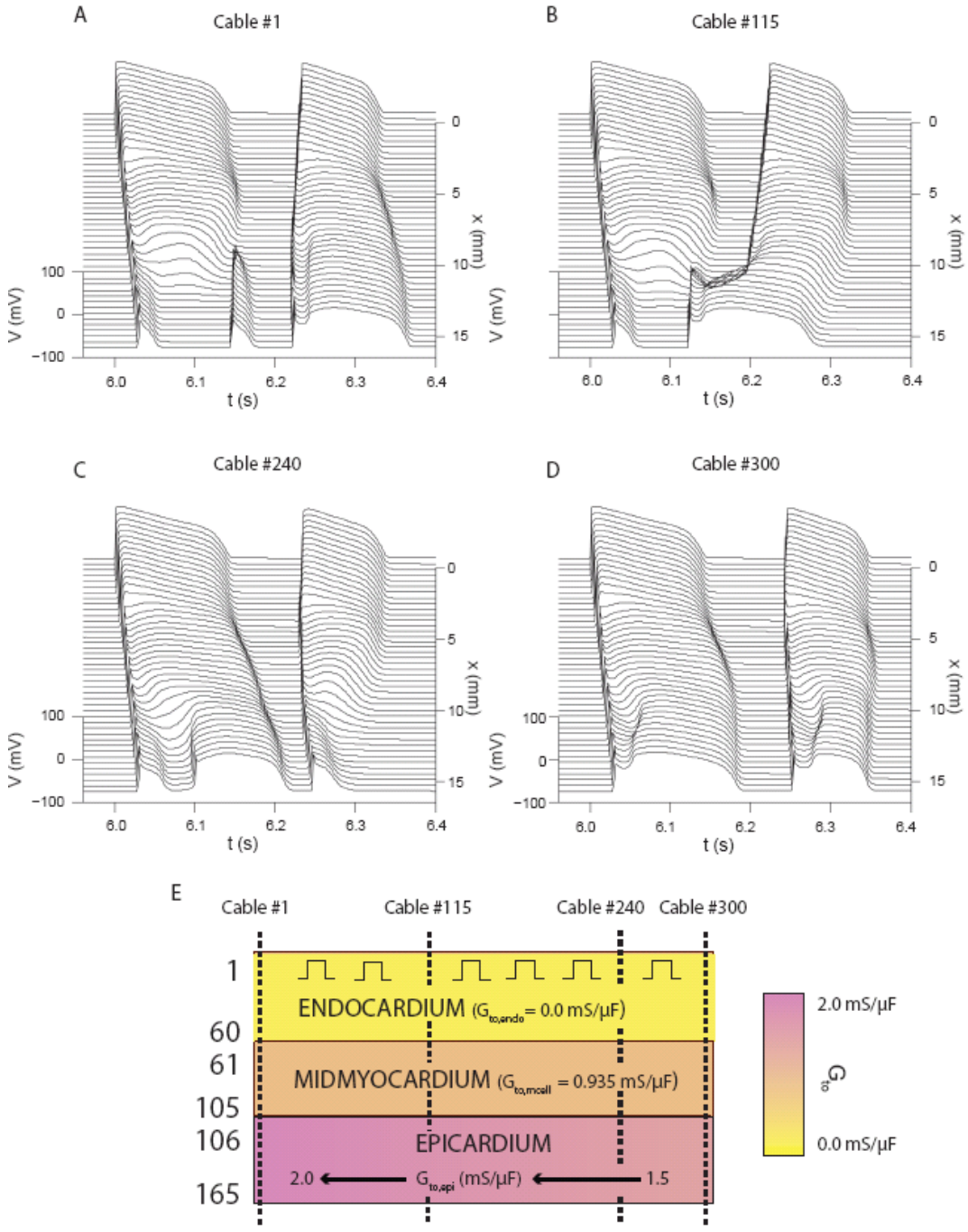

Figure 4.4 APs along virtual cables extracted from the two dimensional simulation in Figure 4.3. **A-D:** AP along cable #1 ($G_{to,epi}$ = 2.0 mS/μF) , #115 ($G_{to,epi}$ = 1.8062 mS/μF), #240 ($G_{to,epi}$ = 1.5937 mS/μF) and #300 ($G_{to,epi}$ = 1.5 mS/μF). See text for details. **E:** Schematic representation of the tissue. Epicardial G_{to} linear gradient between 1.5 to 2.0 mS/μF is shown. Schematic representations of cable locations are shown by dashed vertical lines.

#240 (Figure 4.4A-C). For all other cables (cable #241 to cable #300), the epicardial cells manifested the notch-and-dome morphology (e.g. cable #300, Figure 4.4D). Due to higher $G_{to,epi}$ value ($G_{to,epi}$ = 2.0 mS/μF versus $G_{to,epi}$ = 1.5 mS/μF), cable #1 manifested shorter epicardial APs than cable #300. Hence, repolarization of the epicardium started from cable #1 (t=6.046 s) toward cable #300. At t=6.052 s the epicardium of cable #300 manifested the notch-and-dome morphology (Figures 4.3 and 4D). At t=6.096 s a spiral tip formed as a result of epicardial and/or transmural electrotonic currents; current from phase 2 of cables #241 to #300 propagated horizontally to recovered epicardial regions (cables #1 to #240) and current from the dome phase of midmyocardial cells propagated down the tissue to the epicardium. This created P2R in cable #240, as shown in Figure 4.4C. This re-entrant wave is shown in snapshots of t=6.100 and 6.136 s and also in cable #115 (Figure 4.4B) and cable #1 (Figures 4.4A). At t=6.196 s there was another initiation of a spiral tip, causing abnormal propagation, this time in the transmural direction from the epicardium to the midmyocardium. Current propagated up from the epicardium, creating retrograde P2R (Figure 4.4B). Later, this reentry propagated to the sides of cable #115, such that at t=6.212 s a figure-of-eight occurred. The spiral wave continued to propagate at t=6.237 and 6.260 s. Later, repolarization occurred, starting from the middle of the tissue, where the reentry originated, and continued to the sides (t=6.320 s). At t=6.358 s the tissue was almost fully repolarized. The time from beginning of excitation to full repolarization of the 6^{th} beat was 362 ms, while the normal propagation, as shown in the beat before, took only 162 ms.

4.4.2 Linear epicardial Gto gradient from 0.0 to 2.0 mS/μF

A similar two-dimensional simulation was performed with a different epicardial G_{to} gradient from 0.0 to 2.0 mS/μF. Interestingly, P2R happened in all ten beats in which current propagated from the direction where $G_{to,epi}$=0.0 mS/μF and the notch-and-dome morphology occurred, toward the other direction, where $G_{to,epi}$=2.0 mS/μF and the loss-of-dome morphology was present. Moreover, these P2R occurrences were all confined to the epicardium and did not spread to the midmyocardium, unlike in the other two-dimensional simulation.

4.5 Discussion

We demonstrated that P2R could be arrhythmogenic in two-dimensional tissue and could approximately double the time from excitation to full repolarization relative to normal propagation. To the best of our knowledge, this is the first study that investigates P2R development in two-dimensional transmural tissues.

Overall, most incidences of P2R originated in the epicardium, from the side of the epicardium that had the lower G_{to} value (right), spreading to the other side with the higher G_{to} value (left). In these occurrences the right side of the tissue showed a prolonged notch-and-dome morphology while the left side of the tissue showed the loss-of-dome morphology. This facilitated propagation of electrotonic current from the right side to the left side and initiation of P2R. As shown in Chapter 2, the prolonged notch-and-dome morphology occurred when APs

showed the switching behavior. The loss-of-dome morphology occurred either when G_{to} was increased or when the cells manifested the switching behavior.

Because most P2R incidences initiated in the epicardium, propagating horizontally from one side of the epicardium to another, we examined whether P2R would occur with complete block of epicardial propagation. We hypothesized that in case of such a block, P2R would occur in the epicardium transmurally, starting from the side that borders the midmyocardium and directed to the end of the epicardium (next to the external surface). In a simulation of two-dimensional transmural tissue lacking epicardial diffusion, P2R occurred in 9 out of 10 beats along the transmural direction. We conclude that the epicardium plays a key role in P2R initiation where P2R could develop either along the horizontal axis or along the transmural axis of the epicardium.

4.4.3 P2R incidence in two-dimensional tissues versus one-dimensional cables

It is worthwhile to compare the incidence of reentry in two-dimensional tissues to the incidence of P2R in one-dimensional cables to check whether arrhythmogeneity degenerated as the tissue grew or was suppressed by multidirectional stronger coupling. Both sets of simulations, the two-dimensional simulations and the one-dimensional simulations, were executed in an analogous manner, including usage of the same single cell model, similar initial conditions, and epicardial G_{to} values.

The occurrence of P2R in two-dimensional simulations was 40% in the simulation having a $G_{to,epi}$ gradient between 1.5 and 2.0 mS/μF and 100% in the simulation having 0.0-2.0 mS/μF $G_{to,epi}$ gradient. One-dimensional transmural simulations with these ranges of epicardial G_{to} had 10% P2R incidence (when $G_{to,epi}$=1.5 mS/μF, Figure 3.2A) or less. Furthermore, one-dimensional epicardial cable simulations with linear gradients of G_{to} showed 33% P2R incidence when the epicardial gradient was between 1.5 and 2.0 mS/μF (Figure 2.2A) and 37% when the gradient was between 0.0 and 2.0 mS/μF (Figure 2.2B). Therefore, there is an increase in P2R incidence in the two-dimensional simulations when compared to either epicardial or to transmural one-dimensional simulations. This increase is notable because one might have expected a decrease in P2R occurrence in two-dimensional simulations compared to one-dimensional simulations due to a suppression of local instability when residing in a bigger tissue. Several factors may contribute to this increase in P2R occurrence. In particular, the larger epicardial region essentially scans a range of dome and loss-of-dome dynamics in each beat, thus increasing the possibility of P2R. In addition, in the 2D simulations, the electrotonic current causing propagation of the dome likely has both transmural and epicardial components.

4.4.4 Study limitations

There are two main limitations for this two-dimensional study. First, we assumed isotropic diffusion and did not take into account the different gap junction conductances along the cells' axis [12]. Second, the tissue size was predetermined and invariant. Larger tissue simulations may result in sustained reentry. Even with these limitations, we believe that this two-dimensional

transmural study, together with our previous one-dimensional studies investigating the epicardial and the transmural directions, sheds light on the underlying dynamics and offers insight into the basic mechanism of the phase-2 reentry arrhythmogeneity.

4.5 Conclusion

We found that P2R could be arrhythmogenic in two-dimensional tissues causing abnormal AP propagation and approximately double the time from excitation to full repolarization relative to normal propagation. P2R was facilitated by the switching AP morphology in the epicardium, where cells switch intermittently between the notch-and-dome and loss-of-dome morphologies. To the best of our knowledge, this is the first simulation study that shows P2R in two-dimensional transmural tissue as opposed to two-dimensional epicardial tissue studies, done before [4, 5]. Sustained reentry was not demonstrated in this study, perhaps due to small tissue dimensions (i.e. 3 cm by 1.65 cm), which would be consistent with the critical mass hypothesis [13]. Finally, there was a remarkable increase in P2R incidence in two-dimensional transmural simulations compared to one-dimensional epicardial and transmural simulations.

REFERENCES

1. Miyoshi, S., et al., *Link between SCN5A mutation and the Brugada syndrome ECG phenotype: simulation study.* Circ J, 2005. **69**(5): p. 567-75.
2. Maoz, A., T. Krogh-Madsen, and D.J. Christini, *Instability in action potential morphology underlies phase 2 reentry: a mathematical modeling study.* Heart Rhythm, 2009. **6**(6): p. 813-22.
3. Miyoshi, S., et al., *A mathematical model of phase 2 reentry: role of L-type Ca current.* Am J Physiol Heart Circ Physiol, 2003. **284**(4): p. H1285-94.
4. Cantalapiedra, I.R., et al., *Reexcitation mechanisms in epicardial tissue: role of I(to) density heterogeneities and I(Na) inactivation kinetics.* J Theor Biol, 2009. **259**(4): p. 850-9.
5. Fenton, F., et al., *Basis for the induction of phase two reentry in the Brugada syndrome: Insights from computer simulations.* Heart Rhythm 2004. **1**: p. S224-S225.
6. Kimura, M., et al., *Mechanism of ST elevation and ventricular arrhythmias in an experimental Brugada syndrome model.* Circulation, 2004. **109**(1): p. 125-31.
7. Aiba, T., et al., *Cellular basis for trigger and maintenance of ventricular fibrillation in the Brugada syndrome model: high-resolution optical mapping study.* J Am Coll Cardiol, 2006. **47**(10): p. 2074-85.
8. Morita, H., et al., *Repolarization heterogeneity in the right ventricular outflow tract: correlation with ventricular arrhythmias in Brugada patients and in an in vitro canine Brugada model.* Heart Rhythm, 2008. **5**(5): p. 725-33.

9. Luo, C.H. and Y. Rudy, *A dynamic model of the cardiac ventricular action potential. I. Simulations of ionic currents and concentration changes.* Circ Res, 1994. **74**(6): p. 1071-96.
10. Dumaine, R., et al., *Ionic mechanisms responsible for the electrocardiographic phenotype of the Brugada syndrome are temperature dependent.* Circ Res, 1999. **85**(9): p. 803-9.
11. Rush, S. and H. Larsen, *A practical algorithm for solving dynamic membrane equations.* IEEE Trans Biomed Eng, 1978. **25**(4): p. 389-92.
12. Fenton, F. and A. Karma, *Vortex dynamics in three-dimensional continuous myocardium with fiber rotation: Filament instability and fibrillation.* Chaos, 1998. **8**(1): p. 20-47.
13. Qu, Z., *Critical mass hypothesis revisited: role of dynamical wave stability in spontaneous termination of cardiac fibrillation.* Am J Physiol Heart Circ Physiol, 2006. **290**(1): p. H255-63.

CHAPTER 5

CONCLUSIONS AND FUTURE DIRECTIONS

5.1 Summary of research

The leading hypothesis of Phase-2 reentry (P2R) is that it occurs when a notch-and-dome action-potential (AP) region borders a loss-of-dome action-potential region allowing current from phase-2 to propagate from the region where the dome is maintained to the dome-abolished region. However, our modeling studies suggest that P2R has a more complex initiation mechanism. The mere existence of two regions with different AP morphologies, the notch-and-dome and the loss-of-dome, does not facilitate P2R initiation per se. In fact, it can even prevent P2R from occurring. Indeed, we showed (Chapter 2) that when the two morphologies, the notch-and-dome and the loss-of-dome, were highly stable on a cable, the APs along the cable gradually transformed from one morphology to the other and the action potential duration (APD) gradually changed (i.e., P2R did not occur). Our most important finding is that the main factor facilitating P2R is a switching AP morphology caused by an ionic current imbalance. With such instability, cells can switch intermittently between the notch-and-dome and the loss-of-dome morphologies, which can trigger P2R.

P2R development in the epicardial direction of the right ventricle (RV) was studied in Chapter 2. The RV epicardium inherently has high values of the repolarizing current, I_{to}, and therefore is more prone to loss-of-dome AP development. We found that when the switching behavior was present in the cable, P2R occurred. This finding held true both for completely homogeneous

cables and for heterogeneous cables. In addition, we showed that for heterogeneous cables, the type of G_{to} gradient did not change these results.

P2R development in the transmural direction throughout the ventricular wall was investigated and discussed in Chapter 3. We found that P2R can indeed occur in the transmural direction and was always initiated in the epicardium regardless of whether stimuli were applied to the epicardial or the endocardial end of the cable. P2R was facilitated by the switching AP morphology in the epicardium. This switching behavior developed in the epicardium in the side that bordered the midmyocardium due to electrotonic current propagating from the midmyocardium and due to intrinsic properties of the epicardium. The finding that transmural P2R always stem from the epicardium, together with higher incidence of epicardial P2R when compared to transmural P2R incidence, suggest that the epicardium is more susceptible for P2R development. This is consistent with experimental studies [1, 2].

A two-dimensional P2R study was explored in Chapter 4. This study investigates two-dimensional transmural tissues, combining the epicardial (Chapter 2) and transmural (Chapter 3) one-dimensional studies. We found that P2R could be arrhythmogenic in two-dimensional tissues. Simulations demonstrated that abnormal AP propagation results from extensive prolongation of the time from beginning of excitation to full repolarization relative to normal propagation. P2R occurrences originated from the epicardium and were facilitated by the switching AP morphology in the epicardium. To the best of our knowledge, this is the first study that investigates P2R in two-dimensional transmural tissue. Moreover, a remarkable increase in P2R incidence in two-dimensional transmural

simulations compared to one-dimensional epicardial and transmural simulations was demonstrated.

To summarize, the goal of my thesis was to understand the underlying mechanism of P2R initiation. Using these three computational studies we have illuminated the fundamental underlying dynamics of the model system and have therefore introduced a plausible theory for the basic mechanism of the P2R arrhythmogeneity substrate clinically.

5.2 Future directions and discussion

5.2.1 Specificity of I_{to}

One of the weaknesses common to all of the studies in this thesis lies in the method of simulating heterogeneity. In order to simulate ionic heterogeneity in the RV, we only used gradients in the expression levels of one current, the transient outward current, I_{to}. We elaborate on the rationale for that here.

First, all other computational studies that investigated P2R [3-6] altered only G_{to} in the epicardium. Since we believed that all of these studies altered G_{to} incorrectly (i.e., we are aware of no experimental data supporting the existence of such discontinuous G_{to}), our first priority and focus was to correct the methods by which G_{to} was varied. We believe that our continuous gradient method is more realistic and could provide a better understanding of the mechanism of P2R development.

Second, there is evidence of heterogeneity of I_{to} expression level in canine left ventricle (LV) myocytes [7] - I_{to} amplitude is significantly larger in apical than in basal cells. In addition, canine myocytes from the right ventricular free wall show disparity in peak current density, with I_{to} density varied between 70-152% of the mean value [8].

However, investigating the system under variation of G_{to} alone, does make our findings more difficult to generalize. In order to strengthen the conclusions that the switching behavior is a key factor in P2R initiation, it is important to extend the study not to be solely dependent on gradients in I_{to}. To do so, we suggest several approaches:

(I) Alternative epicardial ionic gradients

This approach consists of applying different ionic gradients (e.g., in the sodium current or in the L-type calcium current) to the epicardium, to show that the switching behavior is not dependent only on an I_{to} gradient. Such a study should use the basic framework our studies followed, starting from single-cell simulations, progressing to cable simulations and simulating two-dimensional tissues with ionic gradients in the epicardium. For each current, a range of its maximum conductance values (G_{Na} or $G_{Ca,L}$) will be used to detect where the switching behavior range is. This range would be considered physiologically relevant if it is in agreement with pathological data of patients who have deficiency in ionic-channel function (i.e. Brugada syndrome patients who have known mutation in I_{Na} [9] or $I_{Ca,L}$ [10] function). A pathologically-relevant scenario would

show a wide range of G_{Na} or $G_{Ca,L}$ values showing the switching behavior and the loss-of-dome morphology as well as reasonable absolute decrease values for these variables (e.g. 30-70% of the WT value). Support for such a study was reported in a study by Vecchietti et al [11]. In this simulation study, the switching behavior was evident where I_{Na} was blocked by 40% in the presence of the Y1795H SCN5A mutation, occurring in some Brugada patient families. The Y1795H mutation causes a negative shift of the inactivation curve (making the channel less available).

(II) Reduced–model analysis

Another approach to show that the switching behavior is not solely determined by manipulations of I_{to}, would be to reduce the single-cell ventricular model we used, the LRd model, to a simplified non-ionic model. An example for such a reduced model is the four-variable model developed by Bueno-Orovio et al [12] to model the human ventricular action potential. This model can reproduce APs from the epicardium, endocardium, and midmyocardium, as well as epicardial prolonged notch-and-dome and loss-of-dome morphologies. Using such a model, one could vary parameters representative of generic inward and outward conductances to investigate the occurrence of switching behavior and P2R. By so doing, one could separate the occurrences of these dynamics from specific ionic mechanisms, thereby offering support for the generality of the mechanism. Furthermore, if a reduction of the model to a three-variable model is possible, one would be able to plot the system in phase-space to visualize the relationships between variables. In such a scenario, depending on the parameters of the model, when either the notch-and-dome or the loss-of-dome morphologies occur,

a period-1 solution would appear. When the system manifests the switching behavior, a period-2 (or higher) solution would appear on the phase-space map.

5.2.2 Three-dimensional simulations

Adding a third dimension to the model would provide a more realistic simulation, combining epicardial ionic heterogeneity with transmural heterogeneity. It is difficult to predict the different patterns that will emerge. However, we will describe here how we expect the system to behave based on our two-dimensional simulations of Chapter 4. First, P2R would be expected to develop in the epicardium, propagating from one side of the epicardium to the other, initiating a spiral wave in the epicardium, due to midmyocardial refractoriness. Then, when the midmyocardium is recovered, the epicardial spiral wave would be able to propagate transmurally, creating a retrograde transmural scroll wave in the midmyocardium.

Such dynamics are consistent with the development of polymorphic VT and VF. In an experimental study of P2R, 9 out of 12 of canine right ventricular preparations administered with pilsicainide (sodium channel blocker) and pinacidil (a K_{ATP} channel opener) displayed VT that degenerated into sustained VT [1]. In another study where transmural wedges of dimensions from 2x1x0.7 cm to 3x1.5x1 cm were dissected from the free wall of the RV of male dogs, VT (terminated within 5 s) and VF (sustained more than 5 s) occurred [2]. In this study a drug combination of terfenadine (I_{Na} and $I_{Ca,L}$ blocker), pinacidil and pilsicainide was used.

A second phase to such a three-dimensional study may include incorporating anisotropy to represent the different layers of cells, arranged in fibers, in the ventricular wall. It is known that electrical signals propagate faster in the direction that is parallel to the fibers than perpendicular to them and that the fibers themselves rotate transmurally across the ventricle [13]. Incorporating such complex orientations would contribute to better and more accurate modelling of the three-dimensional simulation.

5.2.3 Mutation-based study

As discussed in Chapter 1.3.3, the Brugada syndrome inheritance follows an autosomal dominant mode of transmission. Mutations in the SCN5A gene that encodes the α-subunit of the sodium channel were identified. Some such mutations have been studied in expression systems, which enable probing of their electrophysiological characteristics (e.g. reduced sodium channel expression, voltage- and time-dependence I_{Na} activation and inactivation shift and slower recovery from inactivation of the sodium channel). Therefore, a study that models these mutations based on their known kinetics is both feasible and beneficial. It would investigate whether these characteristics are all arrhythmogenic and whether some of them are more susceptible to P2R initiation than others.

A second phase to such a study may include incorporating drug models into the system. Drugs that change the ionic balance at the end of phase-1 or the beginning of phase-2 may be offered as therapeutic solutions to Brugada patients. A comprehensive modeling study that simulates both mutations and drugs could

shed light on possible therapies for Brugada syndrome, in addition to ICD implantation.

REFERENCES

1. Kimura, M., et al., *Mechanism of ST elevation and ventricular arrhythmias in an experimental Brugada syndrome model.* Circulation, 2004. **109**(1): p. 125-31.
2. Aiba, T., et al., *Cellular basis for trigger and maintenance of ventricular fibrillation in the Brugada syndrome model: high-resolution optical mapping study.* J Am Coll Cardiol, 2006. **47**(10): p. 2074-85.
3. Miyoshi, S., et al., *A mathematical model of phase 2 reentry: role of L-type Ca current.* Am J Physiol Heart Circ Physiol, 2003. **284**(4): p. H1285-94.
4. Miyoshi, S., et al., *Link between SCN5A mutation and the Brugada syndrome ECG phenotype: simulation study.* Circ J, 2005. **69**(5): p. 567-75.
5. Fenton, F., et al., *Basis for the induction of phase two reentry in the Brugada syndrome: Insights from computer simulations.* Heart Rhythm 2004. **1**: p. S224-S225.
6. Cantalapiedra, I.R., et al., *Reexcitation mechanisms in epicardial tissue: role of I(to) density heterogeneities and I(Na) inactivation kinetics.* J Theor Biol, 2009. **259**(4): p. 850-9.
7. Szentadrassy, N., et al., *Apico-basal inhomogeneity in distribution of ion channels in canine and human ventricular myocardium.* Cardiovasc Res, 2005. **65**(4): p. 851-60.
8. Di Diego, J.M., Z.Q. Sun, and C. Antzelevitch, *I(to) and action potential notch are smaller in left vs. right canine ventricular epicardium.* Am J Physiol, 1996. **271**(2 Pt 2): p. H548-61.
9. Tan, H.L., et al., *Genetic control of sodium channel function.* Cardiovasc Res, 2003. **57**(4): p. 961-73.

10. Cordeiro, J.M., et al., *Accelerated inactivation of the L-type calcium current due to a mutation in CACNB2b underlies Brugada syndrome.* J Mol Cell Cardiol, 2009. **46**(5): p. 695-703.
11. Vecchietti, S., et al., *In silico assessment of Y1795C and Y1795H SCN5A mutations: implication for inherited arrhythmogenic syndromes.* Am J Physiol Heart Circ Physiol, 2007. **292**(1): p. H56-65.
12. Bueno-Orovio, A., E.M. Cherry, and F.H. Fenton, *Minimal model for human ventricular action potentials in tissue.* J Theor Biol, 2008. **253**(3): p. 544-60.
13. Fenton, F. and A. Karma, *Vortex dynamics in three-dimensional continuous myocardium with fiber rotation: Filament instability and fibrillation.* Chaos, 1998. **8**(1): p. 20-47.